Alma Mater Studiorum - Università di Bologna

DOTTORATO DI RICERCA IN

AUTOMOTIVE PER UNA MOBILITÀ INTELLIGENTE

Ciclo 34

Settore Concorsuale: 09/C1 - MACCHINE E SISTEMI PER L'ENERGIA E L'AMBIENTE

Settore Scientifico Disciplinare: ING-IND/08 - MACCHINE A FLUIDO

MODELING OF ELECTRIC HYBRID VEHICLES BASED ON INNOVATIVE ENERGY STORAGE TECHNOLOGIES FOR SUPER SPORTS CARS APPLICATIONS

Presentata da: Alessandro Franceschi

Coordinatore Dottorato

Nicolò Cavina

Supervisore

Nicolò Cavina

Esame finale anno 2022

Contents

List of Figures

List of Tables

List of Abbreviations

4WD	4-Wheel Drive
BMEP	Brake Mean Effective Pressure
BSFC	Brake Specific Fuel Consumption
CB	Charge Blended
CD	Charge Depleting
CFC	Chlorofluorocarbon
CO	Carbon Monoxide
CO2	Carbon Dioxide
CS	Charge Sustaining
DP	Double Polarization
ECMS	Equivalent Consumption Minimization Strategy
ECU	Engine Control Unit
EDLC	Electric Double Layer Capacitor
EM	Electric Machine
EMS	Energy Management Strategy
EV	Electric Vehicle
FC	Fuel Consumption
FTP-75	Federal Test Procedure
GUI	Graphic User Interface
HESS	Hybrid Energy Storage System
HEV	Hybrid Electric Vehicle
ICE	Internal Combustion Engine
IMEP	Indicated Mean Effective Pressure
ISFC	Indicated Specific Fuel Consumption
LHV	Lower Heating Value
LiC	Lithium-Ion Capacitor
MPC	Model Predictive Control
NEDC	New European Driving Cycle
PDT	Pulsed Discharge Test
PHEV	Plug-in Hybrid Electric Vehicle
PI	Proportional-Integral
PMP	Pontryagin's Minimum Principle
RBS	Rule Based Strategy
RC	Resistor-Capacitor
RPM	Revolutions per Minute
SI	Spark Ignition
SoC	State of Charge
THC	Total Hydrocarbons
WLTC	Worldwide harmonized Light-duty vehicles Test Cycle
WLTP	Worldwide harmonized Light-duty vehicles Test Procedure

Abstract

Today, the contribution of the transportation sector on greenhouse gases is evident. The fast consumption of fossil fuels and its impact on the environment has given a strong impetus to the development of vehicles with better fuel economy. Hybrid electric vehicles fit into this context with different targets, starting from the reduction of emissions and fuel consumption, but also for performance and comfort enhancement. Hybrid electric vehicles serve as a strong alternative on drivability and performance to conventional internal combustion engine-based vehicles.

Vehicles exist with various missions; super sport cars usually aim to reach peak performance and to guarantee a great driving experience to the driver, but great attention must also be paid to fuel consumption. According to the vehicle mission, hybrid electric vehicles can differ in the powertrain configuration and the choice of the energy storage system. Nowadays, hybrid electric vehicles represent one of the main solutions for the reduction of greenhouse gases in the automotive sector.

Targeting the reduction of CO_2, manufacturers are working on various electric hybrid vehicles configurations that may differ in terms of topology (series, parallel, power-split, …) and architecture (P0, P1, P2, P3 and P4 if considering a parallel configuration). Most of such solutions adopt high-voltage batteries as energy storage systems for the electric propulsion, but other technologies could provide additional advantages, especially for specific applications where the need for managing high electric power demands becomes crucial, both during traction and regeneration.

Lamborghini has recently invested in the development of hybrid super sport cars, due to performance and comfort reasons, with the possibility to reduce fuel consumption. This research activity has been conducted as a joint collaboration between the University of Bologna and the sportscar manufacturer, to analyze the impact of innovative energy storage solutions on the hybrid vehicle performance. In particular, capacitors have been studied and modeled to analyze the pros and cons of such solution with respect to batteries. To this aim, a full simulation environment has been developed and validated to provide a concept design tool capable of reproducing the hybrid vehicle behavior on regulated emission cycles and real driving conditions, allowing to compare the effects of different energy storage solutions, considering also "hybrid" systems, where both batteries and capacitors are employed on the same vehicle.

The target is to dispose of a reliable tool capable of precise results and able to foresee the performance and behavior of future vehicles, with a particular focus on fuel consumption and longitudinal performance, based on a minimal amount of data while achieving good accuracy. Therefore, this work intends to give reliable instruments capable of shortening the times associated to the vehicle concept phase.

In addition, the target of the research activity is to deepen the study of hybrid electric super sports cars in the early concept development phase, focusing on defining the control strategies

and on choosing the energy storage system's technology that best suits the needs of the super sports cars. This dissertation covers the key steps that have been carried out in the research project.

At first, it is presented a short but necessary introduction of the topics, to point out the fundamental characteristics of the hybrid electric vehicles and to clarify the differences between capacitors, typically associated with high power density and low energy density, and batteries, typically limited on the charge and discharge power. Then, a longitudinal dynamics model is presented and validated, and the electric components are introduced. The longitudinal dynamics model will be capable to reproduce the behavior of both conventional vehicles based on an internal combustion engine, and hybrid vehicles.

In the following chapters, various controllers are explained, as they will be implemented as energy management strategies (EMS) for the studied vehicles. Later, three hybrid vehicle configurations are described as these represent the core of this dissertation. The vehicles presented show an evolution in the complexity of the hybrid system, both on the powertrain side and the control one.

At last, the results of the activity are presented along with the conclusions. The research project demonstrates how hybrid electric super sport vehicles based on energy storage systems consisting solely of capacitors or "hybrids", can meet demands for comfort, performance and even fuel economy.

Introduction

Earth's climate has changed throughout history, and most of the climate changes are attributed to variations in Earth's orbit that change the amount of solar energy the planet receives. The current warming trend is of particular significance because most of it is extremely likely to be the result of human activity since the mid-20th century, and proceeding at a rate that is unprecedented over millennia [1].

Certain gases in the atmosphere block heat from escaping and "force" climate change causing longer and more intense heat waves, loss of sea ice, accelerated sea level rise, global temperature rise, …

The current and projected implications of climate change for the society and the sustainable development are such that actions are required, as energy consumption mitigation and a shift to a lower-carbon economy [2].

Some of the gases participating to the greenhouse effect are [3]:

- Water vapor,
- Carbon dioxide (CO2),
- Methane,
- Nitrous Oxide,
- Chlorofluorocarbons (CFCs),
- …

The transportation sector contributes to the greenhouse gas emissions especially through carbon dioxide (CO2). The emissions are the product of the combustion of hydrocarbons-based products, like gasoline, in internal combustion engines (ICEs) [4,5]. Also, small amounts of methane, nitrous oxide and hydrofluorocarbon are emitted. Solutions need to be adopted to actively reduce greenhouse gas emissions, as the global heating must be limited. A variety of opportunities associated with transportation could be adopted and are nowadays explored.

The automotive sector has focused on the improvement of existing technologies and on new proposals related to the reduction of CO2 emissions [6–9]. Now, the electrification process is trending since electric vehicles (EVs) or hybrid electric vehicles (xHEVs) can reduce the fossil fuels consumption while maintaining performance comparable to the ones of conventional ICE vehicles [5,10].

On one side, electrification is seen as a great opportunity to challenge climate change, especially in some aspects of road transportation [11]. On the other side, it brings along some issues related to the technologies, that have not yet been overcome [5,12].

A hybrid powertrain uses two or more distinct power sources to move the vehicle. The term refers to various hybrid topologies that could combine an ICE as a primary energy source and a secondary energy source of various nature. The most common topologies are [13]:

- Electrical, that typically includes a battery for the energy storage and an electric motor/generator as energy converter,
- Mechanical, that foresees the usage of a high-speed flywheel both to accumulate and provide the recovered energy,
- Hydraulic, where the auxiliary energy storage system is a hydraulic accumulator and the energy converter is a hydraulic motor/pump; this solution is suitable for specific applications such as construction equipment, garbage trucks, …, because of the weights and sizes of the additional components,
- …

According to the size of the electric energy storage system and Electric Machines (EMs), different hybridization levels can be defined [11,14,15]:

- Micro Hybrid, in which the electric machine is an integrated starter generator (only Stop/Start and recuperation capabilities),
- Mild Hybrid, where the small size of the electric components allows limited maneuvers in pure-electric mode,
- Full Hybrid, which includes powerful motors and large battery sizes; in this case pure-electric mode is admissible,
- Plug-in Hybrid Electric Vehicle (PHEV), the powertrain architecture is similar to the full hybrid, but the battery can be externally recharged and is typically larger,
- Range-extender electric vehicles, for which the electric propulsion is the main contribution to the propulsion and the engine is the auxiliary energy converter.

Table 1. Overview of HEV characteristics.

Functions	Start/Stop	Regenerative Braking	Boost	Electric Drive	External Charge
Conventional	Possible	0	0	0	0
Micro Hybrid	1	Minimum	0	0	0
Mild Hybrid	1	1	Minimum	Limited	0
Full Hybrid	1	1	1	1	0
Plug-in Hybrid	1	1	1	1	1
Extended Range	1	1	1	1	1
Battery Electric Vehicle	1	1	0	1	1

Moreover, various powertrain architectures can be defined depending on the architecture [5,11,14,15]:

- Series, where the wheels are powered only through the EM, while the ICE is connected to a generator and provides energy to the battery. Typically Full, Plug-in and Extended Range Hybrids.

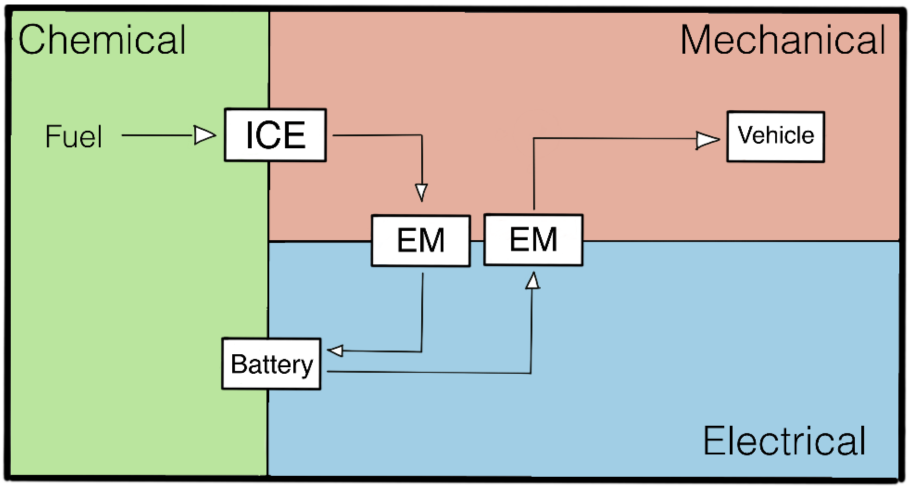

Figure 1. Series HEV energy flow.

- Parallel, that allows to have the summation of the torques derived from the ICE and the EM before or after the transmission. Typically Micro, Mild, Full and Plug-in Hybrids.

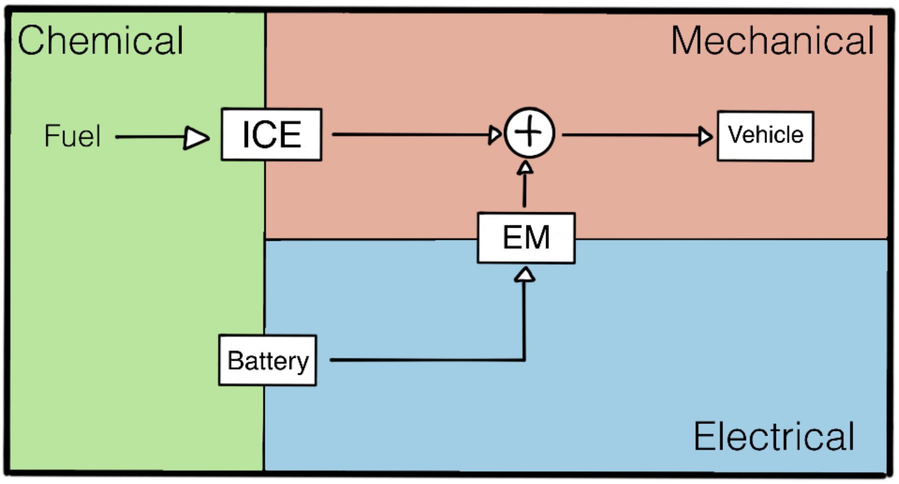

Figure 2. Parallel HEV energy flow.

- Power-split, that foresees the possibility of managing the powertrain both in series and parallel configurations through the connection of the engine and the EMs to a power split device like a planetary gear set. Typically Mild, Full, Plug-in Hybrids.

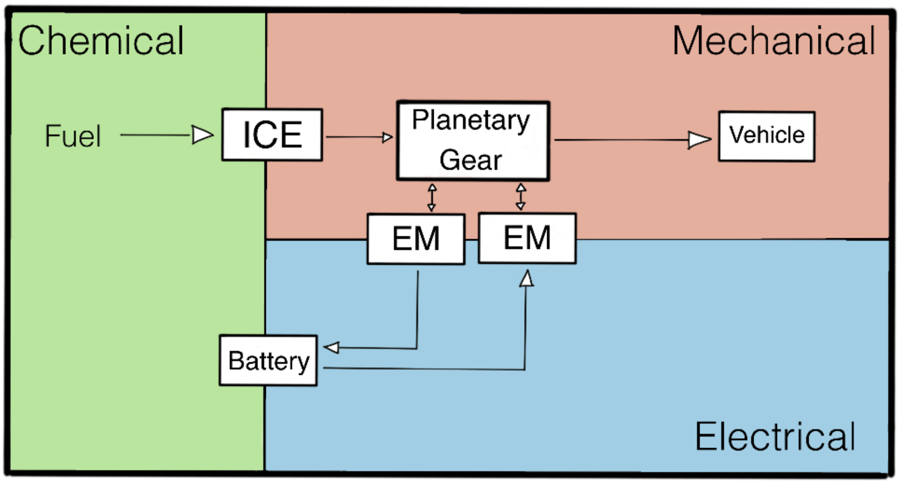

Figure 3. Power-split HEV energy flow.

- Series/Parallel, that sees the engagement/disengagement of one or two clutches to change the powertrain configuration from series to parallel and vice versa. Typically, Full and Plug-in Hybrids.

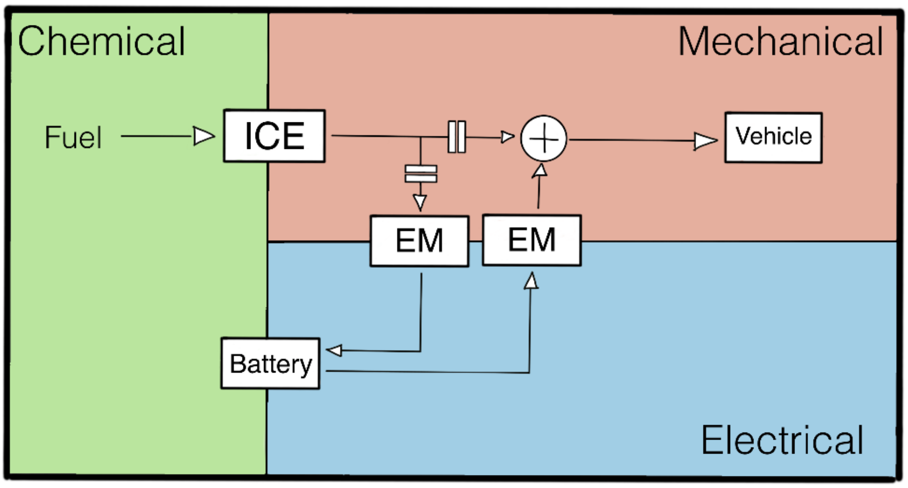

Figure 4. Series/Parallel HEV energy flow.

Focusing on the parallel architecture, the position of the EM defines more in detail the characteristics of the vehicle, as shown in Figure 5 [15]:

- P0, the EM is connected directly to the ICE, typically with belts,
- P1, the EM is positioned between the ICE and the primary shaft of the gearbox, but it can be detached from the gearbox, and it can start the engine without carrying other inertias,
- P2, the EM is positioned between the ICE and the primary shaft of the gearbox, but it can be disconnected from the ICE to avoid the losses of the ICE itself,
- P3, the EM is positioned at the secondary shaft of the gearbox,
- P4, the EM is connected to the wheels and permanently disconnected from the ICE.

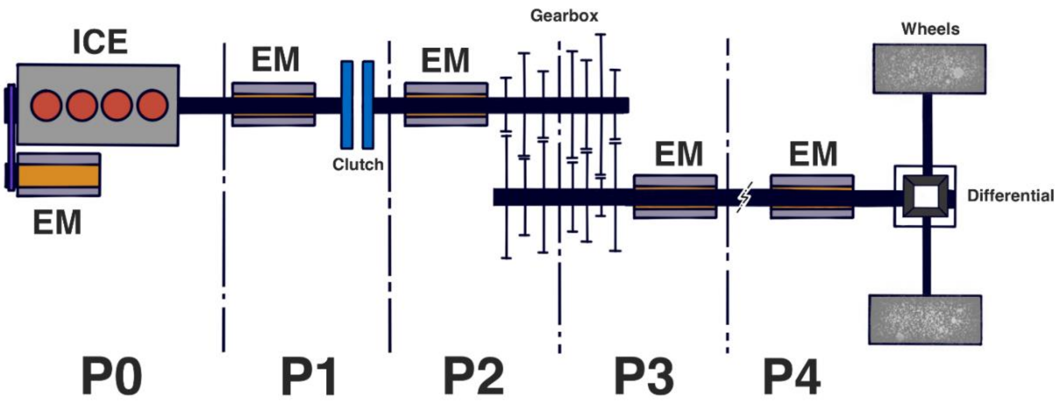

Figure 5. Various EM positioning in parallel architecture.

The impact of hybrid electric vehicles on global warming, that would make them a good solution for the reduction of CO2 emissions, depends on the hybrid control strategies that are adopted. Various strategies exist that can target fuel economy, as [11]:

- Load point shift, where the torque requested to the engine is augmented, in order to increase its efficiency, and part of such power is used to recharge the battery,
- Kinetic energy recuperation, that allows to recover energy during braking phases instead of using mechanical brakes,
- Electric driving, that allows to cover the power request uniquely with the electric machine,
- Start/Stop, that allows to avoid idle phases for the engine, switching it off when not needed and restarting it using the electric machine,
- Boost, that allows to downsize the engine to guarantee higher efficiency and to use the electric machine as a booster.

The activation of these hybrid control strategies depends on the amount of energy and power made available by the hybrid powertrain. In particular, it strongly depends on the energy storage system that has been adopted.

Some strategies are related to high energy requirements. For example, the electrical driving when the internal combustion engine is inefficient, or in in urban areas, is possible only when high energy content is available. On the other hand, other strategies are strictly related to high power requirements, both in charge and discharge, as it is for kinetic energy recuperation or boost. To fully recover the kinetic energy available in braking phases, high charging power is needed, while high discharge power is requested when in boost mode.

High power requirements from the energy storage system become essential if we refer to super sports cars. Typically, this kind of vehicles shows a specific need for high power especially when driven in sport mode or when they are driven on track, generating high accelerations and decelerations. Power could be needed also to target comfort, covering the torque gap that is generated during gear shifts in single clutch transmissions.

The current dissertation deepens the study of energy storage systems, starting from batteries and ending with Lithium-Ion Capacitors (LiCs), with a particular focus on applications on super sport cars. The contribution of this activity highlights how high-power density systems can help to achieve the targets mentioned above, pointing out how capacitors can be an alternative to batteries for super sports cars applications.

Referring to electrochemical batteries, they are a key component in hybrid electric and electric vehicles, capable of transforming chemical energy in electrical energy and vice versa. As shown in Figure 6 batteries are equipped with two electrodes of different chemical composition, immersed in an electrolyte, and separated by a membrane. The membrane allows the passage of small ions, which are formed if the electrodes are connected through an external electrical circuit (Faradaic process). This circuit makes it possible to pass electrons produced by oxygenation. The anode, electrically negative, is the electrode where the oxidation takes place (loss of electrons). The cathode, electrically positive, is defined as the electrode where it takes place the reduction process (electron acquisition). The batteries used in the automotive sector are all rechargeable (defined as secondary). They can be divided into two categories depending on the type of electrolyte adopted, the batteries working at room temperature use an aqueous or non-aqueous electrolyte, those at high temperature an electrolyte solid or molten. The most common technologies are [5]:

- Acid lead,
- Metal nickel hydride,
- Lithium, including lithium ions and polymer of lithium metal,
- Molten salts, including nickel-sodium chloride,
- Air-metal, including air-lithium and zinc-air.

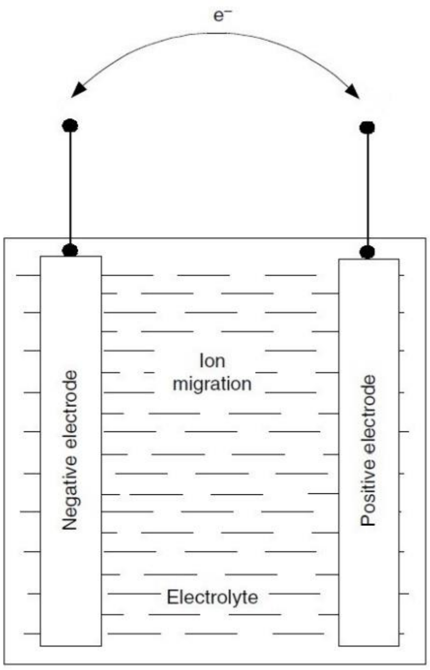

Figure 6. Battery scheme [5].

The power generated by a battery is given by the product of voltage and current, where the voltage depends on the chemistry of the elements adopted. One of the main features of the batteries is the high energy content and low power values, which result in high charging and discharging times as it is explained in [15,16]. On the other hand, capacitors can be of various types, starting from the simplest format of two plates consisting of conductive material and separated by a dielectric up to capacitors formed by two plates of conductive material separated by an electrolyte fluid and a membrane. Unlike batteries, they do not undergo chemical changes to the structure [5,15].

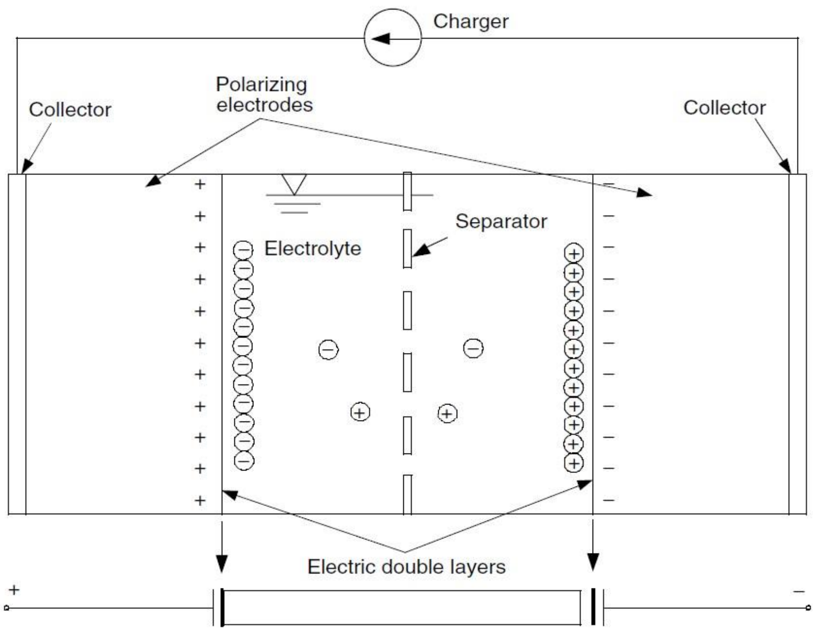

Figure 7. Electrical double layer capacitor scheme [5].

Electrical Double Layer Capacitors (EDLCs) consist of two electrodes composed of high surface area carbon, characterized by a high polarizability and electrical conductivity, and separated by an electrolyte. More in detail, in EDLCs charge carriers are distributed into the bulk of the polarized carbons electrodes over a relatively large distance that is inversely related to the charge-carrier density. Then, two layers are formed. The first is formed on the electrolyte side and it is a compact layer of ions of the same charge (but different sign with respect to the electrode surface), called the Inner Helmholtz Plane, at the closest distance from the electrode. The second is a diffuse layer, that occurs in order to balance the electrode charge, called the Outer Helmholtz Plane. The capacitance can be expressed as follows:

$$C = A\frac{\varepsilon}{l}$$

I

Where $\varepsilon\ [\frac{F}{m}]$ is the dielectric permittivity, $A[m^2]$ is the electrode surface area and $l[m]$ is the double layer thickness. Due to the high surface areas and the low thickness, the capacitance of EDLCs reaches values above 1000F.

One of the characteristics of EDLCs is that they are based on non-Faradaic processes, meaning that the carbon electrodes store charge electrostatically. However, also pseudocapacitors exist, that feature battery-like electrodes that are charged/discharged by fast and reversible redox processes.

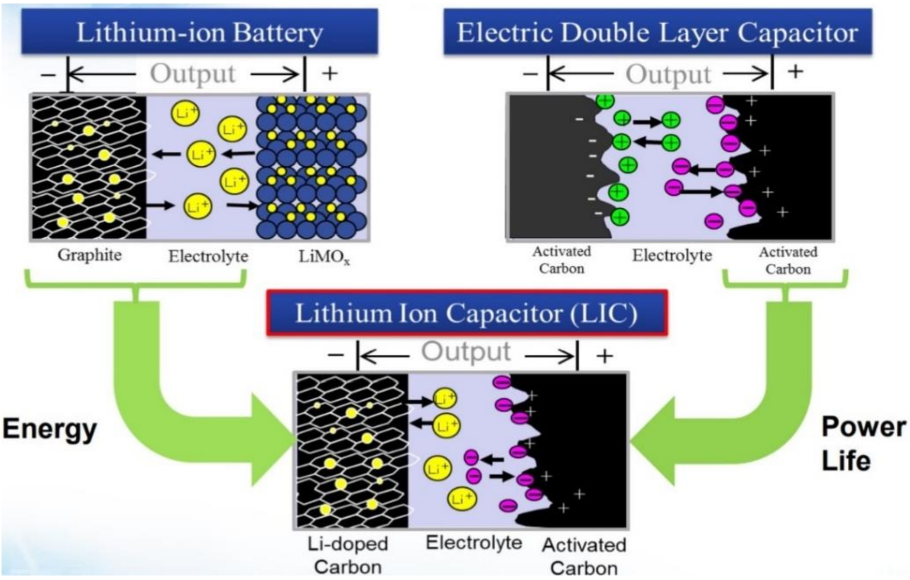

Figure 8. Lithium Ion Capacitor [17].

At last, hybrid capacitors feature positive and negative electrode materials of different nature that are charged/discharged via different electrostatic and faradic modes. Lithium-Ion capacitors, shown in Figure 8, belong to this group as they combine the activated Carbon cathode of an EDLC with the Li-doped Carbon anode of Lithium-Ion Batteries, to guarantee both power and energy. The energy density that is achieved is 3 times larger than the one of ordinary super capacitors.

The other advantages of capacitors are represented by the high number of cycles they can run until the end of life, and the symmetrical behavior in charge and discharge, differently from batteries that are typically limited by the low cycle life and the asymmetry in charge and discharge.

Both batteries and capacitors can be connected in series or parallel configurations. The word 'cell' can be used to describe the single electrochemical unit, and usually multiple cells are connected together to form a pack of batteries or capacitors. When cells are connected in series the output voltage increases while the current stays the same. High voltage configurations require many cells connected in series and they require careful cell matching. In fact, an aged or faulty cell will have a lower capacity than the others, hence causing imbalance and preventing the string from reaching the nominal voltage. A single cell failing would cause a failure on the entire string.

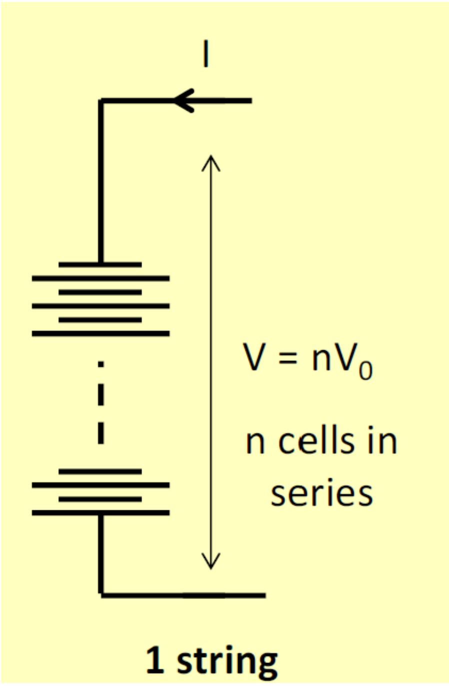

Figure 9. Cell in series configuration.

On the other hand, cells connected in parallel divide the current among the cells while maintaining the same voltage. Parallel connections allow the pack to sustain higher currents without the need of larger cells. Moreover, a cell that develops high resistance or fails will not change the pack, but it will reduce the total capacity. However, an electrical short would mean that the faulty cell starts draining energy from the other cells, causing a fire hazard, making security systems as fuses essential.

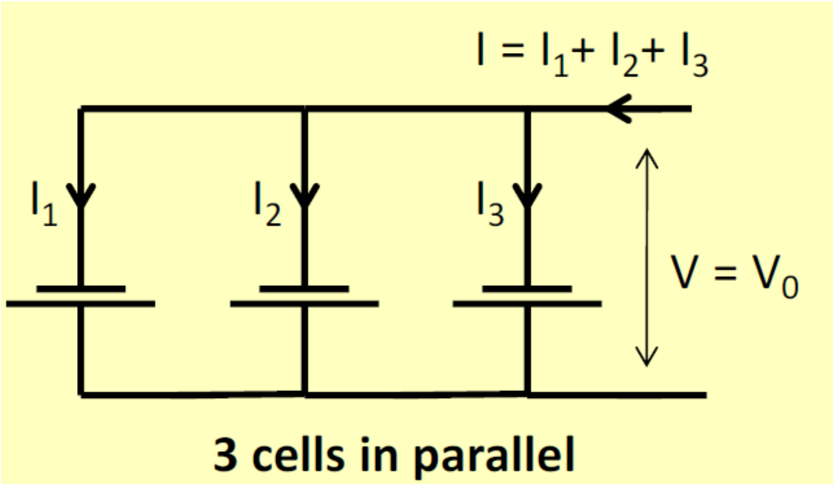

Figure 10. Cells in parallel configuration.

The pack configuration can be defined depending on the number of cells in series, expressed by the letter s, and the number of cells in parallel, expressed by the letter p. For example, if the configuration is a 14s2p, that would mean that the pack is made of 14 cells in series and 2 parallels.

Apart from the voltage and current, cells are usually defined by the internal resistance R that defines the overall resistance within the cell, the more it increases, the more the cell efficiency decreases and more of the charging energy is converted into heat.

For a series configuration, the equivalent resistance of the pack R_{eq} is given by:

$$R_{eq} = R_1 + R_2 + \cdots + R_n$$

II

For a parallel configuration, the equivalent resistance of the pack R_{eq} is given by:

$$\frac{1}{R_{eq}} = \frac{1}{R_1} + \frac{1}{R_2} + \cdots + \frac{1}{R_n}$$

III

For capacitors, the capacitance parameter C is also introduced as it defines the ratio of the amount of electric charge Q stored to a difference in electric potential ΔV.

$$C = \frac{\mathrm{Q}}{\Delta V}$$

IV

For a series configuration, the equivalent capacitance of the pack C_{eq} is given by:

$$\frac{1}{C_{eq}} = \frac{1}{C_1} + \frac{1}{C_2} + \cdots + \frac{1}{C_n}$$

V

For a parallel configuration, the equivalent capacitance of the pack C_{eq} is given by:

$$C_{eq} = C_1 + C_2 + \cdots + C_n$$

VI

1. Longitudinal Dynamics Model

The longitudinal dynamics model is presented here. The target is to reproduce accurately a super sport car's behavior, targeting the analysis of its fuel consumption, drivability, and comfort. The longitudinal dynamics model can also produce a first analysis on the vehicle performance, taking into account the deformation of the tires computed through the variable wheel radius and the tire slip.

1.1. Literature Review

Several approaches have been investigated and can be found in the literature related to this topic with the main distinction, that is clarified in [13,14], of:

- Backward-facing approach,
- Forward-facing approach.

The backward facing approach that can be found in [18–20] is capable of quasi static simulations. The vehicle is supposed to always meet the required speed profile, calculating the required force to accelerate and decelerate it at each time step. An approach of this kind can easily implement experimental efficiency maps, moreover it allows simple integration routines and gives fast simulations. On the other side, it does not take into account dynamic effects, and it is not suitable for an appropriate and realistic description of the real control signals of the vehicle.

If that is the target of the model, a forward-facing approach like the one found in [21] is needed. A system of this kind can include dynamic models and high frequency effects, using measurable and realistic control signals and torques. Detailed simulations are obtained, and the model is more realistic and appropriate for control development. On the other side, smaller time steps are required to provide stability and accuracy, and this results in a lower simulation speed.

Various software and models exist for reproducing the longitudinal dynamics behavior of a vehicle, and some of them can be found in [19,22–24].

[19] has been developed at the Eidgenössische Technische Hochschule Zürich, on MATLAB/Simulink with a quasi-static approach, and it cannot capture dynamic phenomena. Data input takes place thanks to Simulink masks and the software makes available a wide library of models reproducing the vehicle powertrain components. [18] presents the QSS toolbox and some case studies solved with this tool, while the theoretical background can be found also in [20].

[22] has been developed from the Environmental Protection Agency and it simulates the whole vehicle on MATLAB/Simulink. It has been developed to estimate the greenhouse gases emissions and it allows to simulate a great variety of vehicles by defining the architecture of the vehicle, also thanks to a Graphic User Interface (GUI). Its structure is extensively described in [25]. The software has been used to model a midsized car as in [26], where the study targets

minimum greenhouse gases emissions by comparing various combinations of existing technologies included in the software's library, which is extended and includes vehicles of various sizes.

[23] has been produced by the National Renewable Energy Laboratory, it allows to run a quick analysis on performance and fuel consumption on MATLAB/Simulink. The software is quasi-static, the GUI is easily accessible, and it allows to modify various aspects of the vehicle. [27,28] show some of the results that can be obtained with ADVISOR, using the wide library available through the software.

[24] has been produced by the Joint Research Centre of the European Commission on Python, and it allows to estimate CO2 emissions. The software is open source and uses Excel for data input and output.

Another forward-facing model is shown in [29]. This work is a master thesis focused on the longitudinal dynamics of a conventional super sport car Lamborghini Murciélago [30], and it is developed internally at Automobili Lamborghini S.p.A., making it a perfect baseline for the current research project.

Other vehicle simulation tools are commercially available, as Autonomie [31], AVL-CRUISE [32], GT-Drive [33], Ricardo IGNITE [34], …

Commercial vehicle simulation tools usually guarantee the chance to model the entire vehicle and to model virtually any vehicle architecture, but they come at a cost. Moreover, commercial tools not always guarantee transparency and easy public access since they do not guarantee access to the code.

1.2. Research Project Contribution

The current research project focuses on the development of a longitudinal dynamics forward-facing model. The need for a model of this kind is clear for pre-concept and concept phases, as it allows to predict and quantify the effects of proposed changes in vehicle characteristics and parameters.

A reliable longitudinal dynamics' model capable of reproducing faithfully the behavior of real vehicles is realized. The focus is not on passenger cars, as it is in the majority of the previously analyzed software, but rather on super sport cars.

The various software analyzed [19,22–24,31–34] show a good starting point for the building of a longitudinal dynamics' model and the possibility to choose one of these as a baseline is considered, as their pros and cons are evaluated. However, the decision to strictly stick to one of these models could excessively limit the possibility to modify the vehicle in concept phase. So, the necessity to develop a model within the company is made evident. The model is designed to specifically reproduce the behavior of super sport cars from Automobili Lamborghini, ensuring a reliability that cannot be found in any other software. Moreover, the possibility to develop and keep internally the know-how is a strong benefit for the vehicle manufacturer, as it allows for better control towards the design process.

According to this, the MATLAB/Simulink simulation environment is chosen. This decision makes [24] not fit for the current activity, however the choice to use Excel for data input is evaluated and maintained as it can be easily integrated with MATLAB. Moreover, [19,23] being quasi static models are inadequate, but represent a strong baseline for the modeling of the single vehicle components. [22] is a forward-facing model, but it does not include super sport car vehicles in its library, which represent the core of this research activity.

The chance to freely work on every model component is considered of great importance as it allows to explore any possibility in concept phase and it gives the chance to intervene on any element. This makes all the commercial tools [31–34] inadequate for our work.

Therefore, the baseline for the current research project is the master thesis shown in [29] as it represents the best solution among the ones analyzed. The longitudinal vehicle model from [29] describes in fact a super sport car, and it is developed internally at Automobili Lamborghini S.p.A. on MATLAB/Simulink. These elements make it an excellent starting point.

The vehicle is based on the forward-facing model structure, and the landmark of the vehicle model consists in the longitudinal dynamics' equations. A complete analysis of longitudinal dynamics can be found in [35,36].

A driving cycle represents the input to the whole model. As in [19,22,23], emission cycles are included in the model in order to simulate CO2 emissions on the same procedures that can be run on the vehicle test bench. This allows to have a baseline for the validation of the model. However, also real driving cycles acquired on road are introduced in the model and can be used for simulation purposes.

Accurate description of the possible choices that can be done with respect to the driver modeling is present in [37,38]. A proportional integral controller is here adopted to reproduce the longitudinal driver behavior, as in [29].

Vehicle resistances are based on two different solutions. At first, experimental data for the aerodynamic forces are introduced [36] and the vehicle resistances are completed through an experimental campaign on the vehicle test bench capable of quantifying the rolling resistance of the entire vehicle. Secondly, experimental data indicating the vehicle coast-down performance are adopted as in [26,39].

With respect to the powertrain, according to [29] the driver pedal command is directly linked to the engine torque as it indicates the percentage of the maximum available torque. However, in the current work data from the engine control unit (ECU) and from an experimental campaign on the engine test bench are introduced into the vehicle model. This allows to detach the direct link from the driver pedal command and the engine torque, making the subsequent development of hybrid vehicles easier.

A clutch model is introduced. [40] shows the complete analysis of an automotive clutch during engaging and disengaging, but the level of detail that is reached is not needed in the current work. So, the clutch is here modeled focusing only on the torque gap that takes place during disengagement, making the model simple and the simulations fast. The torque transmission chain is completed through the introduction of the gear ratios of the gearbox and the differentials.

Wheels and braking are modeled as in [29]. As a first approximation these models are simple but can be considered reliable. However, the braking model has been revised to fit the introduction of the regenerative braking function for hybrid control, making it possible to split the torque between mechanical braking and negative electrical torque.

The gear shift maps are updated with respect to [29], and the same is done for the fuel consumption maps. The software shown in [19,26,27,29] are all based on experimental maps for the computation of fuel consumption as the choice to work with a brake specific fuel consumption map is common and refers to the theoretical background shown in [4].

However, here the choice is revised according to [29] and a new map of indicated specific fuel consumption that is based on experimental campaigns on the engine test bench is computed. The oil temperature dependency is also considered: in [27] the thermal model of the engine is realized, while here a simpler configuration based on experimental data is considered, as in [29].

The modeling activity for the conventional vehicle is then concluded. The validation of the longitudinal dynamics model was run through experimental testing on the full vehicle. In order to validate the single components, specific experimental physical quantities were kept into account and used as input for the submodels. The simulated output results were then compared to experimental data. One of the main experimental activities that are run on the entire vehicle is represented by the chassis dynamometer testing, for example through emission cycles (New European Driving Cycle (NEDC), Federal Test Procedure (FTP)-75, Worldwide harmonized Light-duty vehicles Test Procedure (WLTP), …), or real driving. Experimental data from chassis dynamometer testing will be used as a comparison, in addition to experimental results from tests on specific components, if present.

The chassis dynamometer equipment allows to determine the total hydrocarbons (THC), carbon monoxide (CO), CO2 emissions and through regulations it is possible to calculate the fuel consumption (FC) for the given emission cycle (L/100km).

Since introducing further instrumentation on the vehicle represents a cost and would involve modifications to the vehicle, also ECU estimations will be used as a comparison with simulated data in addition to experimental results from tests on specific components, when present.

Electric components are introduced in the following chapters as the hybrid powertrain is explained. This represents the major contribution with respect to the previously analyzed works.

1.3. Model Structure

The longitudinal dynamics model adopted in this dissertation is composed of a driving cycle input, a proportional-integral (PI) controller (driver) acting as the accelerator and braking pedal, an engine model subsystem, a gearbox model, a tire model, and the longitudinal dynamics equations. In a second phase, the electric system is introduced.

The input is given from a speed cycle, function of time, and it can be chosen between the main emission cycles and some real experimental driving cycles. The actual speed is subtracted to the target speed and the error is introduced in the PI controller which simulates the driver's behavior. The output, acting as the requested pedal position, is the input for the vehicle subsystems and determines the vehicle performance, as shown in Figure 11.

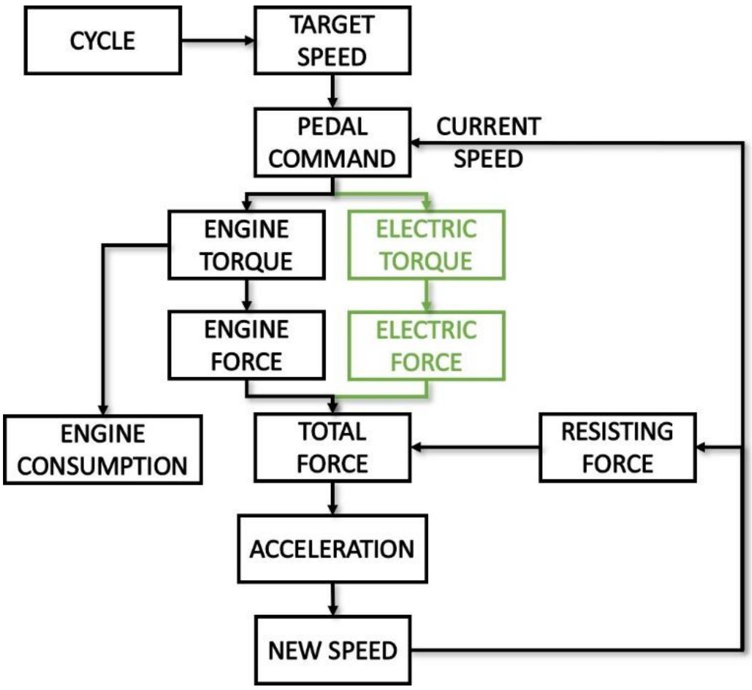

Figure 11. Longitudinal dynamics model structure.

Part of the vehicle components were modeled and validated, while others were directly based on experimental data (typically provided by suppliers), due to the trade-off between the simulation accuracy and the simulation speed. Once the model is validated, it represents a powerful tool for future hybrid architecture analysis and strategy development.

1.4. Vehicle Dynamics

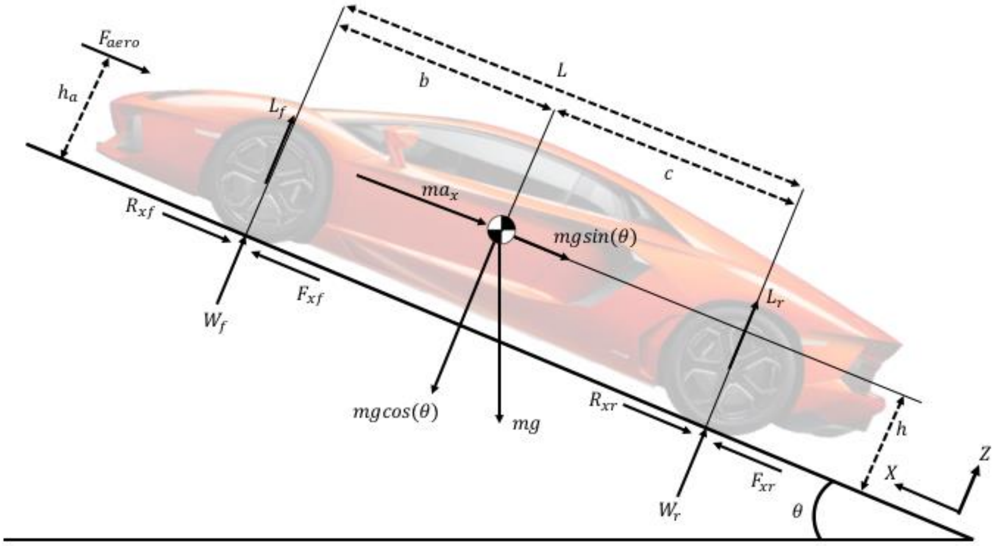

Figure 12. Vehicle Dynamics.

The longitudinal dynamics model is based on the equilibrium along the X and Z direction shown in Figure 12, in addition to the momentum equilibrium. In VII are reported the equations for the longitudinal dynamics:

$$F_{xf} + F_{xr} - m \cdot a_x = F_{aero} + R_{xf} + R_{xr} + m \cdot g \cdot sin(\theta)$$

VII

Solving VII, where $F_{xf} + F_{xr}$ express the longitudinal traction force for the front and rear wheels respectively, F_{aero} is the aerodynamic force, $R_{xf} + R_{xr}$ are the rolling resistances produced on each axle, the longitudinal acceleration can be determined and, by integration, the longitudinal speed. The target of the longitudinal dynamics model is the simulation of emissions cycles or real driving cycles for the chosen vehicle. The starting point is represented by the driving cycle choice, which takes place through an implemented pop-up menu that includes both emission driving cycles and real experimental driving cycles, obtained from testing on road.

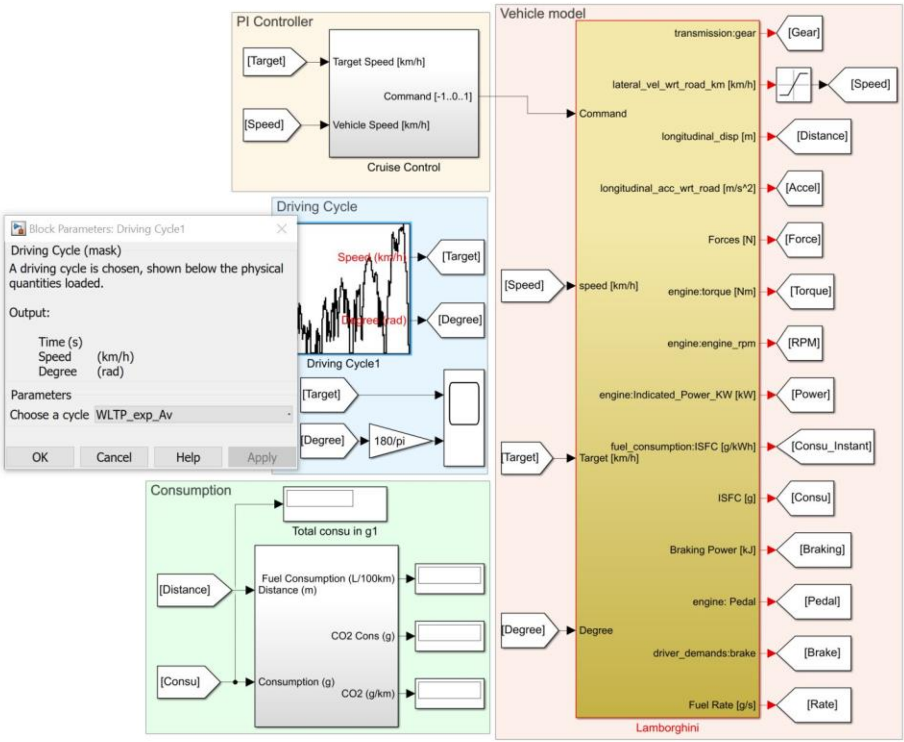

Figure 13. Longitudinal dynamics scheme.

The structure of the longitudinal dynamics model realized on MATLAB/Simulink is reported in Figure 13. The chosen driving cycle generates a target speed, a time-dependent quantity that is the input for the following submodels. The model focuses on the powertrain components. When possible, components are based on experimental black box models, guaranteeing low simulation time but less accuracy (especially for the dynamic behavior of the model), otherwise they would be physically modeled and experimentally validated.

1.5. PI Driver

The PI controller is based on a proportional component and an integral one, it takes as input the error between the target speed and the measured one. The proportional component depending on k_P reacts rapidly to the error variation, but it is not capable of cancelling the error. On the other side, the integral component k_I reacts slowly but can eventually nullify the error.

$$P(t) = k_P \cdot e(t) + k_I \cdot \int_0^t e(t) \cdot dt$$

VIII

The PI controller output is normalized between -1 and 1, representing three different cases:

- If it is positive, the car must accelerate to reach the target speed. This signal matches the accelerator driver pedal,
- If it is equal to zero, the target speed is reached,

- If it is negative, the vehicle must brake.

1.6. Vehicle Resistances

Vehicle resistances are due to aerodynamic forces and rolling resistances, and the first ones can be modeled as:

$$F_{aero} = \frac{1}{2}\rho C_x S v^2$$

IX

Where $\rho[\frac{kg}{m^3}]$ is the air density, v $[\frac{m}{s}]$ is the vehicle speed, keeping into account the direction and speed of the wind, C_x $[-]$ is the longitudinal drag coefficient and S $[m^2]$ is the frontal area. The last two parameters are determined through experimental tests, but they are not addressed here since the testing had already been done.

1.6.1. Rolling Resistance Model

The rolling resistance model has been identified from an experimental test campaign. The test had the aim to measure the force/torque moving both the wheels of the car and the gearbox shafts, with the clutch open. In this way, the losses of wheels and gearbox could be quantified.

The behavior of the vehicle on the chassis dynamometer was analyzed at different gearbox oil temperatures, different vehicle speeds and different gears since the losses depend on all these parameters. The clutch was kept open in order to avoid the resistant contribution of the engine. The results show that the power losses can be modeled as:

$$P = P_{2nd} + k \cdot \omega^n$$

X

Losses for the secondary gearbox shaft, P_{2nd}, depend on speed, oil type and temperature, presence of auxiliary elements. Losses for the primary gearbox shaft are modelled as $k \cdot \omega^n$, where k includes rolling resistances and contact frictions between gear wheels (dependent on torque, rotational speed, design, and gear ratio) and where ω^n is indicative of the dependency from speed (and gear ratio). n can be assumed equal to 2.

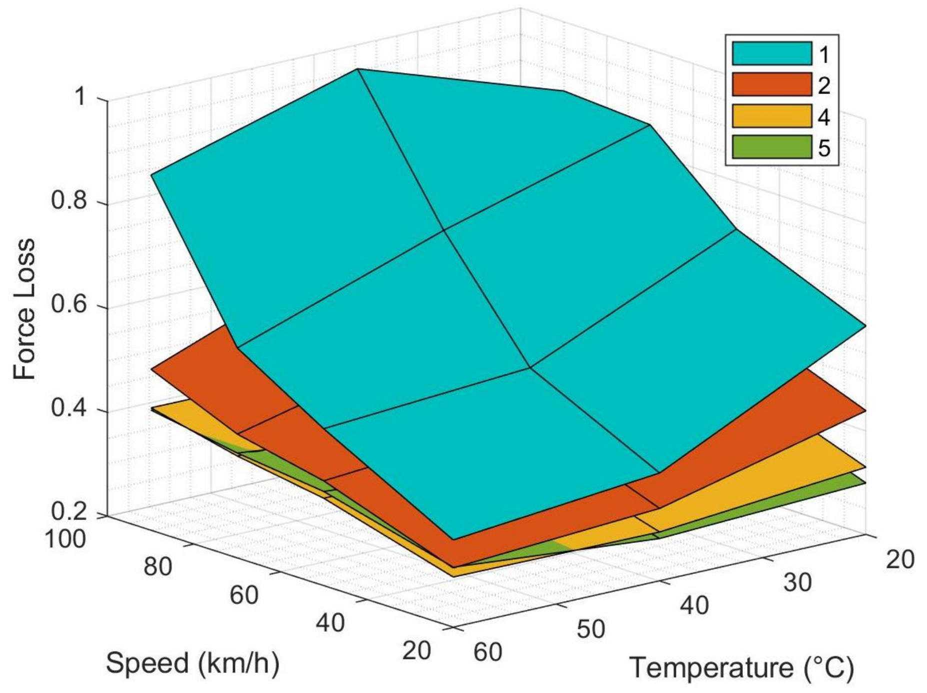

Figure 14. Normalized force loss determined through experimental testing.

Figure 14 shows the force loss variation at various gears engaged. The oil temperature dependency is linked with the oil viscosity variation. At low temperatures corresponds a high viscosity, that generates higher losses. On the other side, high speeds are associated with high rotational frictions and force losses. The choice of a higher gear allows to reduce the rotational speed of the primary gearbox shaft, with a resulting lower force loss.

1.6.2. Coast-Down Model

Vehicle resistances could be also based on experimental data. Vehicle tests have been run to determine the dependency of the resistant force with speed, according to the following coast-down equation:

$$F_{res} = F_0 + F_1 \cdot v + F_2 \cdot v^2$$

XI

Where $v[\frac{km}{h}]$ is the vehicle speed, F_0[N], $F_1[\frac{N}{km/h}]$ and $F_2[\frac{N}{(km/h)^2}]$ are the vehicle coast-down coefficients. According to this formula, the F_{res} already models the aerodynamics, rolling and all the vehicle resistances. This approach is easily implementable, but requires experimental testing on the specific vehicle, or on the most similar vehicle available. On the other side, data of this kind can be easily shared due to the ease of use of the model.

The choice to work with one method or the other depends on the specific situation, and on the availability of experimental data. In the following chapters, as vehicle configurations are introduced, it will be specified which method is used for the calculation of resistances.

1.7. Powertrain

The powertrain is composed of various parts, including the engine and all the elements that mechanically deliver the torque to the wheels. The vehicle model aims to reproduce faithfully the real behavior and is often based on experimental data to achieve simulation speed without losing accuracy. The ECU torque map from the real vehicle is introduced into the model. The driver pedal and the engine RPMs enter this map and identify the ICE torque request. The V12 spark ignition (SI) engine is modeled on data from an experimental campaign on the engine test bench, shown in Figure 15 for the engine fitted on a Lamborghini Aventador.

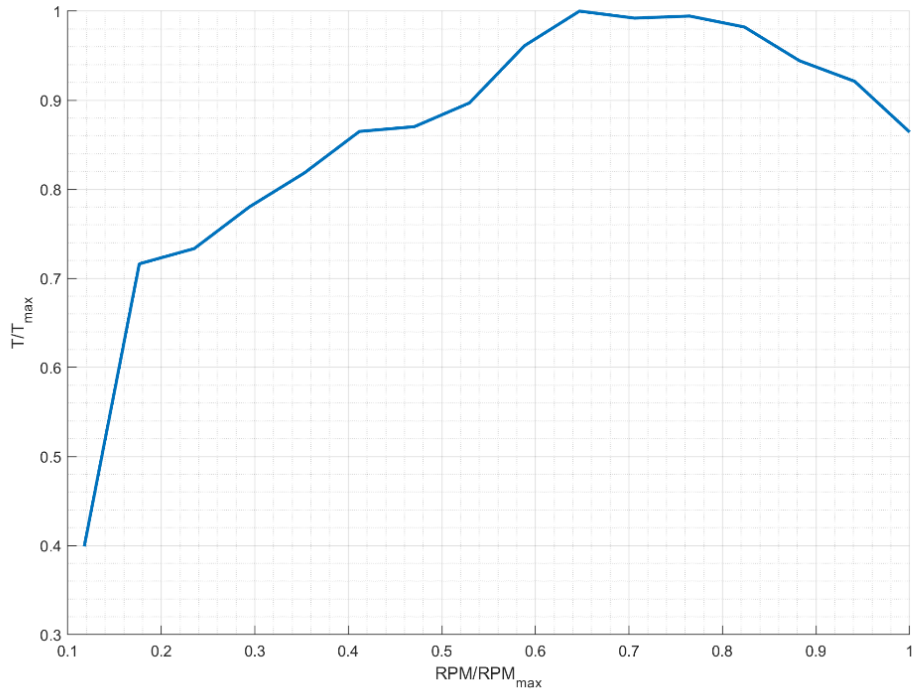

Figure 15. Engine torque curve for a Lamborghini Aventador.

The same experimental campaign has been carried out for the V12 engine fitted on the Lamborghini Aventador SVJ, and the curve can be found in Figure 16.

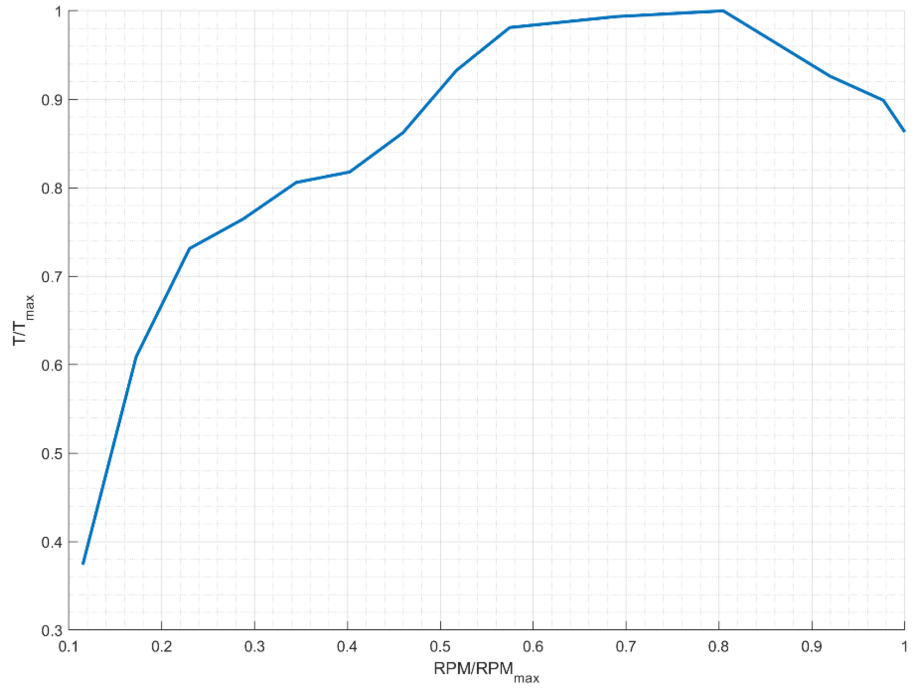

Figure 16. Engine torque curve for a Lamborghini Aventador SVJ.

In the following chapters, as vehicle configurations are introduced, it will be clarified which engine has been fitted on the model.

Once the torque request from the ECU map is known, it enters the V12 SI engine model and the actual torque from the ICE is computed. Engine frictions are computed according to [4,29] and their computation is needed to determine the actual engine torque and subsequently the engine consumption. In particular, the pumping and mechanical losses will be introduced in the model, in addition to an approximation of the losses due to external equipment. The reader is referred to [29] for the complete analysis of the calculation of the engine losses.

Oil temperature dependency is considered in the current model as it plays an important role on the global performance. Oil temperature impacts heavily on oil viscosity, as shown in Figure 17, generating great losses when the oil is cold. Typically, vehicles that run emission cycles start cold, so a warm-up phase is always present. The warm-up phase of emission cycles represents one of the most controversial intervals for fuel consumption analysis.

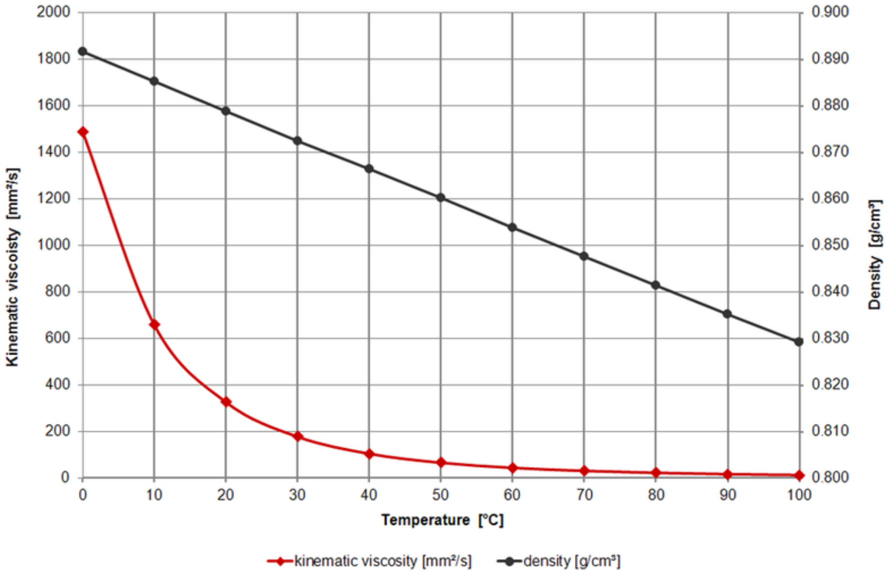

Figure 17. Oil viscosity 15W-40 from [41].

Depending on the cycle and on the oil characteristics, various temperature profiles are implemented in the model to accurately describe the oil behavior, as no model reproducing the oil heating is present in the simulation. The experimental values of the oil temperature are available for all the driving cycles that have been tested, also the real driving cycles on road.

In Figure 18, the temperature profile for a Worldwide harmonized Light-duty vehicles Test Cycle (WLTC) Class 3b is reported as an example, normalized with respect to the maximum temperature achieved during the cycle. It is evident that the oil starts cold in the first phase of the cycle.

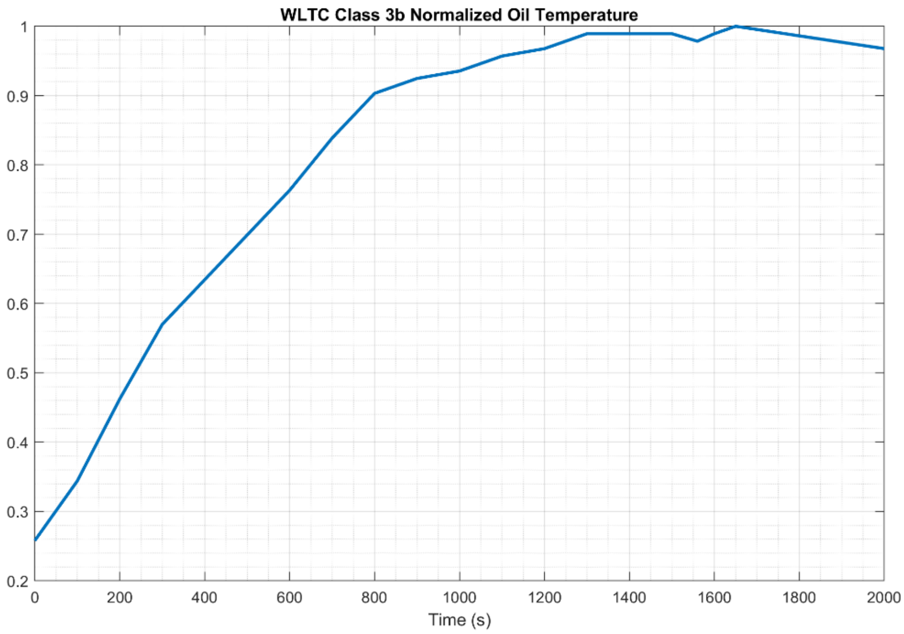

Figure 18. Oil temperature normalized curve.

The actual torque generated by the ICE is passed to the transmission and the gearbox shafts through a clutch. The clutch model is simple and simulates the torque gap during gear shifts by interrupting the torque transmission from the ICE to the primary gearbox shaft when the gear shifts, as the vehicle that is modeled is fitted with a single clutch transmission. The torque is then passed to the gearbox shafts and multiplied by the gear ratios, to the wheels. Hybrid powertrain components are not present in the conventional vehicle model and will be introduced in a second phase to reproduce the hybrid configuration.

1.8. Braking

The braking model is simplified as it is represented only by an imaginary force acting when the vehicle needs to decelerate. This is not impactful on fuel consumption as braking does not burn any fuel during the cycles and does not take part in the acceleration tests [29]. The braking force is determined as follows, m is the mass of the vehicle, g is the gravity force, mu is the friction coefficient and $P(t)$ is the PI driver braking request (if negative) from VIII.

$$F_{brake} = \frac{1}{2} \cdot m \cdot g \cdot mu \cdot P(t)$$

XII

However, the braking model acquires new importance when hybrid behavior is introduced. In fact, regenerative braking is one of the most important hybrid control functions for the reduction of fuel consumption. As the braking force required by the PI driver is computed, it will be split into the conventional mechanical braking and the regenerative braking. The regenerative braking request will be supplied by the EMs.

1.9. Wheels

The wheels participate in generating rolling resistance as friction occurs between the tire and the road. The biggest contribution to rolling resistance is due to the fact that materials are subject to deformation, especially tires. As wheels rotate, tires and road are deformed depending on their stiffness. On one side, the deformation of road is negligible, on the other side, the tire is made of elastic material and its deformation must be considered. The deformation of tires sees a flattening at the contact patch and a non-symmetric distribution of the load during the rotation of the tire. Therefore, the radius varies depending on where it is measured, and it is different from the unloaded radius. In order to find the proper value, an effective wheel radius model is introduced depending only on the tire structure, the speed and the radius of the unloaded wheel [29]:

$$R_e = k_0 r_w + k_1 v + k_2 v^2$$

XIII

The k_i coefficients match experimental data, r_w is the unloaded radius and v is the vehicle speed in $\frac{m}{s}$.

Another aspect of the tire modeling is related to the tire slip. Accurate formulation of the problem can be found in [36] and the most common model is the magic formula found in [42]. For the current model, the formulation proposed in [29] is adopted, as this allows to keep the overall model simple and fast. According to [29] the tire slip can be supposed dependent on the gear engaged, the model is acceptable in first approximation as the vehicle runs mainly emission cycles, where the acceleration is typically small.

Table 2. Slip and friction coefficients.

Gear [-]	1	2	3	4	5	6	7
Slip [%]	15	12	10	8	4	3	2
μ [-]	1.34	1.32	1.29	1.22	0.86	0.69	0.49

1.10. Gear Shift

The gear shift map implemented in the model is the same that is fitted on the real vehicle. The speed target at which the gear is shifted is defined through the actual gear and the pedal value. A map indicating the upper threshold and one indicating the lower threshold are introduced in the vehicle model. When the actual speed of the vehicle goes over or under the threshold, a gear shift takes place, the clutch opens and closes, and the gear ratio values are updated.

In Figure 19 the gear upshift thresholds are shown. If we supposed to be on an accelerating vehicle starting from null speed with a pedal constantly equal to 50%, we would be moving horizontally from the left axis of the graph to the right as the speed increases, and we would see a gear shift every time we meet one of the curves, starting from first gear up to the seventh gear.

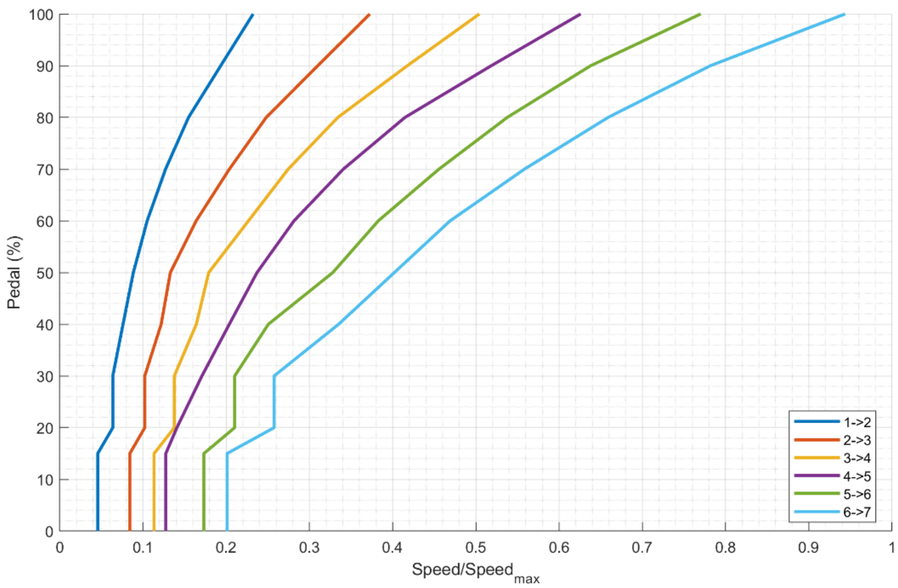

Figure 19. Upshift map.

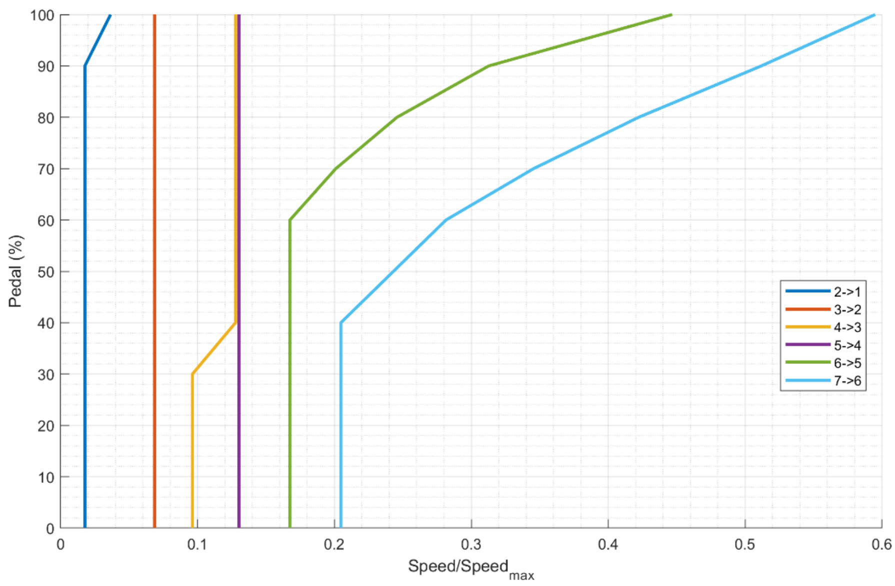

Figure 20. Downshift map.

In Figure 20 the gear downshift thresholds are shown. According to this graph, if we were on a decelerating vehicle moving at high speed with a pedal equal to 50%, we would be moving horizontally from the right of the graph to the left. Every time we meet a curve, we would be shifting down a gear starting from the seventh gear to the first one.

1.11. Fuel Consumption

The fuel consumption is computed thanks to maps based on experimental data. The ICE working point is determined, and the map indicates the fuel consumption in $\frac{g}{kWh}$ associated with that working point. By multiplying with the total power expressed by the ICE and integrating in time, fuel consumption is determined. The fuel consumption map has great importance in the longitudinal dynamics vehicle model as simulations will be run on emission cycles to determine the overall fuel consumption of the vehicle.

The most common way to compute the fuel consumption is to use a Brake Specific Fuel Consumption (BSFC) map determined from the test bench, but this kind of formulation carries some problems, especially if it is used on a vehicle model running an emission cycle, as explained in [29,43]. First of all, the BSFC map cannot take into account the cold oil frictions, making it difficult to properly compute fuel consumption during the first phases of the cycle. Moreover, when computing BSFC, the denominator considers the torque value going to the wheels and this makes situations with open clutch flawed. Another thing that needs to be kept into account is that when testing super sport cars that produce very high torque values, test benches become inaccurate in measuring low torques. This makes the BSFC inaccurate when torque becomes low, which is exactly where emission cycles make the vehicle work.

The formulation in XIV from [29,43] is then adopted, and values for engine idling are extrapolated. $ISFC$ is the Indicated Specific Fuel Consumption, $BMEP$ is the Brake Mean Effective Pressure, $IMEP$ is the Indicated Mean Effective Pressure.

$$ISFC = \frac{BMEP}{IMEP} BSFC$$

XIV

This map is still defined in $\frac{g}{kWh}$, but differently from before it is based on $IMEP$. This is possible thanks to the computation of the engine losses that allows to determine the $IMEP$ value, keeping into account the oil temperature dependency.

1.12. Model Validation

The whole model validation is based on data determined through a WLTC Class 3b. Experimental physical quantities are chosen as inputs and the simulation is run. The resulting simulated outputs are compared to the experimental data available, that are represented by the estimations of the ECU and the measurements run on the chassis dynamometer. During the first analysis, the validation process is run on the model of a conventional Lamborghini Aventador, with no hybrid components. The model simulation is run taking the target speed of a WLTC Class 3b as input.

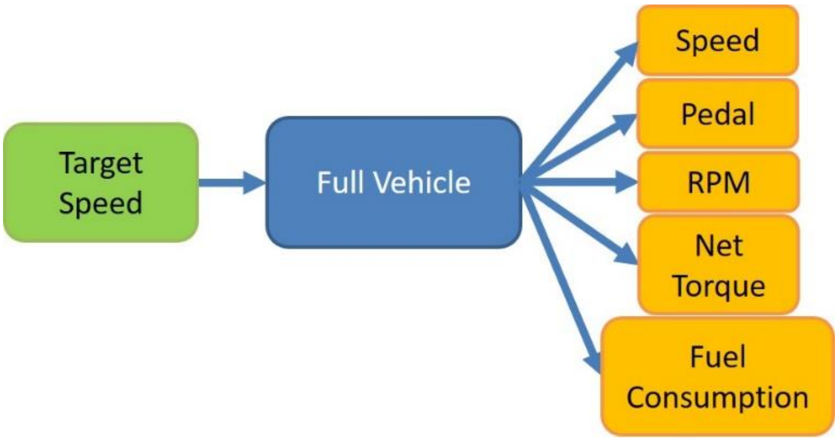

Figure 21. Complete vehicle and driver simulation.

The 'Full Vehicle' model comprehends all the submodels that have been introduced until now and the PI driver.

Table 3. WLTC Class 3b simulated fuel consumption, conventional vehicle.

	Phase 1	Phase 2	Phase 3	Phase 4	Combined
Simulated %	100	56	44	43	53
1. Error %	+3,4	-6,5	-2,8	-5,5	-2,6
2. Error %	+2,6	-1,0	+2,0	-1,6	+0,3

The WLTC Class 3b phases are defined as follows [44] and the cycle is shown in Figure 22:

- Phase 1: 0s – 589s
- Phase 2: 590s – 1023s
- Phase 3: 1024s – 1478s

- Phase 4: 1479s – 1800s

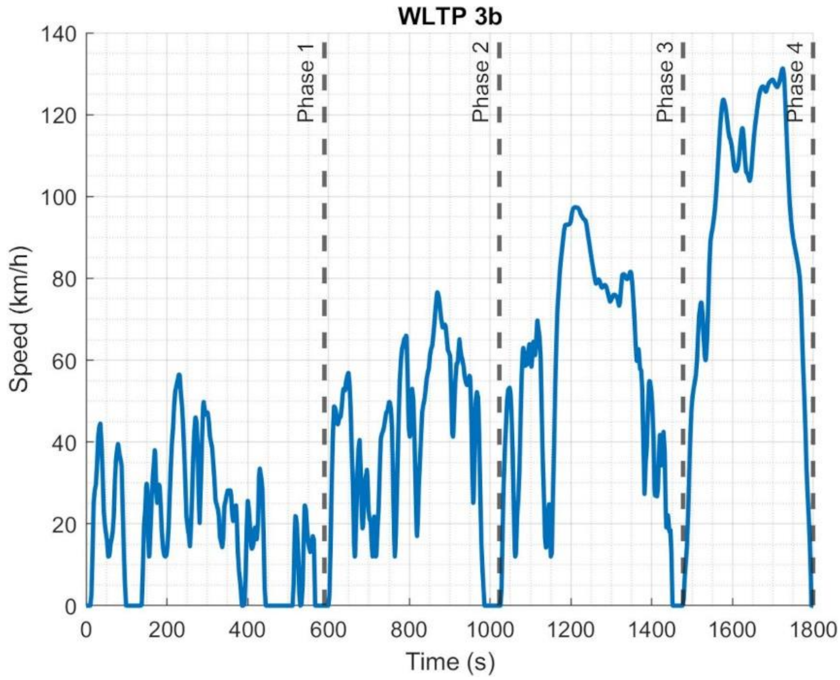

Figure 22. WLTC Class 3b.

The results in Table 3 are normalized with respect to the maximum simulated fuel consumption value obtained during the various phases. The simulated values are compared with two different experimental tests and the error is reported (%).

The fuel consumption evaluation is based on the ISFC experimental map, linearly interpolated. The simulated fuel consumption will be used as an element of comparison for different strategy configurations when introducing the hybrid components.

The results in Table 3 show that the model accuracy is generally within ±5%, and at the same time they clearly highlight the great variability associated with the real driver's behavior, which is particularly influent during rapid accelerations and decelerations. In fact, even a small driver pedal difference can result in a great torque (and, consequently, fuel consumption) difference, since super sport cars are characterized by a wide torque range.

This variation has a strong impact on the vehicle performance [45]. Different drivers on the same vehicle (or the same driver on the same cycle but during separate moments of the day) can produce significantly different fuel consumption results due to different driving styles. A variation in the accelerator pedal value is linked with a different torque request value and, eventually, with a different emission value as it can be seen in [46,47]. The idea of a PI tuning is not applicable, in fact we could fit the behavior of a single driver in a defined moment, but not the behavior of all the drivers in every moment. Then the decision is to not modify the PI.

2. Hybrid Powertrains

The current chapter illustrates the various solutions that were adopted to realize a hybrid super sport car model.

2.1. Literature Review

As explained in the Introduction, the automotive market is now in the middle of a transition; the need to reduce fuel consumption is evident, and the adoption of hybrid electric powertrains is considered one of the most promising solutions.

In [5,14] a complete analysis of various hybrid architectures is proposed, while [11] focuses on a parallel hybrid architecture pointing out the results that can be reached deepening the study of the hybrid control strategies. [13,15] introduce hybrid architectures with a focus on the modeling and control activities.

The super sport cars' market is not exempt from the electrical transformation and various companies have already announced they want to reach the target of an hybrid electric fleet [48–50]. However, the super sport cars' market shows necessities that are different from the ones typically associated with the passenger cars' market and a baseline, or standard technology is still far from being set. Due to this, proper tools are needed to support the electrification process as various solutions should be deepened.

The first hybrid electric vehicle that is analyzed is a Lamborghini Aventador. The Lamborghini Aventador series gearbox is an Independent Shift Rod gearbox with a single clutch belonging to the Automated Manual Transmission family and during gear shifts, as all the single clutch gearbox do, it generates a torque gap. A gear shift is a fast process, lasting approximately 0.2 s in STRADA mode (the vehicle setting commonly used during city drive), but can have a strong impact on the passengers' comfort.

Nowadays, various technologies are available to improve this behavior. Dual clutch transmissions enable smooth gear changes with almost no torque interruption, allowing to reach faster accelerations and lower fuel consumption. Lamborghini's first dual-clutch transmission is available in the Lamborghini Huracán, named "Doppia Frizione" (meaning 'Dual Clutch') [51].

Other solutions are linked with torque fill strategies. For example, a hybrid system could be introduced as seen in [52], where a parallel HEV solution is proposed. Another solution is registered by Ford Global Technologies, where a solution for torque filling through a hybrid powertrain is proposed [53]. Both solutions are based on the usage of batteries as energy storage systems.

The innovative solution provided by Lamborghini is based on a 48V EM connected to the wheels in P3 position for performance and comfort enhancement, especially at low loads and speeds. The P3 configuration introduces an EM directly coupled to the gearbox secondary shaft, thanks to a dedicated coupling/decoupling system. Thanks to this parallel hybrid configuration, the electrical torque can be delivered directly to the rear wheels and power the vehicle.

To guarantee the right traction force in fast transients like the gear shifts, it is necessary for the energy storage system to be characterized by high power values. Typically, common batteries guarantee high energy values (meaning a high electric range in automotive applications) but cannot guarantee high power performance, so they work well at supplying low and steady loads but are inefficient at high charge/discharge rates that impose severe stress and reduce the battery life span. [5,11,12,15,16] focus on the various types of batteries existing at the time and that are commonly adopted in the automotive market.

On the other side, capacitors are characterized by a long cycle life and high-power density but have the great disadvantage of a low energy density as shown in [5,12]. In [54–56] innovative solutions related to the materials for anode and cathode of the capacitors are reported. The adoption of innovative materials could lead to an enlargement in energy and power density of the system.

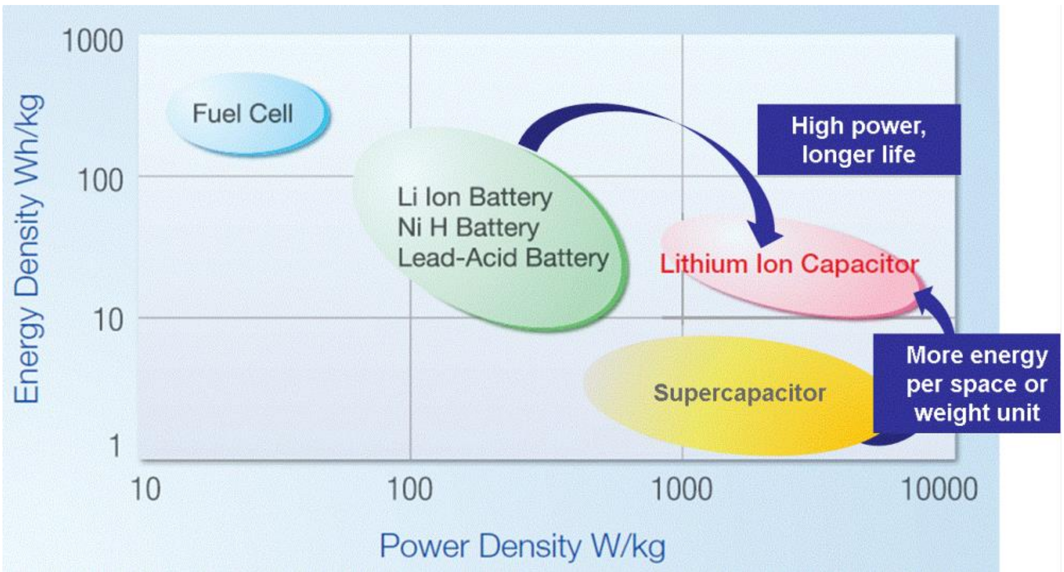

Figure 23. Ragone plot of various energy storage systems [57].

As shown in Figure 23, the Ragone plot illustrates how different energy storage technologies relate one to another. It is evident that capacitors are associated with higher power density values and lower energy density values with respect to batteries. LiCs represent a hybrid solution that achieves higher energy density values than common capacitors, reaching approximately $5 - 13\,\frac{Wh}{kg}$ [57], while Li-Ion batteries typically reach $100 - 250\,\frac{Wh}{kg}$ [58].

As initially explained in Introduction, LiCs are derived from EDLC [5], they combine the activated Carbon cathode of an EDLC with the Li-doped Carbon anode of Lithium-Ion Batteries, to guarantee both power and energy.

In common automotive applications, they are adopted only for few operations, like Start&Stop [59], and, since it is considered difficult to use capacitors alone as an energy storage reservoir [5,60], they may be used as auxiliaries in combination with other energy storage systems (Lithium-Ion Batteries, Fuel Cells, …) [61–63]. The hybrid energy storage systems allow to decouple the specific energy and specific power requirements, and while the capacitors cover the power request, the main battery-based energy storage system can be optimized for the energy request and cycle life.

Li-Ion Batteries usually are introduced as energy storage reservoir and they are more commonly installed in hybrid electric vehicles and electric vehicles due to the high energy content that they can provide [64]. Typically, common batteries guarantee high energy values (meaning a high electric range in automotive applications) but cannot guarantee high power performance [5,65]. Lithium-Ion Batteries are commonly modeled as in [15,16], by choosing the level of complexity that is needed.

Various capacitors model configurations exist and reproduce accurately the behavior. For example, Zubieta and Bonert model [66] shows a complex configuration, working with 8 different parameters and increasing the number of circuit branches. This configuration is capable to reproduce a wide range of phenomena.

Capacitors and batteries could also be combined in series or parallel configuration as explained in Introduction to generate a single storage system, called Hybrid Energy Storage System, or HESS. With respect to this, various configurations exist [5] and the research on this topic has been increasing in the last years [67–70].

A series connection between batteries and capacitors would lead to a high-voltage system where the single cells are run by the same current. In that case, the current and power would be limited by the battery in charge and discharge, making the presence of capacitors useless.

On the other side, a parallel connection would allow to maintain the same voltage across batteries and capacitors, while the current would be split between the two different packs of cells. Hypothetically, this would allow to run a higher current on the capacitors while respecting the limits of the battery. To this aim, the capacitors could be sized to cover high power requests, while the batteries could be sized to cover the energy request.

The parallel configuration between batteries and capacitors is defined also ‘passive’ configuration. This is the simplest hybrid configuration that can be designed.

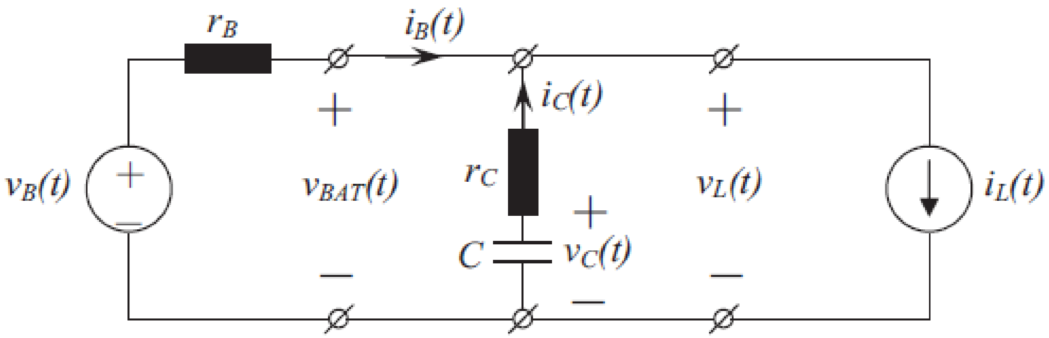

Figure 24. Passive hybrid topology [71].

In Figure 24 a passive hybrid topology is shown. On the left there is the battery with a terminal voltage $v_{BAT}(t)$, internal voltage $v_B(t)$, internal resistance r_B and a current $i_B(t)$. The battery is connected in parallel with a capacitor characterized by an internal voltage $v_C(t)$, a capacitance C, an internal resistance r_C and a current $i_C(t)$. On the right it is present the load with a terminal voltage $v_L(t)$ and a current $i_L(t)$.

The introduction of DC-DC converters to interface the capacitors and the battery could lead to higher reliability and control flexibility, optimizing the power sharing regarding efficiency. In this case, HESS could guarantee higher performance since capacitors could provide most of the entire pulse load while batteries provide the average and constant part of the load [70,72,73].

When a DC-DC converter is introduced to interface capacitors and batteries with a parallel connection, the configuration is called ‘active’ or ‘semi-active’. In active and semi-active topology, one or more DC-DC converters are used to control the flow of current to and from the system components. A fully active configuration is one where two DC-DC converters are introduced to interface batteries and capacitors, the reader is referred to [71] for a complete analysis of these configurations. On the other side, a semi-active configuration is one where only one DC-DC converter is used. The alternatives are explained also in [71,74]. The nomenclature of Figure 24 is maintained in the following semi-active configurations:

- Parallel semi-active hybrid, Figure 25: the converter is between the load and the power sources, $i_S(t)$ is the current supplied by the battery-ultracapacitor branch and $\eta_{DC-DC,L}$ is the efficiency of the converter,

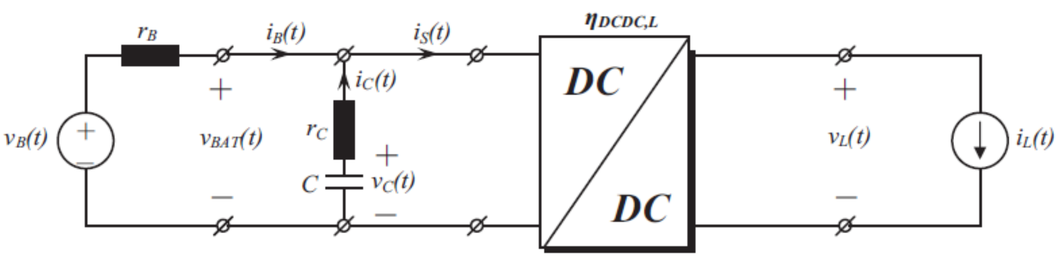

Figure 25. Parallel semi-active hybrid topology [71].

- Battery semi-active hybrid, Figure 26: the converter is between the battery and the load, connecting the capacitor directly to the load side, $\eta_{DC-DC,BAT}$ is the efficiency of the converter, and $i_{L,AVE}(t)$ is the current flowing from the battery branch.

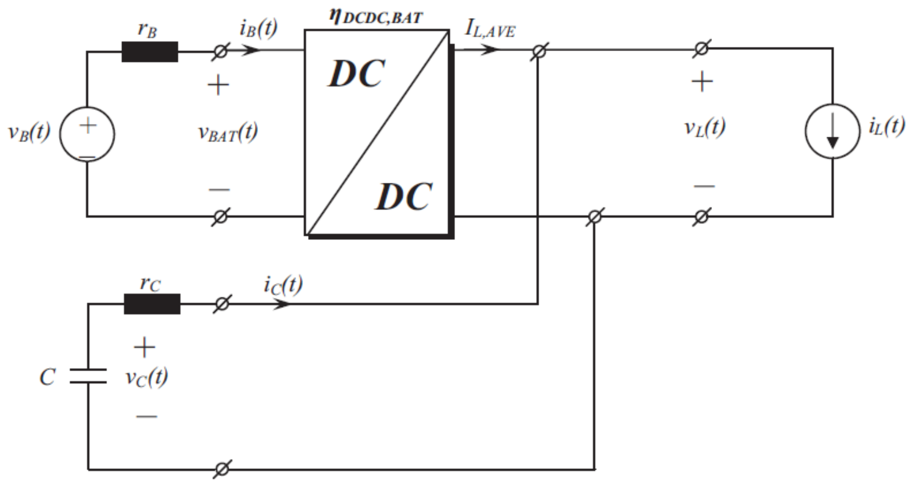

Figure 26. Battery semi-active hybrid topology [71].

- Capacitor semi-active hybrid, Figure 27: the converter is between the capacitor and the load, with the battery directly connected with the load, $\eta_{DC-DC,UC}$ is the efficiency of the converter, $i_{L,DYN}(t)$ is the current flowing from the capacitor branch and $v_{UC}(t)$ is the capacitor nominal voltage.

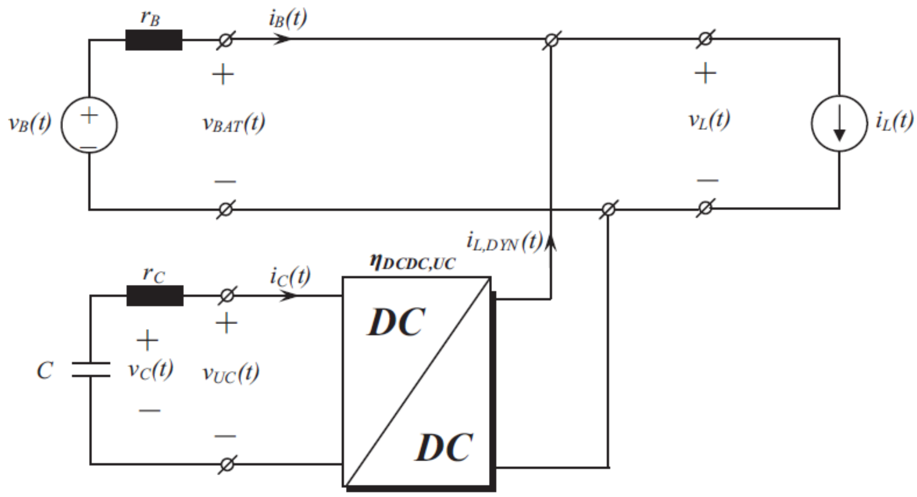

Figure 27. Capacitor semi-active hybrid topology [71].

In [70], a comparison between active parallel and series configurations is carried out. It is shown that active hybrids that use two DC-DC converters in series solve problems for capacitors but have a lower global efficiency and they need to add a full-rating DC-DC converter. On the other side, a parallel configuration has other advantages. It solves problems for battery and capacitors but introduces one DC-DC converter rated at average power and one rated at maximum power bringing complexity, control effort and additional losses.

[69] shows that active configurations can guarantee good results for cost saving, since small size capacitors are linked to low costs for power electronics. Still, energy losses in DC-DC converters are usually the main part of the total HESS energy losses [75]. On the other side, a passive parallel configuration allows to work with less electronics and control circuitry, reducing the overall energy, and power density [70,76]. A configuration of this kind cannot be

actively controlled. Moreover, it limits the usable energy of the capacitors, as their voltage must be equal to the battery's terminal one, reducing the system flexibility.

As explained in [77], the topology of passive HESS is simple, and saving one or two high-power DC-DC converters will save significant cost for the EV or HEV system. Furthermore, passive HESS performance can be easily improved by choosing capacitors with larger capacitance and smaller internal resistance as it is also shown in [74,78,79]. With the fast development of the capacitor's technology in industry, optimizing the battery and capacitor parameters of passive HESS is a feasible way to improve HESS performance. More importantly, simulation research has been done in [78] showing that passive HESS has a higher energy efficiency than active HESS. For the above reasons, passive HESS still has a great application potential in EVs and HEVs.

The various configurations have their own advantages and disadvantages. As described in [71], the passive hybrid is the simplest and cheapest technology, the fully active hybrid gives the best performance, compromising cost and simplicity, and the semi-active hybrid is a trade-off between performance and the circuit complexity and price.

The work done in [12,74] shows how the modeling of a DC/DC converter could be carried out, while the indications in [71] lead to a simpler model that is preferred for our application. Also, [80] explains how fixed ratio DC-DC converters can lower power dissipation, cut costs, and save size, while [81] shows how fixed ratio DC-DCs can be optimized for high efficiency, and it illustrates some specific applications. In [82] fixed-ratio DC-DCs are adopted to satisfy the need for high power and high efficiency systems. So, the introduction of a fixed ratio DC-DC could guarantee comparable performance, saving complexity. The presence of the DC-DC converter allows to control the system guaranteeing high flexibility.

In recent years, researchers have explored various EMSs for the HESSs, which can be divided in online and offline strategies [14,83,84]. The online strategies can be easily implemented in real-world controllers, but generally do not achieve optimal results. In comparison, offline strategies can achieve a globally optimal performance, but they cannot be introduced in real-time applications due to the long computational time, high memory resources requirement, and complete knowledge of the driving conditions [85].

Some common techniques reported in literature for designing an online EMS include rule-based [86], fuzzy logic [87,88], filtering [87]. [75,89] show a way to control the DC/DC converter with an online strategy aiming to a real-time oriented application.

Offline techniques as dynamic programming can be used as a benchmark for optimal performance as in [90]. Other optimization-based EMSs are related to the use of neural networks-based algorithms [91,92] or reinforcement learning [93,94]. To cover the gap between offline optimization and online application, also model predictive control-based strategies could be introduced as in [95]. The current document focuses on real-time oriented models, that must be compatible with the implementation in the control unit on the real car. This makes rule-based and, more in general, online strategies fit for our application.

The hybrid powertrains need to be completed with the introduction of EMs, in particular [5,15] propose a complete analysis of their proper functioning, while [16] proposes a map based approach.

2.2. Research Project Contribution

The current research project starts from the study of an experimentally validated super sport car model and introduces hybrid components to modify the model, making it possible to power the wheels both through the ICE and the EMs, as shown in Figure 2 and Figure 5. The introduction of a hybrid powertrain makes the super sport car's model a powerful concept tool for the vehicle development.

The first vehicle that has been modeled is a Lamborghini Aventador, based on the considerations introduced in 1. The vehicle has been experimentally tested on the chassis dynamometer to determine the rolling resistances, so the rolling resistance model from 1.6.1 has been adopted in the simulations. The conventional Lamborghini Aventador is an all-wheel drive car.

The first target of the research project is to improve the behavior of the conventional vehicle during gear shifts. As in [52,53], a torque fill strategy based on a hybrid powertrain is chosen, but differently from common electric hybrid powertrains, LiCs are introduced in the system to guarantee the required power at the right time due to their characteristics. This solution follows the electrification path but also targets a comfort and performance improvement of the conventional vehicle.

The innovative aspect of the hybrid configuration is represented by the usage of LiCs as the main energy storage system, a high-power density system that differs from the typical energy storage systems adopted on passenger cars.

The work done in [5,66] is taken into account for the LiC modeling. Capacitors are studied in detail, and an experimental campaign on industrial capacitors leads the modeling activity as the choice to work with a simple resistance-capacitor model is justified.

With respect to this first vehicle configuration a single EM is introduced in P3 position, and it has been modeled through a map-based approach as in [16]. The maps are provided by the suppliers of the EM, and they will work with torque request, RPMs, and voltage as inputs, while the output will be a current request to the LiCs' model. This will be explained more in detail in the following chapters.

The second vehicle that has been modeled is a Lamborghini Aventador SVJ. The vehicle is very similar to the previous one, in any case some elements need to be updated, like the engine map and the resistances. In fact, the coast-down model is chosen for this kind of vehicle since no specific tests have been carried out on the resistances in the manner of 1.6.1, while experimental data from coast-down testing are available. The conventional Lamborghini Aventador SVJ is an all-wheel drive car, as the Lamborghini Aventador.

The hybrid powertrain is here enriched by another EM, making the vehicle model more complex. The presence of multiple EMs allows to increase the degree of hybridization and to increase the functionalities of the vehicle. Moreover, it is possible to change the position of the EMs with respect to the rest of the powertrain exploring a variety of possible configurations and analyzing their impact on the vehicle's performance. The configurations that will be explored are P3-P4 and P2-P4.

The focus of this second activity is more related to the hybrid powertrain control strategies. At first, the control strategy model is based on a Rule Based Strategy (RBS), which will target lower fuel consumption results through control rules. Afterwards, an Equivalent Consumption Minimization Strategy (ECMS) is implemented [11,14,16].

The validated model has then been used to develop control strategies aimed at increasing comfort and performance, but also to expand the hybrid system capabilities by widening the LiC working range, and to study the possibility of implementing CO_2 reduction-oriented control functions. These topics are explained in detail in the section Control Strategies.

As this second configuration takes into account various EMs, the positioning introduced in [15] and Figure 5 is adopted. P3-P4 and P2-P4 configurations have in fact been considered.

The energy storage system continues to be a uniquely LiC-based one and the current work aims to explore the capabilities of the hybrid vehicle, by targeting not only performance and comfort, but also fuel economy.

The EMs that are introduced on the second vehicle are different from the EM introduced in P3 position in the first vehicle configuration. So, the EMs' maps are updated with data coming from an experimental campaign run by the suppliers. The output of these maps will be a power request to the LiCs' model. As the input of the LiCs' model changes, the LiCs' model itself is modified to fit the new requirement. The modeling activity is based on [19].

The innovative choice to focus on capacitors instead of batteries is due to the nature of the vehicle that is studied. The research project is in fact based on the study of a super sport car that because of its characteristics has high demands of power as well as energy. Therefore, it is decided to deepen the possibilities offered by storage systems that aim mainly at high power density, bearing in mind the need to improve their energy potential [54–56]. This choice is particularly suited for performance but requires efforts on the system's control to target fuel economy.

Following this path, the third configuration that is analyzed maintains the second vehicle configuration that has been previously studied but focuses on the improvements achievable through modifications on the energy storage system. Instead of working with a single energy storage system (LiCs or batteries), the possibility to combine both in a single system is explored. The activity starting point is the work presented in [74].

At first, a Lithium-Ion Battery is modeled according to [16]. The modeling activity is based on experimental data and the model is validated.

A passive HESS configuration is studied, and its theoretical behavior is deepened as in [74,79]. The system could significantly level the peak current of the batteries and reduce the battery voltage drop, consisting of a simple solution to be introduced on a vehicle. The analysis guarantees a complete understanding of the system's behavior and can serve as the basis for the evaluation of new concepts.

Later, the passive HESS is introduced in the complete vehicle model for a P2-P4 configuration, to power a hybrid powertrain and analyze its performance on a WLTC Class 3b. The control strategies that are chosen to power the vehicle are an RBS and an ECMS.

Then, a semi-active configuration is modeled as it guarantees greater control and flexibility. This solution allows to fully use the capacitors' energy and to actively control the system. The DC-DC converter could be modeled according to the work done in [12,74], but that level of accuracy is not needed at this point of the work. So, the indications in [71] are followed and a simpler system is modeled.

The DC-DC converter control is based on the work done in [75,89], where the average power load is determined and sent to the battery, while the peak power request is satisfied by the LiCs. This allows to achieve a nearly constant battery current, to guarantee performance improving.

At last, a fixed ratio DC-DC will be introduced. As it will be explained in the following chapters, the control strategy for this converter aims to maintain the battery terminal voltage equal to the load voltage. This should guarantee comparable performance, saving complexity. [80] explains how fixed ratio DC-DC can lower power dissipation, cut costs, and save size. Later, the semi-active HESS is introduced into the complete vehicle model, and it is simulated on a WLTC Class 3b.

Both the control strategies are modeled with MATLAB/Simulink, and they are eventually simulated on the full vehicle model. The simulations' results are compared with the ones obtained for a conventional vehicle and the ones obtained for a hybrid vehicle whose energy storage system is based only on capacitors.

This allows to understand the benefits of the hybrid storage system with respect to a conventional powertrain or a hybrid powertrain with an energy storage exclusively based on capacitors.

At last, the semi-active configuration is tested for performance. In particular, a HESS is specifically designed to achieve full energy recuperation during a 200-0 km/h braking and then the hybrid powertrain is tested for a 0-200 km/h acceleration.

The analysis brings interesting considerations as the combined system is introduced into the vehicle model and its impact on emission cycles can be studied. HESS have been studied in small scale applications [74] or in limited configurations [79], but in our case, the work is directly run on a large scale by combining the single systems in a configuration that reaches a voltage high enough to be fitted on a real super sport car. This way, the impact on the vehicle's performance and fuel economy can be determined.

2.3. First Configuration, single EM LiC-based

The EM is introduced in P3 position with the main target to provide torque to the wheels during the gear shifts. This feature could mainly guarantee performance and comfort enhancement, especially at low loads and speeds as it can be seen in Figure 28, where a comparison between the traction force of a conventional Aventador and the hybrid configuration is evaluated. The net electric traction force value that is shown in Figure 28, indicates the force that can be given to the wheels by the EM. This solution reduces the gap between single clutch transmissions and Dual Clutch Transmission.

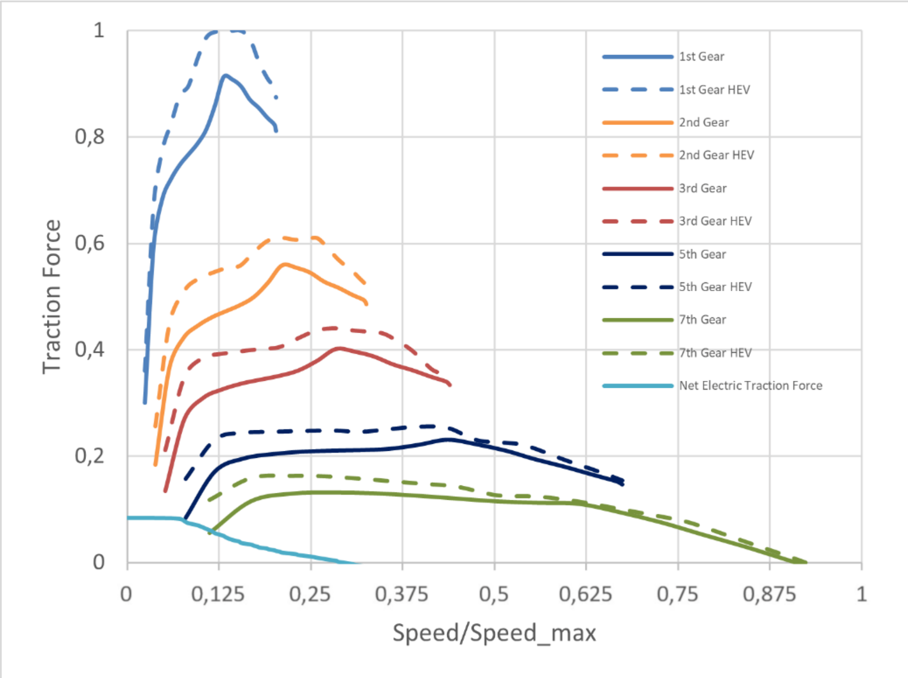

Figure 28. Normalized traction force diagram for Lamborghini Aventador with various gears inserted.

Figure 28 shows with continuous curves the traction force that is given to the wheels by the ICE at various gears inserted. The dotted curves, on the other side, are given by the sum of the continuous lines and the electric contribution.

The EM that is fitted on this vehicle is a traction machine working at 48V, so the energy storage system is dimensioned to work at the same rated voltage. To this aim, the LiC cells which compose the energy accumulation system are arranged in a 14s2p configuration, connected to the EM.

As explained in the Introduction, the 14 cells in series allow to achieve the rated voltage of 48V, as the voltage of the pack is the sum of the single cell voltages in series. On the other side, the decision to work with a 2 parallel configuration allows to increase the capacitance of the pack while reducing the equivalent resistance. This leads to lower energy losses due to heating.

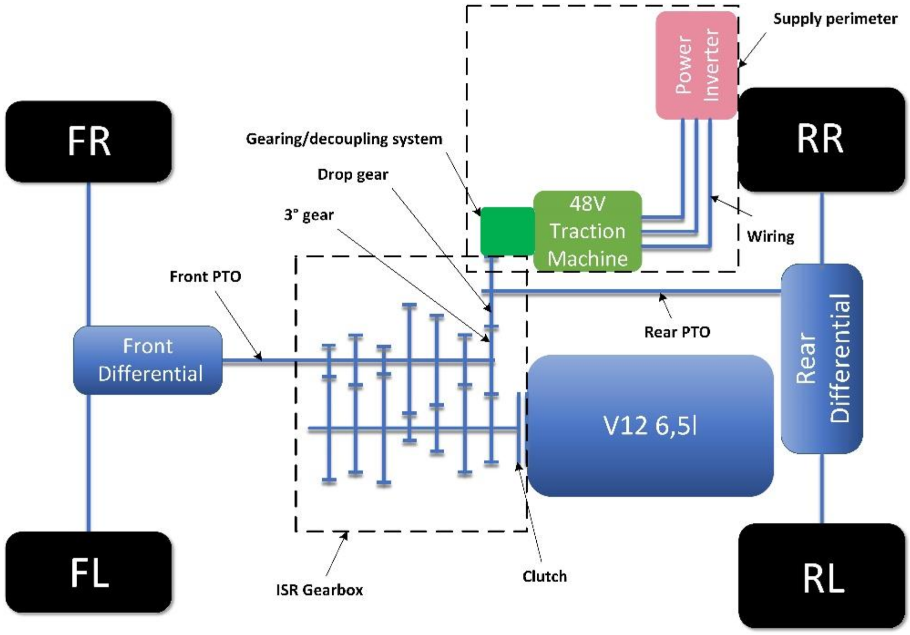

Figure 29. Hybrid powertrain configuration with single EM.

Moreover, a control strategy with a comfort and performance target is introduced in the model. The control strategy is the same introduced on the real vehicle, so every modification can be immediately tested on the road. With the introduction of a control strategy, the LiCs' energy can be managed in the best way, to also respect the technology voltage limits. Moreover, a good energy management can guarantee the chance to make a proper use of the technology, activating, for example, functions as energy recuperation or boost.

The hybrid strategy can activate the EM with four main functions and is further analyzed later to evaluate their impact on the hybrid performance and on fuel economy through simulation comparisons:

- Torque fill, during upshifts,
- Recuperation, if the SoC is too low,
- Electric Boost, in kickdown (accelerator pedal completely pressed) conditions,
- Creeping Function, capable of moving the car at low speeds in full electric if first or reverse gear are engaged.

Fuel economy improvements are not easy to obtain with this kind of application, in fact, the vehicle is characterized by a V12 engine, with a very large displacement that implies high CO2 and fuel consumption values, as all super sport cars do. Moreover, both the hybrid P3 architecture and the LiC energy source have been designed to fulfill comfort and performance targets, rather than fuel economy reduction.

The main components of the electric hybrid system are the EM, the Inverter and the LiC accumulation system. These components have been modeled and integrated into the Simulink model, as shown in the following paragraphs.

2.3.1. EM

The EM and Inverter models are based on experimental results provided by the suppliers, as a single black-box model. The EM's map has torque request, rotational speed, and pack voltage as inputs, while the current request is the output.

The torque request comes from the hybrid control strategy, and it depends on the control functions that are activated. In particular, for the first vehicle configuration the torque request will mainly come from the covering of the torque gap during gear shifts and from energy recuperation during braking.

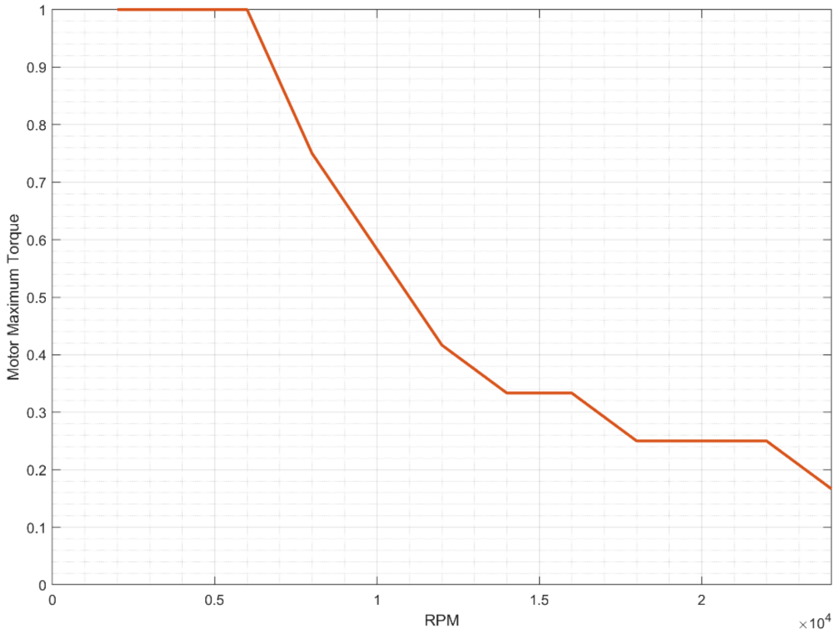

Figure 30. Electric motor maximum torque with respect to motor speed.

The EM is a permanent magnet EM, with a maximum power of 25 kW and a maximum speed of 24000 RPM, designed to provide a better performance during acceleration and gear shifting. The choice of the EM is also linked to the fulfillment of the stringent dimensional constraints.

2.3.2. Lithium-Ion Capacitor Model

In Figure 31, a first approach to the description of the LiC behavior is shown.

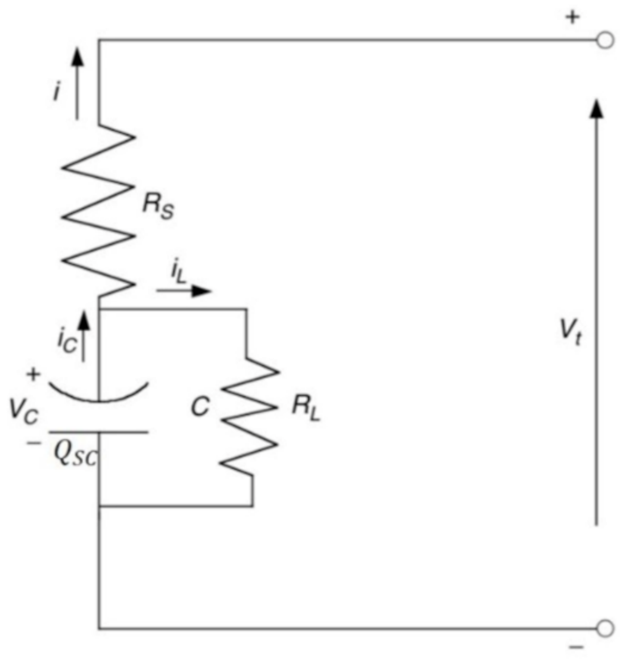

Figure 31. Lithium-Ion capacitor scheme.

The scheme is simple, representing only a series resistance R_s and a capacitance C. The leakage resistance R_L is added to describe in greater detail the operation of the component but could be omitted without losing too much in accuracy. In actual operation, in fact, the leakage current is usually very small [5].

According to Figure 31 the terminal voltage V_t is:

$$V_t = V_c - i \cdot R_s$$

XV

V_c is the internal voltage and i is the flowing current.

Taking into account some basic knowledge on capacitors [5], if C is the capacitance, i_l is the leaking current and R_L is the leakage resistance, the following relationships hold:

$$\frac{\mathrm{d}V_c}{\mathrm{dt}} = -\frac{i_l + i}{C}$$

XVI

$$i_l = \frac{V_c}{R_L}$$

XVII

$$\frac{\mathrm{d}V_c}{\mathrm{dt}} = -\frac{V_c}{C \cdot R_L} - \frac{i}{C}$$

XVIII

Figure 32 shows the model of LiC that has been integrated in the vehicle model, where the current request [A] coming from the EM is the input and the terminal voltage [V] is the output.

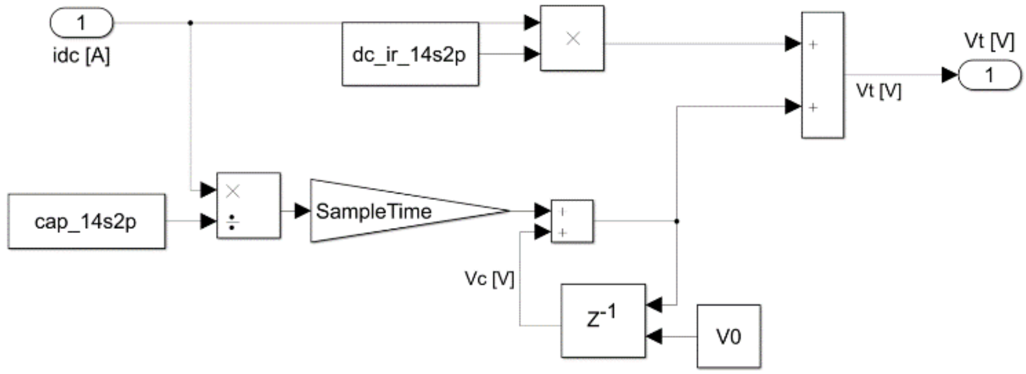

Figure 32. Lithium-Ion capacitor model.

Some state parameters that will be later used to describe the capacitor, are the state of charge (SoC) and the stored energy. The SoC [%] of a pack of capacitors at terminal voltage V_t, minimum voltage V_{min}, maximum voltage V_{max}, is equal to:

$$SoC = \left(\frac{{V_t}^2 - {V_{min}}^2}{{V_{max}}^2 - {V_{min}}^2} \right) \cdot 100$$

XIX

The energy stored E_{cap} $[J]$ for a capacitor of capacitance C, minimum voltage V_{min}, internal voltage V_c, is equal to:

$$E_{cap} = \frac{1}{2} \cdot C \cdot ({V_c}^2 - {V_{min}}^2)$$

XX

Differently from our Resistor-Capacitor (RC) scheme, the configuration adopted in [66] is instead made of three main capacitance terms, that refer respectively to fast, medium, and slow transients, where the medium and long transients' effects can be noticed over respectively 100 s and 1200 s at null current.

To better understand whether the initial scheme of Figure 31 needed to be further developed, a detailed analysis of industrial capacitors from different suppliers has been carried out, since those are the ones used on the vehicle. The various capacitance values have been calculated according to Zubieta and Bonert model [66] and it has been observed that, for industrial capacitors, the term linked to fast transients has the highest values, as it can be seen in Figure 33.

In particular, the fast, medium, and slow capacitance values for two different industrial capacitors have been divided by the corresponding total capacitance. The percentage value for the medium and slow terms is negligible if compared to the fast term.

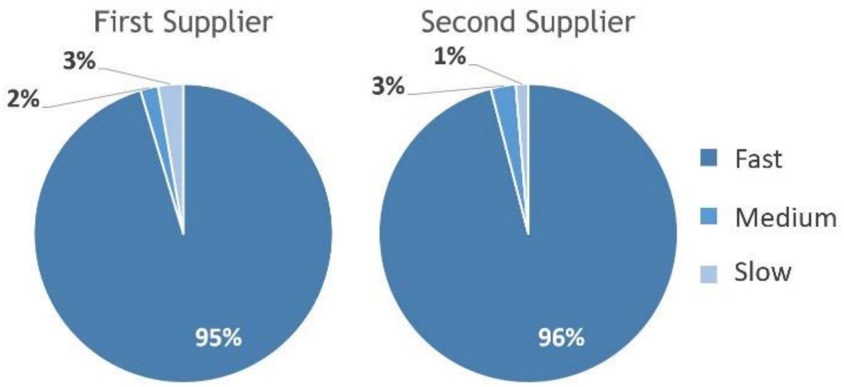

Figure 33. Comparison between two different industrial capacitors.

Moreover, for road applications on HEVs, there is always a power request that varies frequently. So, the LiCs will be almost always kept active, charging, or discharging. For this reason, effects associated with medium and slow transients are not visible since they would require a long resting time of the capacitor at null current. Due to these motivations, these terms are negligible and the choice to work with a single RC circuit branch is justified. The validation is run through experimental data from a road test. Hereafter the procedure is shown.

Figure 34. LiC model validation starting from experimental current.

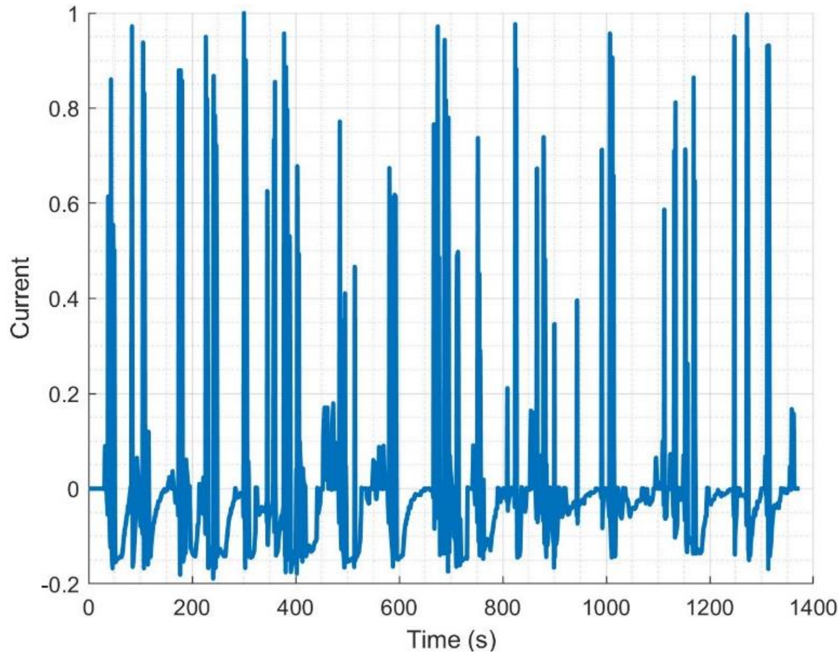

Figure 35. Normalized experimental current profile.

The voltage comparison is shown in Figure 36.

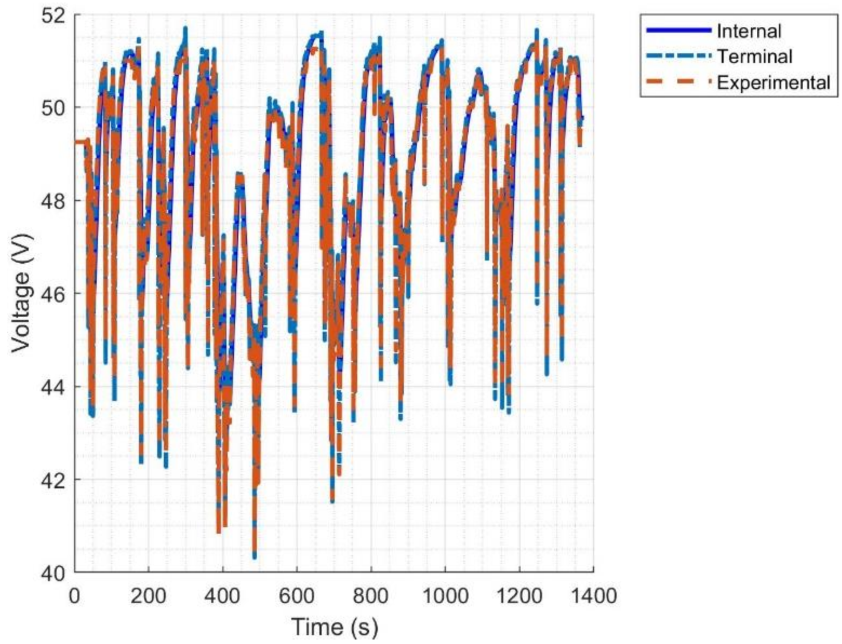

Figure 36. Experimental and simulated voltage comparison.

The graph shows that the simulated voltage trend is close to the experimental one, with a root mean square error of 0.2 V. The results obtained show that the LiC model is reliable.

2.4. Second Configuration, 2 EMs LiC-based

Secondly, a concept for a Lamborghini Aventador SVJ with two EMs is analyzed and implemented in the simulation environment. The EMs parallel configurations that are analyzed are represented by the P3–P4 and P2-P4 positions, as shown in Figure 37. The P4 EM is placed at the front axle, while the rear EM (P2 or P3) is directly coupled with the gearbox. In both cases, the hybrid system can directly power the wheels if requested. For every EM, a proper transmission ratio was designed that could fit the desired speed range.

Figure 37 shows the EMs that are mechanically connected to the shafts. The gear ratios will be dimensioned to keep the motors connected until certain target speeds. The P4 front EM will be disengaged at 190km/h, while the rear EMs will disengage at the vehicle's maximum speed, approximately equal to 350km/h. Thus, they will be able to cover the complete speed range of the vehicle.

As shown in Figure 37, the resulting hybrid Lamborghini Aventador SVJ will be a 4-wheel drive (4WD) vehicle where the front wheels are powered exclusively through the P4 EM that is mechanically connected to the front axle.

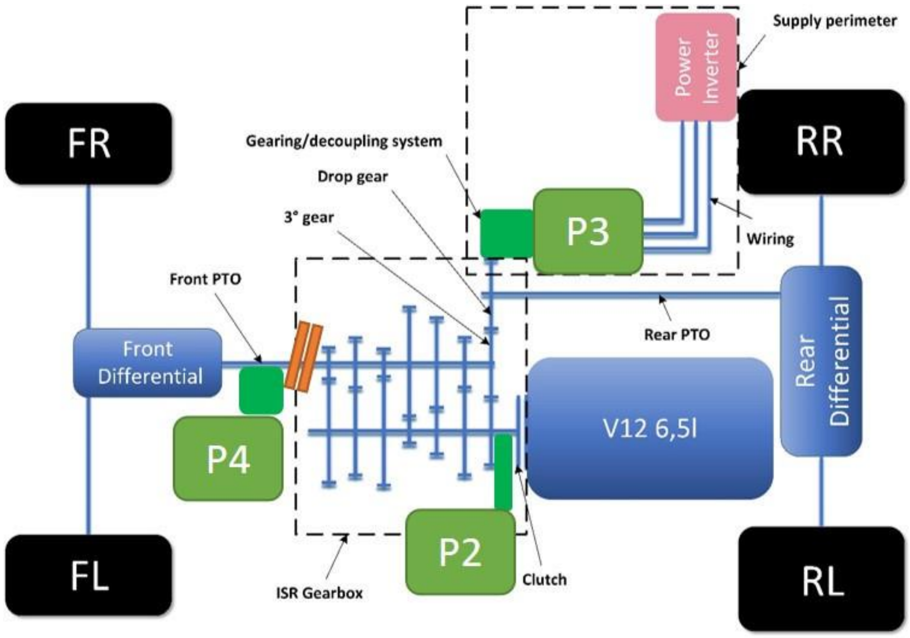

Figure 37. Hybrid powertrain with multiple EMs.

The energy storage system that is evaluated is uniquely based on LiCs. This concept focuses on fuel economy optimization specifically designed for a LiC-based energy storage system, as a new strategy is modeled to take the benefits of the system's characteristics. The application is innovative also for the kind of functions implemented that are usually satisfied through high energy systems [8–10], while in this study, they are destined to a lower energy content system.

As we pointed out before, fuel economy is not easy to improve with this kind of application. In fact, the vehicle is characterized by a V12 engine [96], with a large displacement and high CO2 emissions and fuel consumption values, as all super sport cars do.

The EMs account for a power and torque that are strongly inferior to the one expressed by the ICE (approximately 15%). Consequently, their impact on the performance and on fuel economy is expected to be small, and the percentage of improvements on fuel economy are expected to be quite low. Various hybrid powertrain configurations will be analyzed, and the simulated results will be reported as a comparison between the conventional vehicle and the hybrid configurations.

With the introduction of a control strategy, the electric energy can be managed in the best way to guarantee fuel economy. Moreover, a control strategy is required to respect the technology voltage limits. Also, energy management can guarantee the proper use of the available technology, activating control functions such as energy recuperation or boost.

The masses of the hybrid components will be added in the simulation, and the LiC-based hybrid vehicle is considered to weigh 57kg more than the conventional one.

2.4.1. Transmission Ratios

The EMs mechanical connections are dimensioned with reference to the maximum admissible speed established in the project design phase. As already mentioned, the transmission ratios are dimensioned to guarantee front electric traction and recuperation until 190km/h, when the front EM in P4 position is detached. On the other hand, the P2–P3 EMs will be detached at maximum speed, and they will be able to power the rear wheels over the complete speed vehicle range. These target speed values are compared to the maximum EM speed, equal to 24,000 RPM, and the transmission ratio are determined (Table 4).

Table 4. Transmission ratios for EM connections.

Configuration	Transmission Ratio
Front P4	4.8
Rear P3	3.2
Rear P2	2.84

Since the P2 configuration is positioned at the primary gearbox shaft, the transmission ratio value will be determined keeping into account the gearbox gear ratios. The chosen value will guarantee an EM speed below 24,000 RPM for any inserted gear.

2.4.2. EMs

The EMs models are based on experimental maps that keep into account the contribution of the single EM and the inverter associated with it. Their contribution is described by black-box models based on the results of experimental campaigns run by the suppliers. The two EMs that are introduced in the second vehicle configuration are the same as each other.

The EMs' maps have torque request, rotational speed, and pack voltage as inputs, while the power request is the output. The torque request comes from the hybrid control strategy, and it depends on the control functions that are activated. In particular, for the second vehicle configuration the torque request will mainly come from an electric traction request and from energy recuperation during braking.

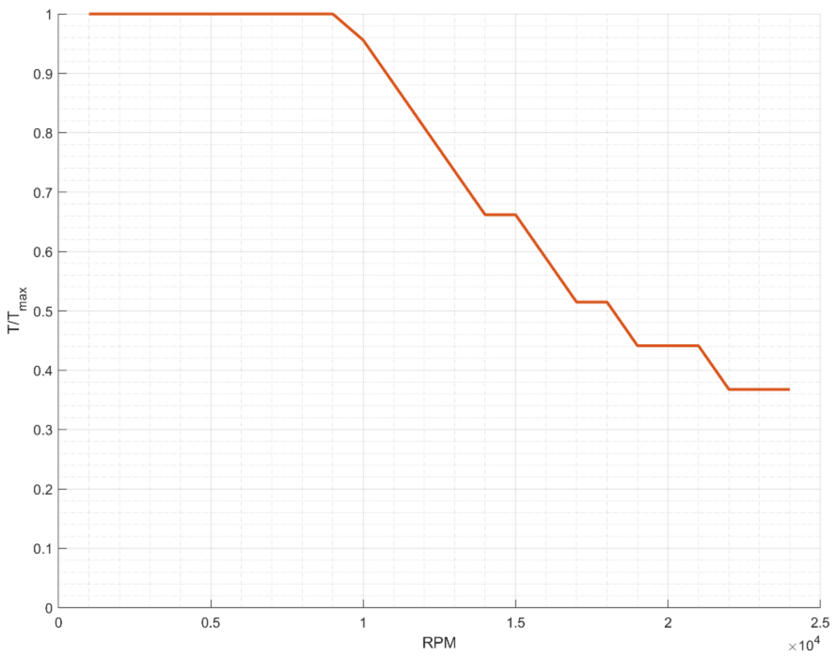

Figure 38. Electric motor maximum torque with respect to motor speed.

All the EMs are assumed to be identical. Every EM guarantees a maximum torque of 68 Nm and a maximum power of 65 kW. The EMs can run up to 24,000 RPM.

2.4.3. Lithium-Ion Capacitor Model

Differently from the first configuration, the EMs here will output a power request instead of a current's one. So, the LiC model is adapted to have a power input instead of a current input. The scheme that is taken into account is the same seen in Figure 31. The scheme is simple, representing only a series resistance R_s and a capacitance C [5]. As already explained, the leakage resistance R_L allows to describe a more detailed model but could be omitted without losing too much in accuracy. Defining Q_{SC} the charge stored within the LiC, and C the capacitance, the voltage V_c can be calculated as follows:

$$V_c = \frac{Q_{SC}}{C}$$

XXI

According to Kirchhoff's rule, the terminal power is given by:

$$P = i \cdot (R_s \cdot i + \frac{Q_{SC}}{C})$$

XXII

Thus, the current i can be determined as [14]:

$$i = \frac{-\frac{Q_{SC}}{C} + \sqrt{\left(\frac{Q_{SC}}{C}\right)^2 + 4 \cdot P \cdot R_s}}{2 \cdot R_s}$$

Figure 39 shows the model of LiC that has been integrated in the vehicle model, where the power [W] is the input and the terminal voltage [V] and the current flow [A] are the outputs.

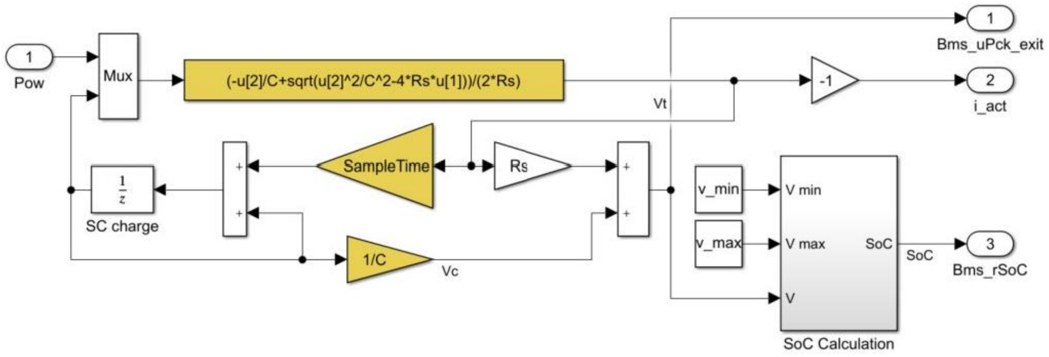

Figure 39. Lithium-Ion capacitor model.

As already explained, the LiC model could be more complicated and detailed, reproducing a wider range of phenomena, but that level of detail is not strictly needed for automotive control-oriented applications. Moreover, the choice to work with a single RC circuit branch was justified before.

Eventually, the model that is described in Figure 39 is based on the same scheme and equations of the model from Figure 32. Therefore, the model is considered reliable due to the validation of the model that was made in Figure 35 and Figure 36.

The two EMs fitted on the vehicle express a maximum power of 130 kW. The LiCs are dimensioned to reach that power value, and that is possible thanks to a 60s1p (60 series cells and 1 parallel string) configuration that stores 0.26 kWh.

The working voltage of the LiCs' pack spans from a minimum voltage of 132 V to a maximum voltage of 228 V, depending on the SoC of the capacitor. As it has been explained in the Introduction, the voltage of the pack is the sum of the single cells' voltages in series configuration.

2.5. Third Configuration, 2 EMs HESS-based

The third configuration that has been analyzed is still based on a Lamborghini Aventador SVJ, with the introduction of two EMs in P2-P4 position and the introduction of a HESS. When speaking of hybrid electric vehicles, the electrical energy source often consists of a chemical battery (for example lithium-ion based), or, as we have seen, capacitors.

The current chapter analyzes the possibility to hybridize the electrical energy source, by combining batteries and capacitors. As shown in Figure 23, the Ragone plot illustrates how different energy storage technologies relate one to another. The idea that is explored is the design of a HESS capable of combining two different technologies to enhance the strengths and peculiarities, while compensating for the disadvantages of the single systems.

A HESS made of a Lithium-Ion Batteries and LiCs is chosen, where the battery can cover the average power request and the capacitors can cover the peak power request. This leads to a system smaller in weight and size than if the battery or the LiCs alone were the energy storage [5]. This chapter analyzes the possibility to implement a passive or semi-active HESS on an already existing longitudinal dynamics vehicle model to evaluate the powertrain's performance.

The vehicle model that is now adopted is the same of the second vehicle configuration but considering only the EMs in P2-P4 configuration. Differently from the previous studies, the main contribution of this work is represented by the deepening on the energy storage systems. The fuel economy optimization will be one of the assessment parameters and the vehicle model will serve as the basis of the activity.

2.5.1. Lithium-Ion Capacitor Model

The LiC model is based on the ones introduced and validated in 2.3.2. The scheme is made of a series resistance and a capacitance, making the model simple but accurate enough to reproduce the real behavior, as shown in Figure 40.

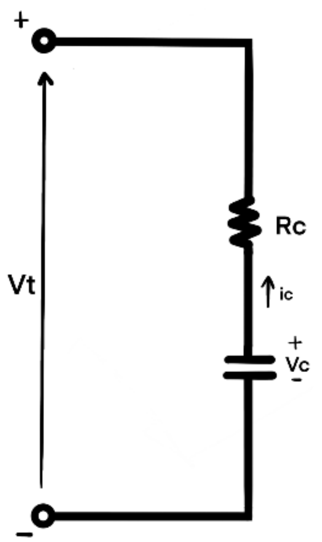

Figure 40. Lithium- Ion capacitor simplified scheme.

Because of the same reasoning done in 2.4.3, the model reproduces the behavior of a 60s1p (60 series and 1 parallel string) that stores 0.26 kWh and could reach over 130 kW of power, satisfying the power request of the EMs. The working voltage spans from 132 V to 228 V.

2.5.2. Lithium-Ion Battery Model

The Li-Ion Battery model is a double polarization (DP) [16] model, made of two RC branches and an internal resistance, as shown in Figure 41.

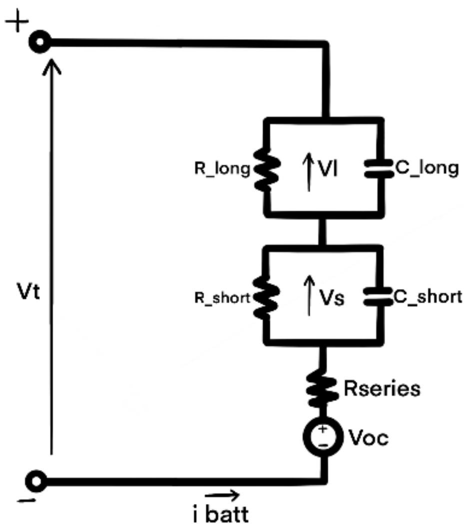

Figure 41. Battery model scheme.

The decision to work with a DP battery model allows to accurately describe the charge/discharge phenomena. The first RC branch is associated with short transients, while the second one is associated with long transients.

The following equations describe the control-oriented battery model, where V_{batt} is the voltage at the battery terminals, I_{batt} is the current flowing through the battery, V_{OC} represents the Open Circuit Voltage, while the R_{series} term indicates the equivalent series resistance and reproduces the sudden effects of a current variation. V_S and V_L respectively indicate the short and long transient voltages, and R_{short}, C_{short}, R_{long}, C_{long} refer to their resistance and capacitance:

$$V_t = V_{OC} - R_{series} \cdot I_{batt} - V_S - V_L$$

XXIV

$$\frac{dV_s}{dt} = -\frac{V_s}{R_{short} \cdot C_{short}} + \frac{I_{batt}}{C_{short}}$$

XXV

$$\frac{dV_L}{dt} = -\frac{V_L}{R_{long} \cdot C_{long}} + \frac{I_{batt}}{C_{long}}$$

XXVI

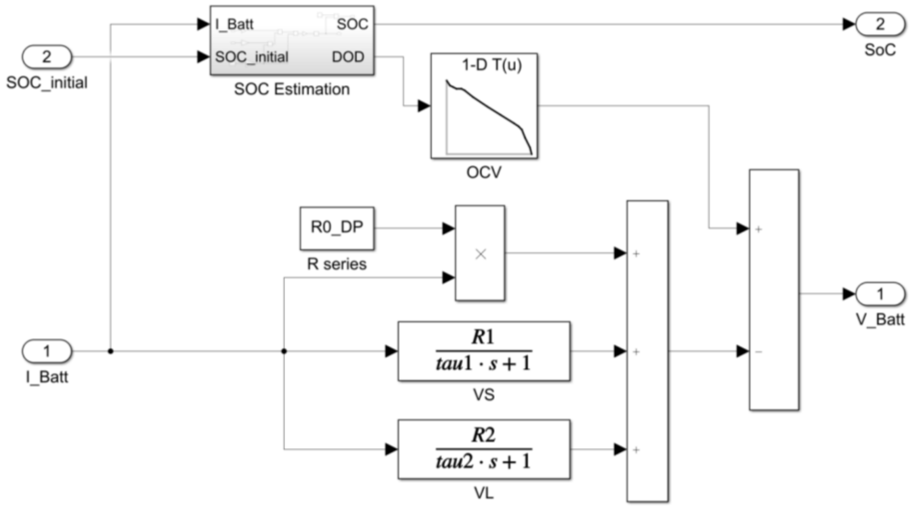

Figure 42. Battery Simulink model.

The state parameters of the battery are the capacity and the SoC. The capacity of a battery is the amount of electric charge that the battery can store, it depends on the discharge conditions because of the chemical reactions happening within the cells.

For a battery pack characterized by a nominal capacity C $[Ah]$ and starting from SoC_0, the SoC can be calculated as follows at a generic instant t, where i is the current flowing in the pack:

$$SoC = SoC_0 - \frac{\int_0^t idt}{C} \cdot 100$$

XXVII

The energy stored in the battery E_{batt} $[kWh]$ can be calculated at a generic instant if the nominal capacity C, the voltage V_{OC} and the SoC are known:

$$E_{batt} = SoC \cdot C \cdot V_{OC}$$

XXVIII

The battery cell has been modeled starting from the experimental testing of a 21700-battery cell (Molicel, INR-21700-P42A) [97].

The battery cell has been experimentally tested through a Pulsed Discharge Test (PDT), shown in Figure 43, to determine its main parameters. The PDT performs the discharge of the battery with discontinuous current, allowing rest time at the end of the current steps (current goes back to 0 A). The rest time is needed to reproduce the cell “relaxation” [98,99] and to study the battery behavior during transients.

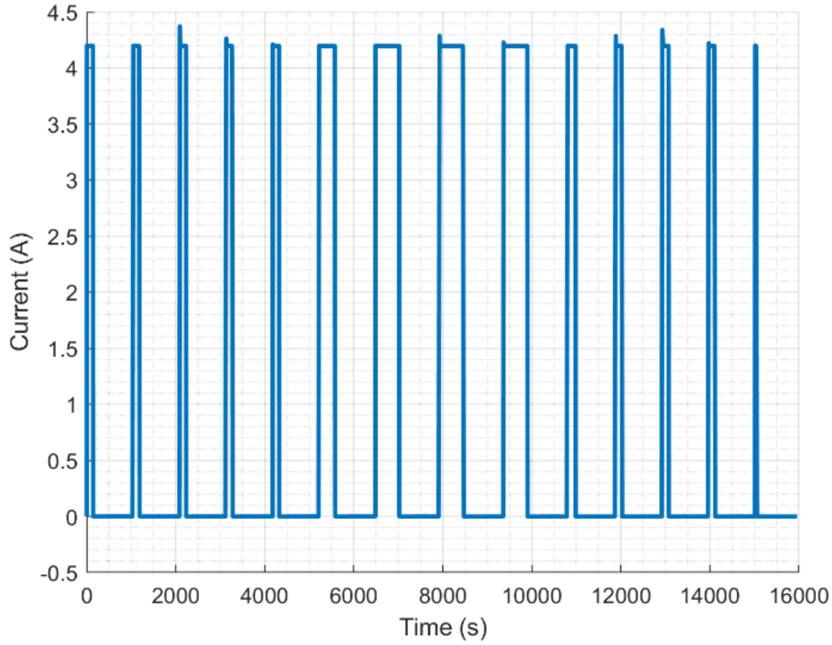

Figure 43. PDT current profile.

The experimental tests take the PDT current shown in Figure 43 as an input and measure the battery voltage variations, that are then reported in Figure 44 under the label 'Experimental'. The study of the voltage profile of the battery allows to determine the parameters needed to complete the battery model, as in [99]. Once the parameters are known and the battery model is complete, it is tested by running a simulation with the current input of Figure 43. This simulation leads to a terminal battery voltage that is reported in Figure 44 under the label 'Simulated'.

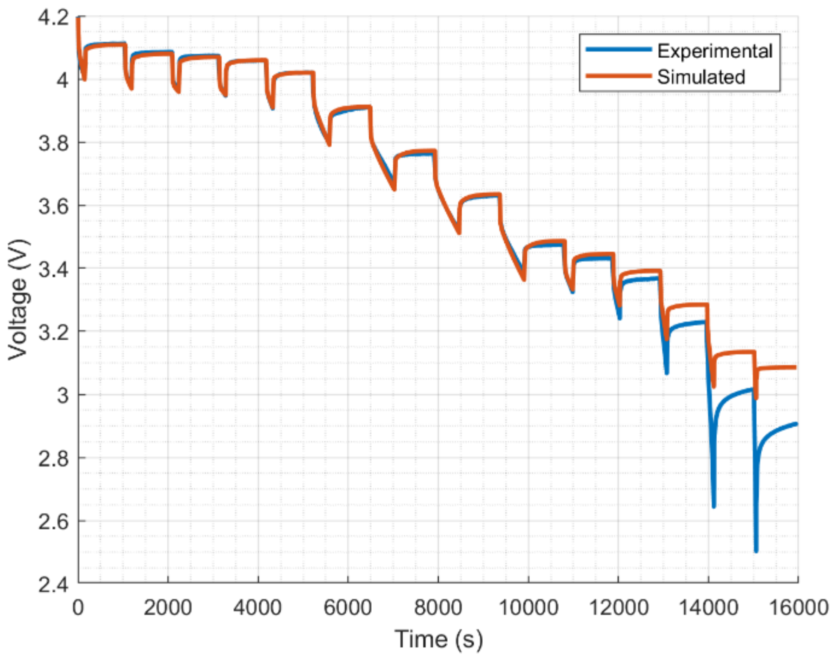

Figure 44. Experimental and simulated terminal battery voltage.

Figure 44 shows that the simulated voltage trend is close to the experimental one, with a root mean square error of 0.07 V. The biggest difference is registered at low voltage when the system reaches its lower limits.

The battery parameters depend on the SoC of the battery pack. However, this dependency is relevant only at very low SoC as it can be seen in Figure 44, where the system will not work during simulations for safety reasons. So, the dependency on SoC is omitted. The battery is also considered to work at ambient temperature, that is maintained constant during simulations, meaning that also the temperature dependency of the parameters is not included in this work. For these reasons, the battery model is considered reliable and faithful to the real functioning of the system in its field of use.

2.5.3. Passive Hybrid Energy Storage System

The first hybrid energy storage considered in this part of the research project is a parallel passive hybrid, that follows the scheme of Figure 45.

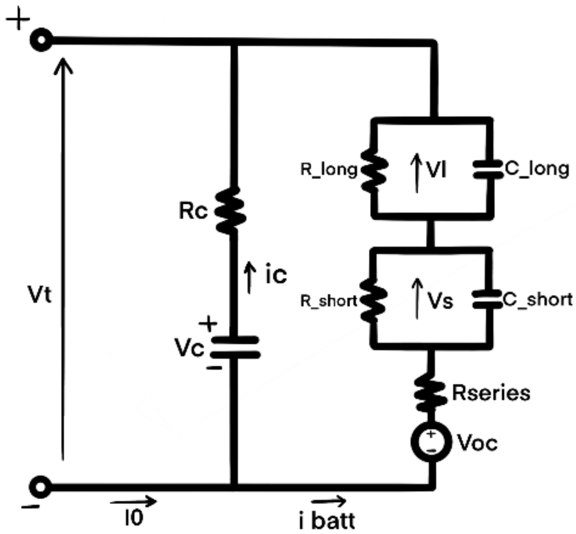

Figure 45. HESS passive scheme.

As explained in 2.4.3 the LiCs are dimensioned to satisfy the power request of the EMs. The first hybrid configuration that is here explained sees the introduction of the battery pack in parallel with the LiCs. Therefore, it will be dimensioned to guarantee a similar voltage range by choosing a proper number of cells in series configuration.

With respect to the number of parallels, the decision is to work with a single branch, since increasing the number of branches in parallel configuration would lead to an increase in the weight and size of the hybrid pack. The current hybrid pack application is destined to a super sport car and needs to respect stringent limits on size and weight.

Therefore, the battery configuration that has been chosen is a 54s1p (54 series and 1 parallel string) that stores 0.79 kWh and could reach approx. 9 kW of power in discharge phase and approx. 0.8 kW in charge phase. The working voltage spans from a minimum working voltage of 160 V to a maximum voltage of 226 V. The maximum discharge current for a single cell is 45

A, while the charge current is equal to -4.2A. The energy contribution of the batteries is three times the one of the LiCs.

The components of the passive hybrid system have been previously described, but the passive hybrid energy storage system needs a deep analysis itself since complexity arises by combining the two systems in parallel. A preliminary analysis is carried out on a simplified system. So, assuming that the battery can be modeled as a single voltage generator and a series resistance, the scheme will be the one in Figure 46:

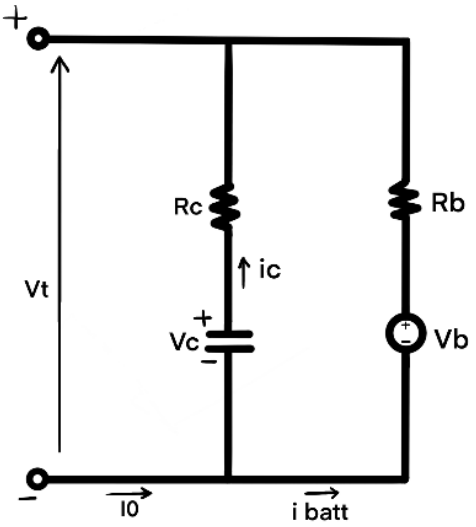

Figure 46. HESS passive simplified equivalent circuit.

As it has been done in [74,78], the circuit is transformed at first in the frequency domain, as it is seen in Figure 47.

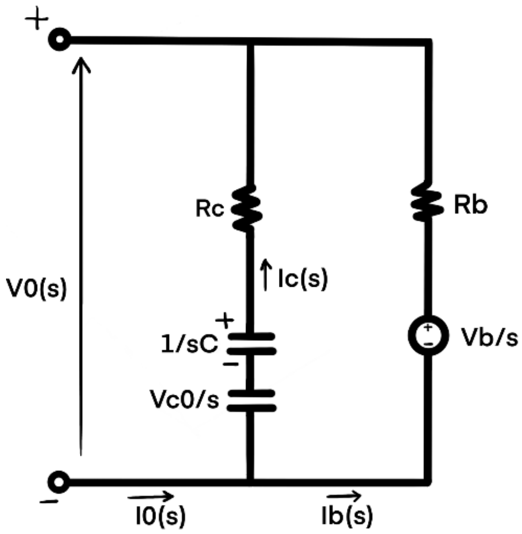

Figure 47. HESS passive circuit in Laplace domain.

This is done by using the Laplace transform, where the current i_c flowing through the capacitor can be transformed given an initial capacitor voltage V_{c0}:

$$i_c = C\frac{dV_c}{dt} \rightarrow I_c(s) = sCV_s - CV_{c0} \rightarrow V(s) = \frac{I(s)}{sC} + \frac{V_{c0}}{s}$$

XXIX

According to the Kirchhoff's voltage and current rules:

$$I_c(s) + I_b(s) = I_0(s)$$

XXX

$$V_0(s) = \frac{V_{c0}}{s} + I_c(s)R_c + I_c(s)\frac{1}{sC} = \frac{V_b}{s} + I_b(s)R_b$$

XXXI

Then, the Thevenin-equivalent circuit is derived as it can be seen in Figure 48.

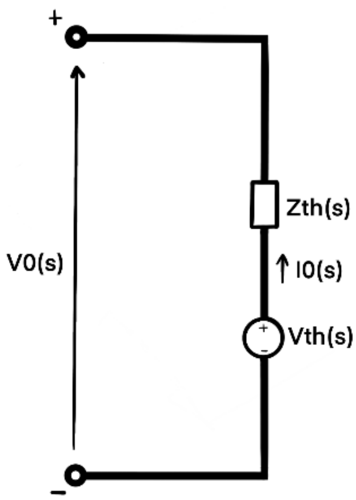

Figure 48. HESS passive Thevenin equivalent circuit.

To describe the output load voltage expressed as V_t in Figure 46, the Thevenin-equivalent circuit is derived. The output voltage in Laplace domain $V_0(s)$ is found analyzing the circuit in open circuit condition. The current $I_c(s) = I_b(s) = I(s)$ circulates in closed loop so:

$$0 = \frac{V_b}{s} - I(s)R_b - I(s)R_c - I\frac{1}{sC} - \frac{V_{c0}}{s}$$

XXXII

$$I(s) = \frac{V_b - V_{c0}}{s(R_b + R_c + \frac{1}{sC})}$$

XXXIII

The Thevenin equivalent voltage $V_{th}(s)$ can be obtained:

$$V_{th}(s) = \frac{V_{c0}}{s} + I(s)R_c + I(s)\frac{1}{sC}$$

XXXIV

Substituting XXXIII into XXXIV, we obtain:

$$V_{th}(s) = \frac{V_{c0}}{s} + \frac{V_b - V_{c0}}{s\left(R_b + R_c + \frac{1}{sC}\right)}(R_c + \frac{1}{sC})$$

XXXV

That can be simplified as:

$$V_{th}(s) = \frac{R_c}{R_b + R_c}V_b\frac{s+\alpha}{s(s+\beta)} + \frac{R_b}{R_b + R_c}V_{c0}\frac{1}{s+\beta}$$

XXXVI

$$Z_{th}(s) = \frac{R_b R_c}{R_b + R_c}\frac{s+\alpha}{s+\beta}$$

XXXVII

Where V_{th} and Z_{th} are respectively the Thevenin equivalent voltage and the Thevenin equivalent impedance, s is the complex frequency, R_c and R_b are the capacitor and battery resistances and V_b is the battery voltage. The capacitor with non-zero initial conditions has been replaced in the Laplace domain by an uncharged capacitor in series with a step-function voltage source with amplitude V_{c0}, and:

$$\alpha = \frac{1}{R_c C_c}$$

XXXVIII

$$\beta = \frac{1}{(R_b + R_c)C_c}$$

XXXIX

Eventually, a real load could be applied, however for an analytical approach an ideal pulsed square load is applied. This allows to capture the fundamental characteristics and the behavior of the system. The pulsed load current has a period T, pulse duty ratio D and it can be expressed for the first N pulses as:

$$i_0(t) = I_0 \sum_{k=0}^{N-1}[\Phi(t-kT) - \Phi(t-(k+D)T)]$$

XL

Where I_0 is the amplitude of the current and $\Phi(\mathrm{t})$ is a unit step function at $\mathrm{t} = 0$. In the frequency domain:

$$I_0(s) = I_0 \sum_{k=0}^{N-1} [\frac{\mathrm{e}^{-\mathrm{kT}\cdot\mathrm{s}}}{s} - \frac{\mathrm{e}^{-(\mathrm{k}+\mathrm{D})\mathrm{T}\cdot\mathrm{s}}}{s}]$$

XLI

With an average value of

$$I_L = DI_0$$

XLII

The inverse Laplace transform of the Thevenin voltage source XXXVI is:

$$v_{th}(t) = V_b + \frac{R_b}{R_b + R_c}(V_{c0} - V_b) \cdot \mathrm{e}^{-\beta \mathrm{t}}$$

XLIII

Where the second term is related to the energy distribution between the capacitor and the battery at the beginning of the discharge. For the given load, the internal voltage drop $V_i(s)$ is:

$$V_i(s) = Z_{th} I_0(s)$$

XLIV

For the chosen current waveform, we have:

$$v_i(t) = R_b I_0 \sum_{k=0}^{N-1} \{\left(1 - \frac{R_b}{R_b + R_c} \mathrm{e}^{-\beta(\mathrm{t}-\mathrm{kT})}\right) \cdot \Phi(t - kT) - \left(1 - \frac{R_b}{R_b + R_c} \mathrm{e}^{-\beta(\mathrm{t}-(\mathrm{k}+\mathrm{D})\mathrm{T})}\right) \cdot \Phi(t - (k + D)T)\}$$

XLV

And the output voltage becomes:

$$V_0(s) = V_{th}(s) - V_i(s)$$

XLVI

$$v_0(t) = v_{th}(t) - v_i(t)$$

XLVII

The currents of the battery and supercapacitors are:

$$i_b(t) = \frac{1}{R_b}(V_b - v_o(t))$$

XLVIII

$$i_c(t) = i_o(t) - i_b(t)$$

XLIX

This analysis is carried on with respect to the steady-state performance, so when the capacitor and battery voltage are equal.

$$V_b = V_{c0}$$

L

This leads to:

$$i_{b,ss}(t) = I_0 \sum_{k=0}^{N-1} \{ \left(1 - \frac{R_b}{R_b + R_c} \mathrm{e}^{-\beta(\mathrm{t}-\mathrm{kT})}\right) \cdot \Phi(t - kT) - \left(1 - \frac{R_b}{R_b + R_c} \mathrm{e}^{-\beta(\mathrm{t}-(\mathrm{k}+\mathrm{D})\mathrm{T})}\right) \cdot \Phi(t - (k + D)T) \}$$

LI

Combining XLIX with XL and LI, we obtain:

$$i_{c,ss}(t) = \frac{R_b I_0}{R_b + R_c} \sum_{k=0}^{N-1} \{ \mathrm{e}^{-\beta(\mathrm{t}-\mathrm{kT})} \cdot \Phi(t - kT) - \mathrm{e}^{-\beta(\mathrm{t}-(\mathrm{k}+\mathrm{D})\mathrm{T})} \cdot \Phi(t - (k + D)T) \}$$

LII

Peak Performance

The target is now to simulate the battery behavior to determine the current peak, that occurs at the end of the pulse load:

$$\mathrm{t} = (\mathrm{k} + \mathrm{D})\mathrm{T}$$

LIII

The battery peak current becomes, for $N \to \infty$:

$$I_{b,peak} = I_0 \left(1 - \frac{R_b}{R_b + R_c} \frac{\mathrm{e}^{-\beta \mathrm{DT}}(1 - \mathrm{e}^{-\beta(1-\mathrm{D})\mathrm{T})})}{1 - \mathrm{e}^{-\beta \mathrm{T}}}\right) = I_0(1 - \zeta_c) = \frac{I_0}{\gamma}$$

LIV

ζ_c is the current sharing factor and γ is the power enhancement factor. This means that without a capacitor, the battery would have to meet the peak load by itself, while the hybrid system can supply a higher load than the battery itself. If I_{rated} is the rated current for the battery, the new possible load current of the hybrid system can be expressed as:

$$I_0 = \gamma \cdot I_{rated}$$

LV

And the instantaneous peak power becomes:

$$P_{peak} = I_0 V_b = \gamma \cdot I_{rated} V_b = \gamma \cdot P_{rated}$$

LVI

The presence of the capacitor allows to make the power enhancement factor larger than one. Considering the eigen frequency of our system for a simplified model $R_b = 1.40\ Ohm$, $R_c = 0.06\ Ohm$ and $C_c = 55\ F$:

$$f_{eigen} = \frac{1}{(R_b + R_c)C_c} = 0.012\ Hz$$

LVII

The power enhancement dependency on frequency and duty cycle is plotted in Figure 49:

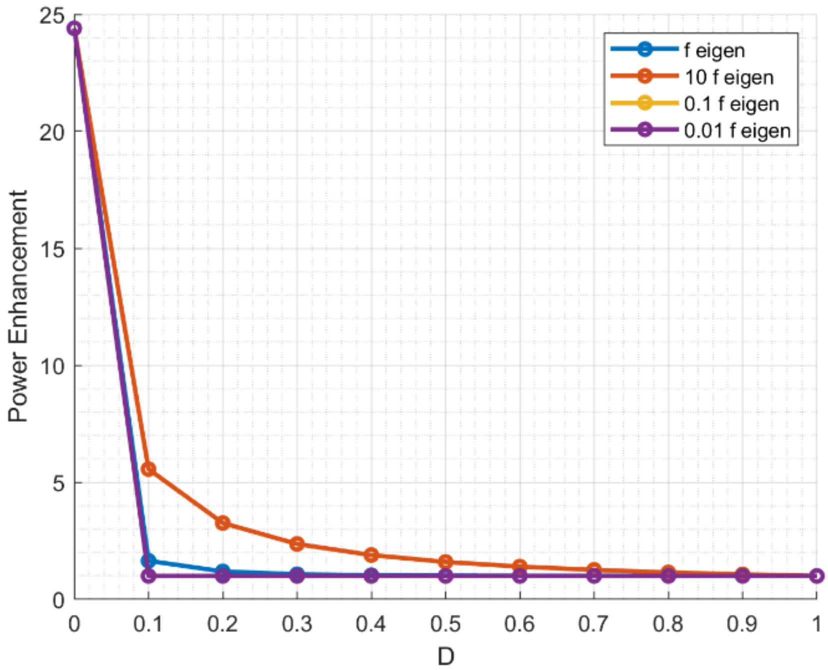

Figure 49. Peak power enhancement dependency on the duty cycle D.

As the frequency grows and becomes way higher than the eigen frequency, the power enhancement reaches a limit close to that of $10 f_{eigen}$. On the other side, the maximum theoretical possible enhancement of output power could be increased 24.4 times the output power of the battery-alone system, as we can obtain for the case of $D = 0$.

By lowering the internal resistance, the capacitor is going to give reduced power losses, since it covers a significant share of the output current.

Another important information that can be carried out from this analysis is that a passive HESS is not capable of delivering the complete capacitor range of power, reducing the flexibility of the system if compared with a capacitor-only energy storage.

Power Saving

Since the capacitors take a high share of current, the losses depend also on their internal resistance, that is usually lower than that of batteries. This results in lower power losses. The analysis can be carried out determining the internal power losses of the hybrid system and introducing a power saving factor. Considering the battery system, the average power of the load pulse train with amplitude V_0, and duty cycle D applied over the load resistance R results in:

$$P_{0,average} = \frac{{V_0}^2}{R} D = \frac{{V_{0,rms}}^2}{R}$$

LVIII

The root mean square load current is:

$$I_{0,rms} = I_0\sqrt{D}$$

LIX

Since the battery here meets the load by itself, $I_{0,rms} = I_{b,rms}$. The total power drawn from the battery and transferred to the load is:

$$P_b = V_b I_{0,rms} - R_b {I_{0,rms}}^2 = V_b\sqrt{D}I_0 - R_b D {I_0}^2 = V_b\sqrt{D}I_0(1 - \frac{R_b\sqrt{D}I_0}{V_b})$$

LX

Since the output voltage of the battery $V_{b,out}$ is the internal voltage V_b minus the voltage drop across the resistance R_b:

$$V_{b,out} = V_b(1 - \frac{R_b\sqrt{D}I_0}{V_b})$$

LXI

$$P_b = V_{b,out} I_{0,rms}$$

LXII

And the internal power losses are:

$$P_{i,b} = R_b {I_{0,rms}}^2$$

LXIII

The root mean square values for the battery and supercapacitor currents when connected together are determined in [74,78]:

$$I_{b,rms} = \sqrt{\frac{1}{T}\int_{nT}^{(n+1)T} [i_{b,ss,nth}]^2 dt} = \sqrt{D} I_0 \lambda(D,T)$$

LXIV

$$\lambda = \sqrt{1 + \frac{R_b}{R_b+R_c} \frac{2\left(1-\mathrm{e}^{-\beta DT}\right)}{\beta DT}\left(\frac{1-\mathrm{e}^{-\beta DT}}{1-\mathrm{e}^{-\beta T}} - 1\right) + \left(\frac{R_b}{R_b+R_c}\right)^2 \frac{(\mathrm{e}^{\beta DT}-1)(1-\mathrm{e}^{-\beta(1-D)T})}{\beta DT(1-\mathrm{e}^{-\beta T})}}$$

LXV

$$I_{c,rms} = \sqrt{\frac{1}{T}\int_{nT}^{(n+1)T} [i_{c,ss,nth}]^2 dt} = \sqrt{D} I_0 \mu(D,T)$$

LXVI

$$\mu = \sqrt{\left(\frac{R_b}{R_b+R_c}\right)^2 \frac{\mathrm{e}^{\beta DT} - \mathrm{e}^{\beta T} - 1 + \mathrm{e}^{\beta(1-D)T})}{\beta DT(1-\mathrm{e}^{\beta T})}}$$

LXVII

The total internal power loss of the hybrid system can be expressed as:

$$P_{i,hybrid} = R_b {I_{b,rms}}^2 + R_c {I_{c,rms}}^2 = R_b D {I_0}^2 \left(\lambda^2 + \frac{R_c}{R_b}\mu^2\right) = R_b D {I_0}^2 (1-\varepsilon)$$

LXVIII

And the power saving factor is defined as:

$$\varepsilon = 1 - \left(\lambda^2 + \frac{R_c}{R_b}\mu^2\right)$$

LXIX

Figure 50 shows the dependency of the power saving factor with respect to the duty cycle D.

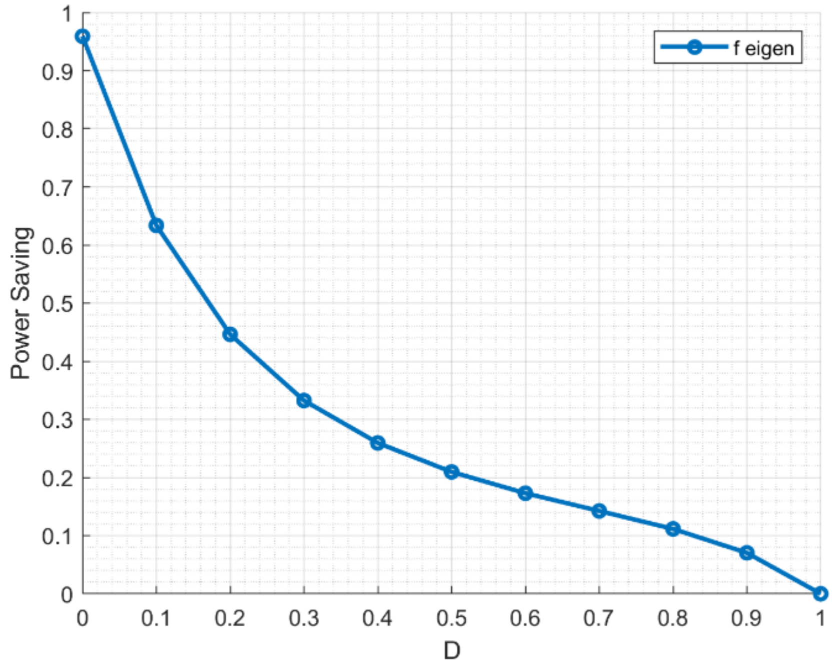

Figure 50. Power saving dependency on the duty cycle D.

If D goes to 1, we approach a constant current and the savings become equal to zero, while the theoretical maximum power saving is given by $D \to 0$:

$$\lim_{D \to 0} \varepsilon = \frac{R_b}{R_b + R_c}$$

LXX

Run Time Extension

The analysis can be concluded looking at the total energy saved by the hybrid system:

$$\Delta W = W_{i,b} - W_{i,hybrid} = R_b D I_0{}^2 \tau_b - R_b D I_0{}^2 (1 - \varepsilon) \tau_{hybrid}$$

LXXI

Where τ_{hybrid} is the total run time of the hybrid system, while τ_b is the total run time of the battery-alone system (assuming it can run to 100% depth of discharge). The saved energy could be formulated as:

$$\Delta W = P_0 \Delta \tau$$

LXXII

Where P_0 is the output power from the system and $\Delta\tau = \tau_{hybrid} - \tau_b$ is the extended run time extension of the system due to the reduced losses. The output hybrid energy is also expressed as:

$$W_0 = P_0 \tau_{hybrid} = W_{total} - W_{i,hybrid} = V_b \sqrt{D} I_0 \tau_b - R_b D I_0{}^2 (1 - \varepsilon) \tau_{hybrid}$$

LXXIII

Combining the equations LXXIII and LXXI in LXXII:

$$\frac{\Delta\tau}{\tau_b} = \frac{\varepsilon\sqrt{D}\delta}{1 - \varepsilon\sqrt{D}\delta}$$

LXXIV

Where $\delta = \frac{R_b I_0}{V_b}$. When $R_b = 0$ the internal voltage drop is zero and the time extended becomes zero because there is no dissipation. On the other side, when the load increases, the dissipation increases and so does δ. If δ is fixed, once the load is known, the run time extension could be evaluated under the variation of D and ε (which depends on D and on the system frequency), as shown in Figure 51.

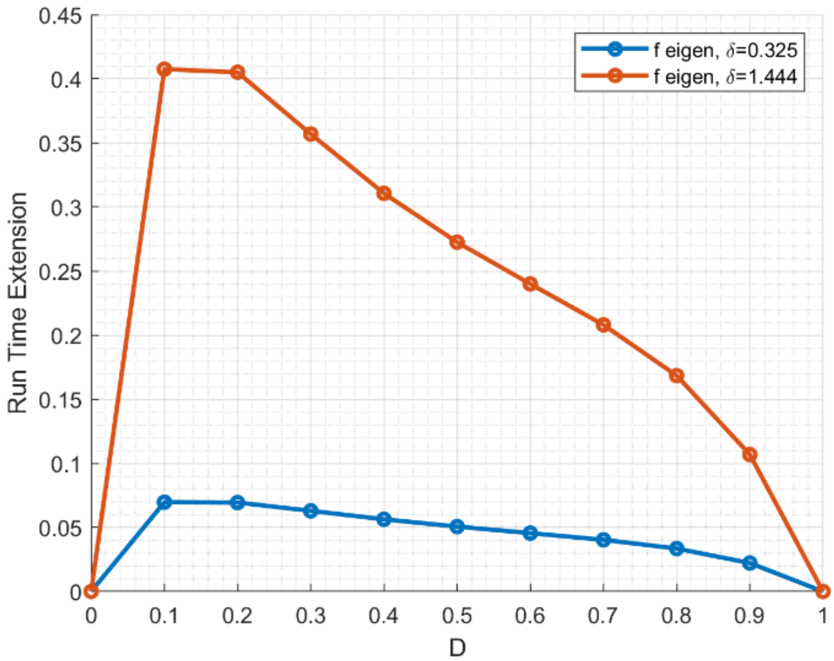

Figure 51. Run time extension dependency on the duty cycle D and on δ.

For $D \rightarrow 0$ the run time extension is zero, while the power saving, and the peak power enhancement have a maximum. This is because the system is not utilized when the current is zero.

The run time extension goes to zero also when D goes to 1, since the situation is one of constant current and the capacitor is not utilized. The run time extension maximum depends also on the frequency of the pulse load and as the frequency becomes lower, the D associated to the maximum is reduced.

Current Model

For our system, a PDT is chosen with $D = 0.2, T = 720\ s, I_0 = 3.4\ A$. A system of this kind is expected to guarantee a $\zeta_c = 0.21, \gamma = 1.26, \varepsilon = 50\%, \frac{\Delta\tau}{\tau_b} = 0.8\%$.

This theoretical analysis of a simplified system allows to formulate the expected behavior of the hybrid system. Since the theoretical analysis has been carried out on a simplified version of the model, the results will slightly differ from the expected ones. The model is realized through MATLAB/Simulink and Simscape Power System, the submodels of the LiC and batteries are modified to simulate the hybrid system as it can be seen in Figure 52 and Figure 53.

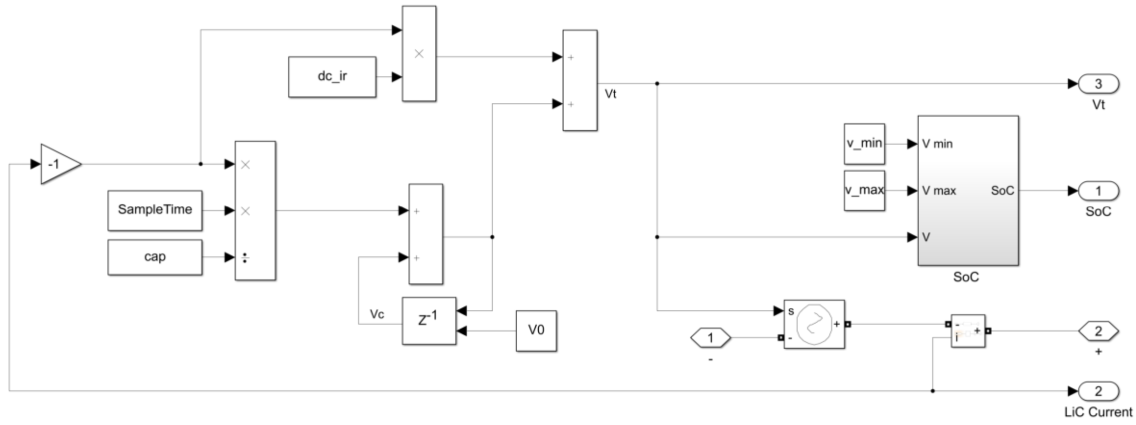

Figure 52. LiC model updated.

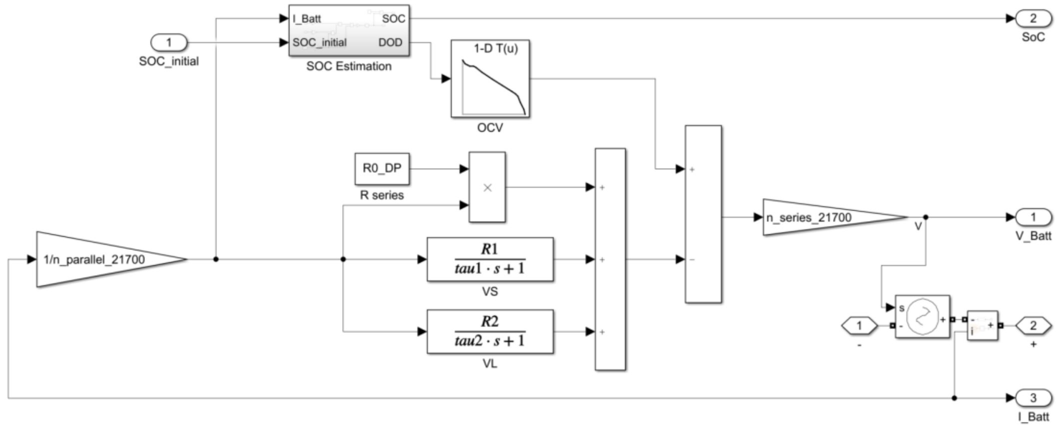

Figure 53. Battery model updated.

A simulation has then been run for the PDT specified previously, and Figure 54 shows the system currents:

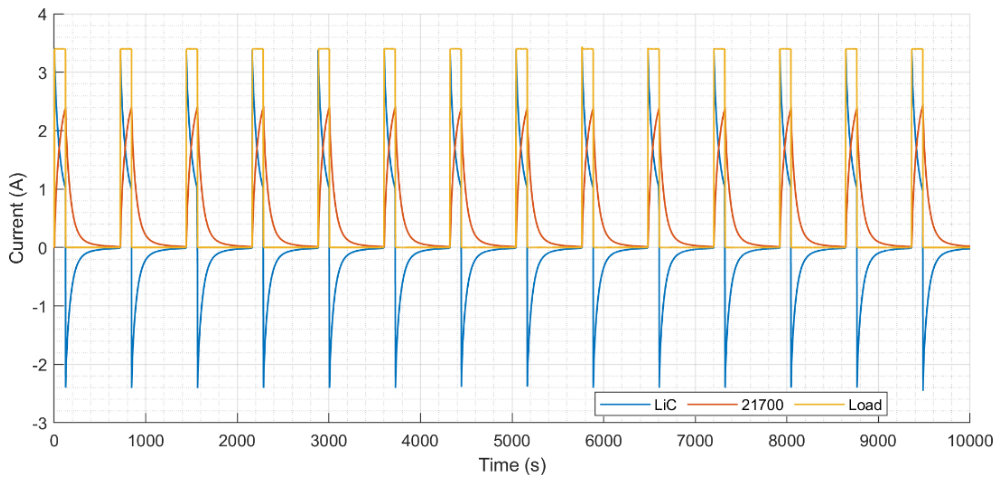

Figure 54. LiCs, battery and PDT current.

In Figure 54 the current load is shown in yellow. As soon as the current request rises to 3.4 A, the HESS is activated and satisfies the current request thanks to the contribution of both the battery and the LiCs. The LiCs power the system in short times due to their high-power values, fulfilling almost all the initial request, while the battery has slower transients. This could be useful during both real driving scenarios and emission cycles as the ones presented in [44], since they are usually characterized by a high variability and they are subject to fast transients.

So, both the battery and capacitors supply current during the load on-state, while the battery charges the capacitors during the load off-state. In this situation, the battery current starts decreasing while the LiCs' current becomes negative to guarantee a sum of currents that is equal to the load request, hence null. Therefore, the instantaneous battery current, which otherwise would be at the same level of the load current request, is reduced considerably due to the assistance of the capacitors, that can relieve peak stresses on the battery, and they positively influence the system performance.

Figure 55 shows the simulated voltage:

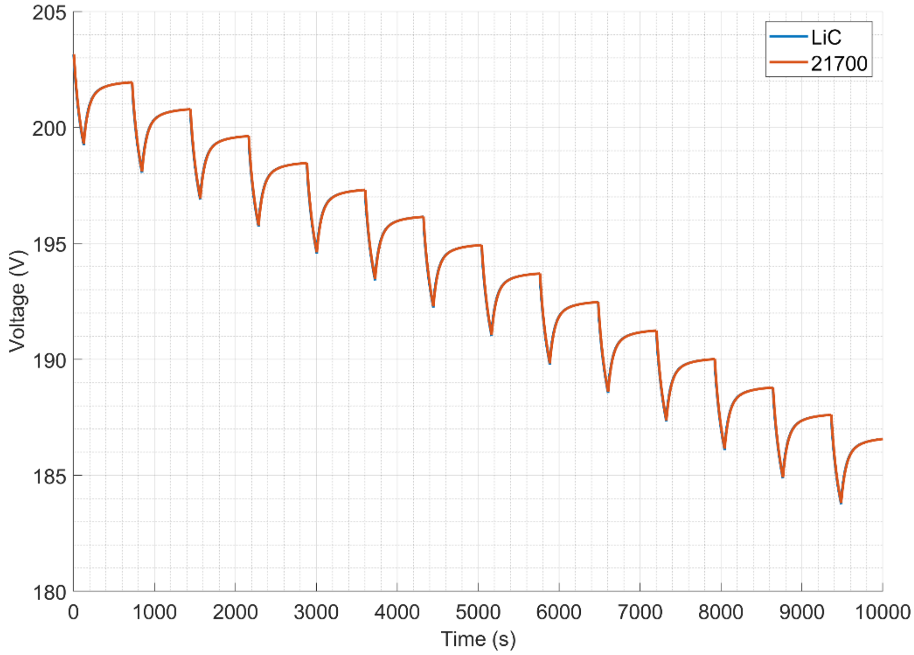

Figure 55. Simulated voltage profile.

Figure 56 shows a comparison between two simulations under the same PDT current input. The voltage profile of the 21700 batteries is shown both for a simulation run for the passive HESS and for the batteries as a stand-alone system. The voltage of the stand-alone batteries reaches values that are lower than the passive HESS, this is due to the presence of the LiCs in the passive configuration, implying a higher energy content.

The comparison between the voltages in Figure 56 shows that the voltage variation of the batteries as a part of the passive HESS is significantly reduced with respect to the batteries as a stand-alone system. This is due to the lower instantaneous current that runs through the system, as shown in Figure 54. The results demonstrate a significant benefit of the hybridization in reducing the fast and large battery terminal voltage transients as explained in [100].

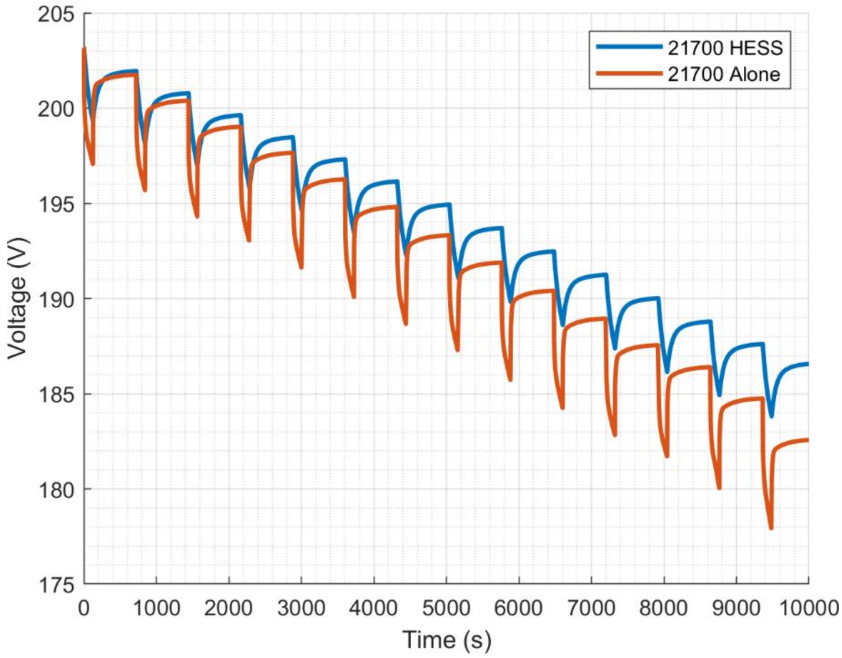

Figure 56. Voltage comparison between a battery alone system and a passive HESS.

It has been verified that for short power pulses the LiCs can supply a large part of the power, reducing the stress on the battery. For longer power pulses, the ratio of the power coming from the battery increases as the voltage of the LiCs drops with theirs SoC. According to the work done in [101], this kind of connection is beneficial when the pulse duration is shorter than 10 seconds and the power electronic complexity needs to be kept at minimum.

A drawback of this configuration is the need to match the voltages of batteries and LiCs, that could become a problem at high voltage. In fact, as explained in [102], a higher energy storage device voltage means the higher potential to have cell imbalances, that could prevent the string from reaching the nominal voltage. It should be kept into account that the usable energy of the LiCs depends on the voltage range of the battery pack. Since the working voltage of the battery is reduced with respect to the one of LiCs, also the energy available from LiCs decreases:

$$E_{LiC} = \frac{1}{2} \cdot c \cdot ({V_{batt,max}}^2 - {V_{batt,min}}^2)$$

LXXV

Where c is the LiCs' capacitance and $V_{batt,max}$, $V_{batt,min}$ are respectively the maximum and minimum battery voltage.

Vehicle Model Implementation

The modeled HESS is introduced in the longitudinal dynamics' vehicle model. The total current request is limited when the HESS voltage is approaching the maximum and minimum values. However, the limit is on the whole passive HESS and no further limitations are introduced on the battery alone.

To verify the feasibility of the passive HESS, a simulation on the whole vehicle model is run for a WLTC Class 3b [44]. The simulation is run for the hybrid vehicle using an RBS for determining the torque or power split between the ICE and the EMs.

Control strategies are deepened in the following chapters. At the moment, it is sufficient to know that here the RBS is a control strategy based on fixed rules that activates the electric propulsion contribution as soon as the SoC reaches a value equal or above 90% and it stops using it when the SoC is equal or below 35%. The resulting current share between LiCs and battery is shown in Figure 57 when tested on a WLTC Class 3b that is shown in Figure 22.

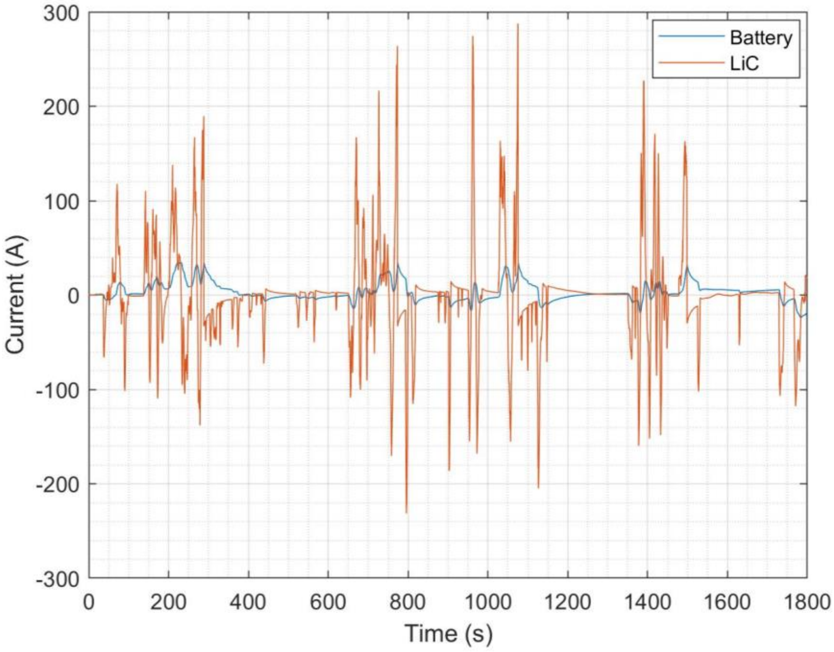

Figure 57. WLTC Class 3b current share for the passive HESS.

The graph shows that under these conditions it is not possible to respect the battery current limits. This is evident for the recuperation phases, in fact the battery limit of -4.2 A is exceeded, especially in the last phase of the cycle where a high-speed braking phase takes place.

In the last braking phase, the current is constantly negative, this resembles a cycle with $D \rightarrow 0$ where the peak performance of the HESS cannot be enhanced. It is evident that under these conditions, a great quantitative of energy coming from regenerative braking would be lost and this would make the presence of the LiCs useless.

The passive HESS has one major drawback which is the limited control possibilities. The load current is shared between the battery and the supercapacitor in a nearly uncontrolled manner, determined predominantly by the internal impedances of the system, as it has been shown in the previous paragraphs.

Control

The simulation that has been run in Figure 57 shows that the passive HESS splits the current between LiCs and batteries in a nearly uncontrolled manner. Therefore, a control strategy is introduced on the vehicle model. The control strategy is composed as it follows:

Table 5. Control strategy for a pack that is charging.

$\lvert i_{batt} \rvert < \lvert i_{batt,lim} \rvert$	$i_{HESS,lim} = \frac{V - V_{batt,max}}{R_{batt}} + \frac{V - V_{LiC,max}}{R_{LiC}}$
$\lvert i_{batt} \rvert = \lvert i_{batt,lim} \rvert$	$i_{HESS,lim} = i_{batt,lim}$

The strategy shown in Table 5 implies that as long as the battery current i_{batt} is lower in absolute value than the battery current limit for charge $i_{batt,lim}$, the limit current for the passive HESS $i_{HESS,lim}$ is given by the sum of the current from the LiCs and the batteries to reach their maximum voltages, respectively $V_{LiC,max}$ and $V_{batt,max}$, calculated thanks to their internal resistances, R_{LiC} and R_{batt}. As soon as the battery current reaches the limit, the limit current for the passive HESS will be set equal to the battery limit.

This is necessary because in a passive HESS we cannot intervene on the battery control alone as the current share is determined by the internal impedances of the system, as it has been shown previously. Instead, we must deal with the entire energy storage.

Table 6. Control strategy for a pack that is discharging.

$\lvert i_{batt} \rvert < \lvert i_{batt,lim} \rvert$	$i_{HESS,lim} = \frac{V - V_{batt,min}}{R_{batt}} + \frac{V - V_{LiC,min}}{R_{LiC}}$
$\lvert i_{batt} \rvert = \lvert i_{batt,lim} \rvert$	$i_{HESS,lim} = i_{batt,lim}$

The strategy shown in Table 6 implies that as long as the battery current i_{batt} is lower in absolute value than the battery current limit for discharge $i_{batt,lim}$, the limit current for the passive HESS $i_{HESS,lim}$ is given by the sum of the current from the LiCs and the batteries to reach their minimum voltages, respectively $V_{LiC,min}$ and $V_{batt,min}$, calculated thanks to their internal resistances, R_{LiC} and R_{batt}. As soon as the battery current reaches the limit, the limit current for the passive HESS will be set equal to the battery limit. This is necessary for the same reason mentioned above.

This control strategy is implemented on the vehicle model, and its impact will be analyzed in the following chapters thanks to simulations on the WLTC Class 3b. In particular, the simulations are run in 4.3.1.

To sum up the analysis that has been run in the previous paragraphs with respect to the passive HESS, it has been demonstrated that the passive HESS is a simple system, that can ensure low weights and small sizes, as well as being inexpensive. However, it has some disadvantages as it needs the voltage of capacitors and batteries to coincide, which means that the capacitors will work in the same voltage range as the batteries, with a consequent limitation on the energy that can be used. In addition, a system of this type presents limited control possibilities.

The introduction of a control strategy over the whole passive HESS protects the batteries from over-current but does not make up for the limits related to the range of operation of the capacitors.

2.5.4. Semi-Active Hybrid Energy Storage System

The introduction of one or more DC-DC converters could be seen as a solution to avoid the problems associated with the passive HESS. A semi-active system as the one shown in Figure 26 and Figure 58 is introduced and modeled.

The semi-active system is capable of interfacing the capacitors and the battery to achieve higher reliability and control flexibility, and to optimize the power sharing [70,72,73]. The presence of a DC-DC converter allows to control the system and to make use of the full voltage range of capacitors. On the other hand, it must be considered that the introduction of a component as the DC-DC converter implies additional costs, a greater size of the system and a greater weight.

The configuration that has been chosen fits a pack of LiCs in 60s1p configuration (as introduced in 2.5.1) connected to the load, so the configuration that is chosen for further evaluations is a battery semi-active hybrid as shown in Figure 58.

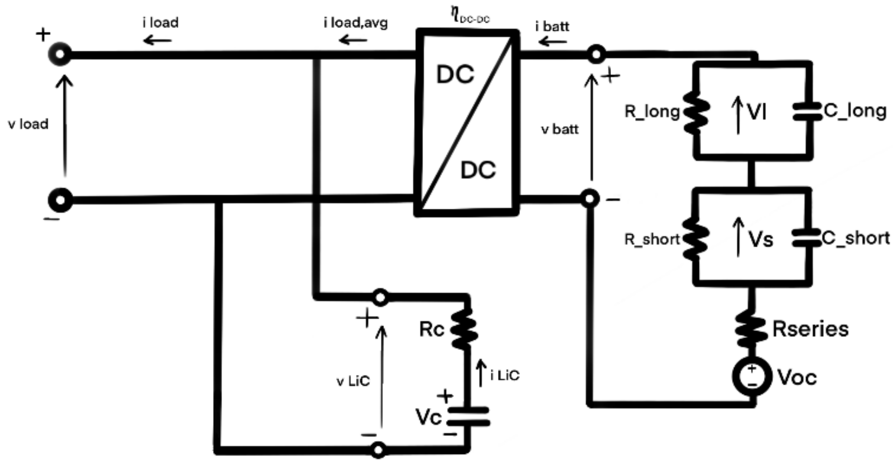

Figure 58. Battery semi-active hybrid energy storage system.

This way, the LiC energy storage is directly connected to the inverter and the EMs, while the DC-DC converter is connected between the battery and the load. This configuration allows to dimension the DC-DC converter for the average power flow, keeping the battery current at a near constant value despite the load current variations. As stated in [71], this allows significant battery performance improving in lifetime, energy efficiency and operating temperature. Moreover, voltage matching between battery and load/LiC is no longer required.

DC-DC Converter

The choice of the converter control logic is linked with the need for a real-time oriented model, compatible with the implementation on the real vehicle control unit. The DC-DC converter could be modeled according to the work done in [12,74], but that level of accuracy is not needed at this point of the work. So, the indications in [71] are followed and a simple system is modeled.

v_{batt} indicates the battery voltage, v_{load} the load voltage, k is the conversion ratio, i_{batt} is the battery current, i_{load} is the load current, η_{DC-DC} is the converter efficiency, i_{LiC} is the LiC current.

$$v_{batt} = \frac{v_{load}}{k}$$

LXXVI

$$i_{batt} = \frac{i_{load}}{\eta_{DC-DC}} k$$

LXXVII

$$i_{LiC} = i_{load} - i_{batt}$$

LXXVIII

The conversion ratio k is adopted instead of an explicit duty cycle dependent conversion ratio. The value of the conversion ratio is related to the working mode of the DC-DC converter. In boost operation $k > 1$, fewer cells in series can be used to form a battery pack with a terminal voltage lower than the load voltage. This reduces the pack size and the internal resistance.

However, as it is explained in [71], in that case the current flowing through the battery pack is higher than the load current, resulting in higher losses due to heating and requiring cells to have higher discharge rate capabilities. When in buck operation, $k < 1$, the battery pack has more cells in series to form a pack with a terminal voltage higher than the load voltage. This would increase the pack size and the internal resistance. In this case the DC-DC converter voltage rating should be chosen according to the maximum voltage of the battery pack. On the other side, the current flowing through the battery pack is lower than the load current, meaning that the losses are reduced, and the cells are required to have lower discharge rate capabilities.

For our simulations, the battery voltage could be higher or lower than the load voltage, meaning that the converter is operating in buck or boost mode respectively.

Converter Control Strategy

The DC-DC converter control is based on the work done in [75,89], where the average power load is determined and requested to the battery, while the peak power request is satisfied by the LiCs. This allows to achieve a nearly constant battery current, to guarantee performance improving in energy efficiency and operating temperature. In particular, the average load power P_{ave} at instant t is determined thanks to the power load P_{load}:

$$P_{ave} = \frac{\int_0^t P_{load}}{t}$$

LXXIX

That value is then divided by the load voltage v_{load} to determine the $i_{load,avg}$:

$$i_{load,avg} = \frac{P_{ave}}{v_{load}}$$

LXXX

Then, the battery current i_{batt} is determined as:

$$i_{batt} = \frac{i_{load,avg}}{\eta_{DC-DC}}$$

LXXXI

While i_{LiC} is determined from LXXVIII. This control strategy is modeled in Simulink, and it can be seen in Figure 59.

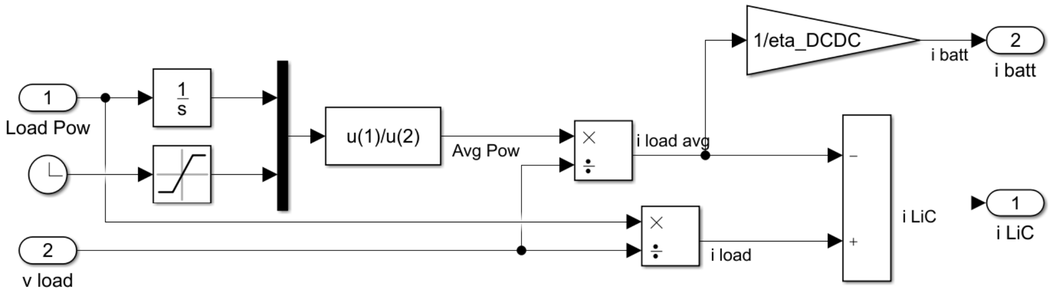

Figure 59. Control algorithm for the DC-DC converter.

As already explained, the powertrain control strategies are the same introduced in the second architecture. So, the power load entering the DC-DC model is given by the RBS or the ECMS. The current output for LiCs and batteries will be limited according to the respective limits, in order not to fail the circuit. The results for the semi-active configuration will be presented in the following chapters, through WLTC 3b simulations.

Fixed Ratio DC-DC

At last, a fixed ratio DC-DC is analyzed as a substitute of the DC-DC converter, with a fixed ratio equal to 1. This should guarantee comparable performance, saving complexity [80].

The control strategy that is here introduced aims to maintain the battery terminal voltage equal to the load voltage. This should simplify as much as possible the structure of the fixed ratio DC-DC that is used. A system of this kind is analyzed to verify its feasibility with the target of optimizing the vehicle fuel economy.

According to the configuration in Figure 58, the load voltage v_{load} corresponds to the LiCs' terminal voltage, and this value corresponds to the one at the terminals of the battery. Since the battery can be seen as a voltage generator v_{batt} and an internal resistance R_0, connected in series run by a current i_{batt}, we will have:

$$v_{load} = v_{batt} - R_0 \cdot i_{batt}$$

LXXXII

The i_{batt} is determined and the i_{LiC} is equal to:

$$i_{LiC} = i_{load} - i_{batt} \cdot \eta_{DC-DC}$$

LXXXIII

The Simulink model for the control algorithm is shown in Figure 60.

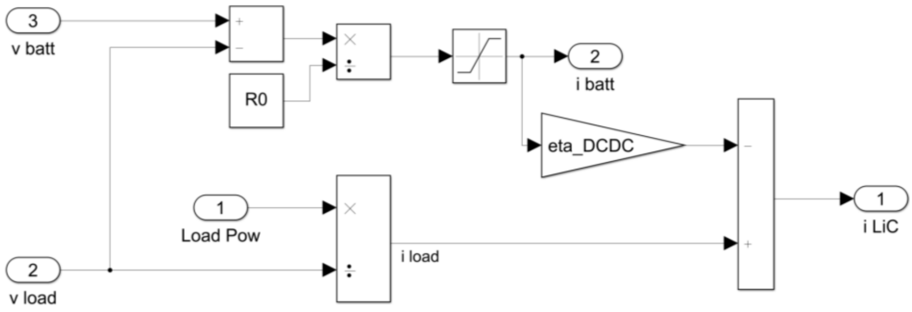

Figure 60. Control algorithm for the fixed ratio DC-DC.

The results for the fixed ratio configuration will be presented in the following chapters, through WLTC 3b simulations. A system of this kind is associated with a lower complexity with respect to the previous DC-DC converter solution.

The disadvantages that are present when DC-DC converters are adopted are represented by the variations of the load voltage during capacitor charging/discharging, that is strictly related to the fact that the capacitor voltage must match the load voltage.

3. Control Strategies

This chapter shows the hybrid powertrain control strategies that have been implemented in the longitudinal dynamics model.

3.1. Literature Review

The control architecture of a HEV usually includes one control unit for each main component and a supervisory controller that receives in input the driver's request and manages the lower-level controllers to satisfy such request according to the powertrain actual conditions. Within the supervisory controller an EMS is implemented, which defines the torque distribution between the energy sources available in the powertrain. In the present dissertation, only parallel hybrid configurations will be considered for the analysis and the development of control strategies.

The EMS reaches various levels of complexity and depends on the powertrain configuration [11,14,83,84]:

- Heuristic controller, with no usage of optimal control theory,
- Sub-optimal controller, with local optimization of the energy management,
- Optimal controller, based on optimal control theory.

3.1.1. Heuristic Control

Heuristic controllers rely on a series of rules that define the powertrain management, some examples can be found in [5,14,16,103–105]. [103] shows how heuristic control can be used to define electric driving mode and it shows the importance of the SoC of the battery as a control parameter. [104,105] show the specific application of heuristic control on a hybrid electric truck in a Simulink environment. The gear shifts, the power split and recharge are defined through control rules and dynamic programming is introduced to support the analysis.

According to the actual conditions of the powertrain, the best control actions to be performed are derived through the implemented strategy. The rules are fixed mathematical rules that aim to maximize the powertrain capabilities, for example, aiming to use as much electrical energy as possible to reduce fuel consumption or shifting the ICE working point to recharge the battery.

This kind of control strategy compares the system variables with thresholds whose reference values were fixed thanks to hypothetical evaluations, the designer's experience, and calibration activities based on experimental tests.

The vehicle behavior can be modeled through simple, low computational effort subsystems or more complex subsystems that could require larger amounts of data and higher computational effort.

This category of EMS is fast, robust and highly real-time capable; therefore, it is widespread and can be seen as the starting point in modeling the vehicle's EMS. On the other hand, a large calibration effort is required and, since no optimal control theory is used in such controllers, their performance is usually far from optimality. Rule-based algorithms can even be derived from the results obtained by means of optimal control approaches.

3.1.2. Sub-Optimal Control

All the controllers making use of the optimal control theory defining and solving the problem instant by instant belong to this family [106,107]. The global solution is a sequence of local optimum solutions, that does not guarantee the global optimum. Two main methodologies have been extensively developed and validated in literature during the last years, namely ECMS and Model Predictive Control, or MPC.

ECMS

ECMS derives from the Pontryagin's Minimum Principle (PMP), that is an analytical method for the minimization/maximization of a given cost-function. The strategy assumes that it is possible to convert, by means of an "equivalence factor", the electrical power consumption in virtual fuel consumption. The sum of the virtual fuel consumption from the battery usage and the actual fuel consumption of the engine becomes the cost-function that is instantaneously minimized.

The main advantage of such controller is the relatively simple implementation and reduced calibration effort, even if the performance, that can achieve results close to the optimal solution, strongly depends on the equivalence factor.

Examples for an ECMS application can be found in [108,109]. [108] shows the implementation of an ECMS, and deepens the analysis by creating an adaptive algorithm capable of estimating the control factors according to the current driving conditions. [109] introduces an ECMS along with optimal control, then extends the ECMS application making it predictive, by guaranteeing further SoC control and utilizing road altitude.

Model Predictive Control (MPC)

The MPC loop makes use of system predicted information [110,111]. A simplified vehicle model fed with historical driving data is used to predict the speed profile over a finite prediction horizon. Once speed and acceleration have been estimated, the optimal control sequence for the time interval of the horizon is calculated. The first element of the optimal control sequence is applied to the powertrain control, then the MPC restarts from the beginning, updating the driving historical data according to the actual feedback from the powertrain.

3.1.3. Optimal Control

The optimal controllers [10,16,84] minimize a given cost-function, for example the fuel consumption, over a given driving mission, for which all the problem variables that are independent from the powertrain operation must be known a priori. This kind of application is then suitable only for off-line implementation, but guarantees global optimal control, useful for benchmarking other controllers.

[112] shows a complete analysis of optimal and sub-optimal control strategies, starting from dynamic programming to achieve a benchmark and then moving to causal control to make the strategy appliable to real vehicles.

Pontryagin's Minimum Principle

PMP is a theorem that aims to solve a global optimal control problem by redefining it through differential equations that represent instantaneous conditions and local optimization [107]. Boundary conditions are imposed both for starting and ending times.

The main drawback is related to the analytical formulation of the problem, meaning that the equations included in the optimal control problem must be derived from a simplified system model. If the simplification makes the model too poor in accuracy, the system representation is not effective, and the optimal control policy found becomes sub-optimal for the real system.

Convex Optimization

This optimization technique assumes that the energy management problem can be formulated in a convex form [113]. The main advantage is that the computation effort needed to solve the problem is independent from the number of system states included in the optimization.

Dynamic Programming

The dynamic programming algorithm derives from Bellman's principle of optimality [112]. The knowledge of the driving conditions for the complete horizon is needed to find a global optimal solution without any simplification of the model and including non-linearities. However, the computational effort increases with the number of variables added to the problem.

3.2. Research Project Contribution

A great variety of hybrid control strategies exist with their pros and cons. The vehicle model serves as a pre-concept and concept tool and the decision that has been taken is to focus on those kinds of strategies that could be introduced on-board the real vehicle. Then, the research project focuses on heuristic control [5,14,16,103–105] and sub-optimal control [106–111], leaving optimal control [10,16,84,107,112,113] for future studies.

At first, the heuristic control is analyzed, with the introduction of an RBS on the vehicle model. The RBS has been implemented on board a 48V prototype, and the concept vehicle model has helped to foresee the impact of the hybrid powertrain on the real vehicle. In particular, the control strategy targets an improvement on the vehicle performance and comfort by covering the torque gap during the gear shifts and activating other hybrid functions, as it will be discussed later.

The battery SoC has been chosen as the main state parameter as in [103], moreover, the braking control is based on the one formulated in [104,105] since it tries to capture as much regenerative braking energy as possible. In particular, the braking action will be exerted mainly by the EM, while the mechanical brakes will come into action only if the required braking power exceeds the regenerative braking capacity.

The torque fill function is based on the one found in [52], where an efficiency improvement during gear shifts is targeted. The torque fill function operates on a parallel hybrid vehicle configuration by activating the electric motor that is commanded to provide a controlled amount and duration of torque during shifts to "fill-in" the torque gap caused by the engine clutch engagement and disengagement.

The RBS is fitted with the presence of LiCs as the main energy storage system, and the control rules that are proposed aim to properly deal with a system characterized by small energy density and high-power density.

Later, the hybrid control strategy is modified to achieve also fuel economy improvements by avoiding fixed calibrated values that are commonly adopted as seen in [11,14], and instead linking the hybrid control to the vehicle speed.

In a subsequent development of the strategy, the focus shifts uniquely on fuel economy. The RBS is modified to adapt to the new target and different control rules are introduced. The new control rules are established through evaluations of the impact on real super sport cars, as the choice to power the vehicle only through the electric powertrain could lead to major complications. For example, arrangements are made not to alter the initial phase of emission cycles, when warm up and catalyst heating take place. In fact, this phase represents the most complex part of the cycles as it can be seen in [114–116].

Further considerations are made for the control strategy. The decision to work with an RBS that targets fuel economy ensures the possibility to work with a simple system. The RBS can provide a high simulation speed since it can work with control rules, but at the same time, it does not guarantee the best working condition for every integration step. In fact, even if the engineering assumptions made for the RBS design make total sense, the rules and calibration are not flexible and cannot be adapted to the driving conditions.

Then, the activity moves to sub-optimal control targeting the minimization of fuel consumption and an ECMS is developed. The ECMS targets exclusively fuel economy, and it is introduced in this work to understand whether the development of a control strategy of that kind is justified by the fuel economy benefits.

The general formulation of the minimization problem refers to any kind of energy storage system and can be found in [11,117]. The ECMS modeling is integrated with the previous work done for the RBS, in fact some control rules are maintained. In particular, the regenerative braking control as in [104,105] is present, moreover the catalyst heating during the warm-up phase of the cycles is not altered.

The research project contribution is also related to the presence of multiple EMs fitted on the powertrain. As explained in [11,16,106,109], the ECMS is set to split torque between the ICE and EMs to achieve the minimization of equivalent fuel consumption. However, the ECMS is here set to split torque also between the multiple EMs, making the strategy formulation more complex and introducing a new control factor that targets fuel economy. Similar activities can be found in [118,119], where powertrains with multiple EMs are analyzed.

The ECMS is set to work with an SoC target that can be chosen depending on the hybrid vehicle mission and the technology that it is used. Here, the SoC target is set constant at first to simulate a Charge Sustaining (CS) mode. Later, the possibilities explored in [11] are evaluated, but since the present work is based on a LiC-based super sports car, an alternative SoC target dependent on speed is formulated similarly as it has been previously done for the RBS. This alternative SoC target formulation is thought to fit better the behavior of LiC that dispose of a high charge and discharge rate, and which can perform a high number of cycles [120,121].

3.3. First Architecture, On-Board RBS Hybrid Control Strategy

The first hybrid RBS strategy that is considered is based on four main functions:

- Torque fill, the EM helps to cover the torque request during upshifts,
- Recuperation, the EM acts as a generator and recovers energy,
- Electric Boost, the EM gives an energy boost in kickdown (accelerator pedal completely pressed) conditions,
- Creeping Function, the EM moves the car at low speeds if first or reverse gear are engaged.

The main target of the control strategy is to guarantee a comfort enhancement, thanks to the torque fill function, activated during gear shifts. The torque fill request depends on the torque actuated at the wheels from the ICE at clutch opening. The actual torque value at the wheels is recalculated as an EM torque request, according to the transmission gear ratios, and it is set as the function output.

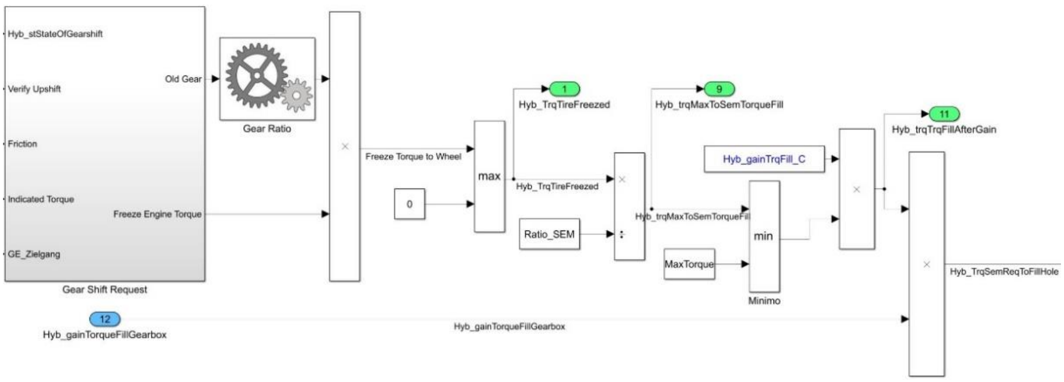

Figure 61. Detail of the block scheme for the torque fill function.

The comfort enhancement can be analyzed looking at the torque flow to the wheels during gear shifts. The electrical torque to the wheels will partially cover the torque gap generated by the clutch opening, that interrupts the ICE torque flow to the wheels.

The maximum torque that can be delivered by the EM has an upper limit that lowers when the EM speed increases and can reach a maximum of 38 Nm (which may result in 780 Nm at the wheels). Due to this limit, the torque gap will be fully covered only at low torque requests at the wheels and low speeds, where the torque gap is felt the most.

A simulation of the hybrid vehicle on a WLTC 3b cycle is run and Figure 62 shows a detail of the normalized torque values at the wheels delivered by the ICE and the EM. The reason why the EM torque at the wheels is not the same for every gear shift must be sought in the algorithms that are implemented for component protection. In fact, the torque delivered by the EM will be limited according to Figure 30, that shows a torque decrease when the rotational speed increases.

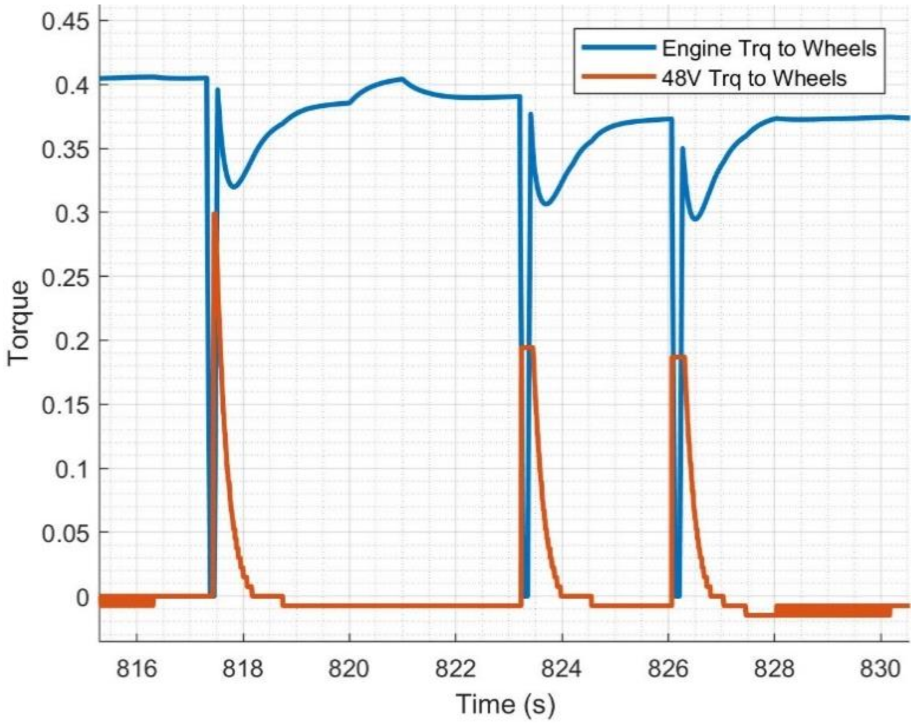

Figure 62. The interruption of the normalized ICE torque to wheels (blue) is partially covered by the EM torque (red).

The graph shows also that the torque from the EM becomes negative after every gear shift. This is due to the regenerative function. The regenerative function is necessary to recover energy when the SoC is too low. The function is activated during braking, but also during normal driving. The aim is to always keep the capacitor at the target value of SoC to cope with the subsequent gear shifts that could take place.

In fact, the EM torque contribution is small and its impact on the V12 torque to the wheels during common driving operations is negligible. The EM torque request for recuperation depends on various quantities, as the braking pressure (Hyp_pBrake), the actual SoC determined through the terminal voltage (Hyb_rSoc48V) and the vehicle speed (PrecisionSpeed).

So, if the speed of the vehicle is greater than a fixed quantity determined through calibration (10 km/h), the regenerative function is activated. In particular, when the SoC Hyb_rSoc48V is greater than a calibrated target SoC value, the strategy will output a constant null torque request regardless of what the state of the car is, whether it is braking or accelerating. This is due to the fact that we are already meeting the energy target to ensure the activation of the hybrid control functions.

Otherwise, if the SoC Hyb_rSoc48V is lower than the target SoC value, the regenerative function depends on the state of the vehicle. If the pedal is pressed and the vehicle is braking, then a torque request dependent on the braking pressure Hyp_pBrake is generated, while if the pedal is not pressed, a torque request dependent on the difference between the actual SoC and the target SoC is generated. The greater is the difference between the actual SoC and the target SoC, the greater will be the torque request for energy recuperation, as we want to keep the SoC at the target value to ensure the activation of the hybrid control functions.

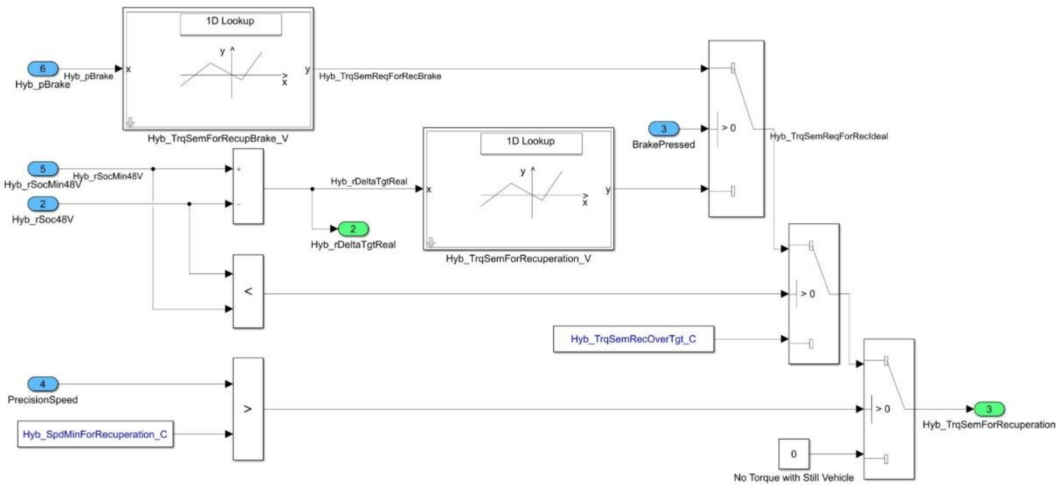

Figure 63. Detail of the block scheme for the regenerative function.

The boost function is activated for performance enhancement, in condition of kickdown (accelerator pedal at maximum). In this situation the EM guarantees the maximum power available.

The creeping function can move a stationary vehicle when the first gear or the reverse gear are engaged and no pressure on the brake is actuated. The gear engagement is required for security reasons, to make sure that the driver really aims to move. The vehicle motion is guaranteed exclusively thanks to the EM, the electric range is obviously limited (approx. 100 m) due to the energy content of the LiC accumulation system.

Figure 64 shows the SoC behavior. Fast discharges and recharges are guaranteed by the high-power values that can be reached. Actual SoC is determined through the terminal voltage, so SoC variations depend both on internal voltage and on the voltage losses due to the internal resistances.

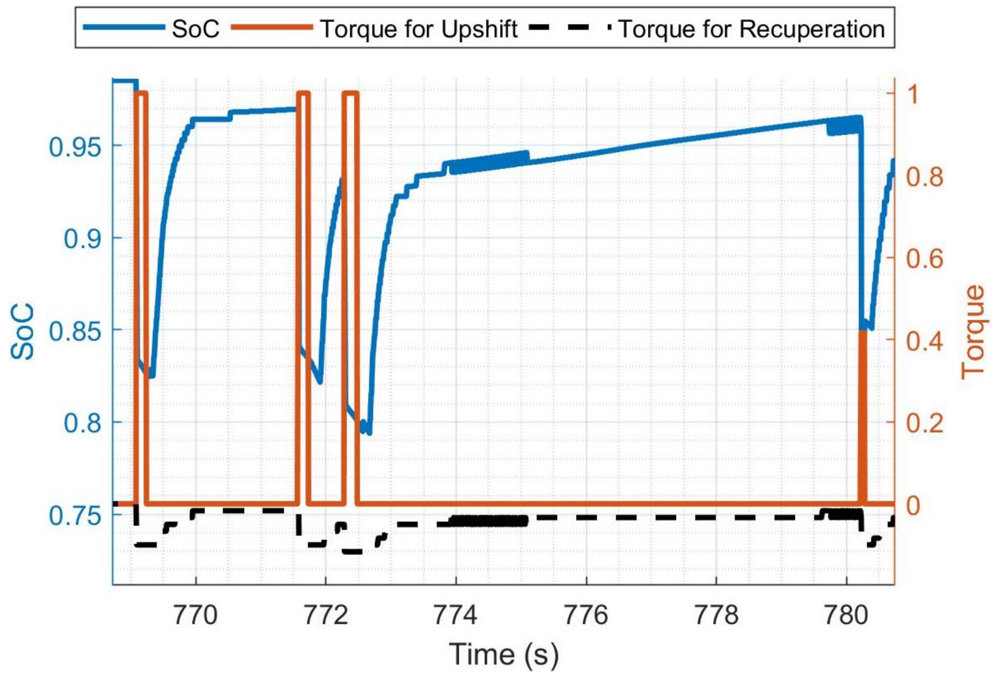

Figure 64. Detail of the SoC at terminals (blue) and normalized EM torque request (black for recuperation and orange for torque fill) during a WLTC Class 3b simulation.

Figure 64 shows the normalized torque request from the EM in a situation in which the vehicle is moving at a speed exceeding 10 km/h, and where some gear shifts occur. Due to this, the EM will try to constantly recover energy to reach the SoC target, however also positive torque requests due to the upshifts will occur.

In case of overlapping between positive and negative torque request, the comfort target will be preferential, and the positive torque fill will overcome as the function output. As soon as the torque fill request is null, the recuperation will be activated.

3.3.1. Strategy Implementation

The aim of the hybrid components that are being considered was, in the first phase of the project, to bring improvements on comfort and performance. As it has been shown in Figure 62 and Figure 64, the hybrid system covers the torque gap during gear shifts, improving the vehicle's comfort.

Figure 65 shows the results of the simulation process for a WLTC Class 3b on the Lamborghini Aventador 48V prototype vehicle. with a focus on the energy storage.

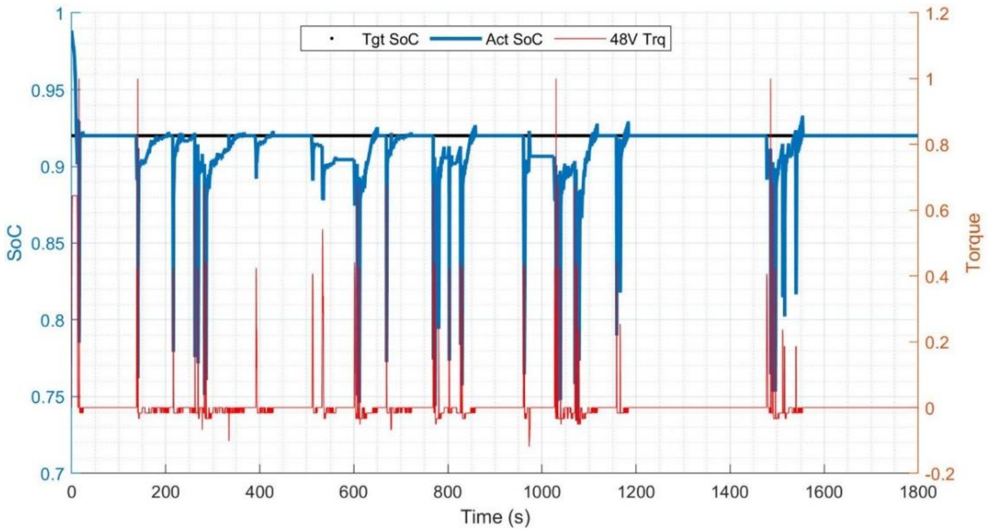

Figure 65. Detail of the Actual SoC (blue) and normalized EM torque (red) during a WLTC Class 3b simulation. In black the fixed Target SoC.

The target SoC value is set as a calibration parameter as it has been explained in the previous paragraph and it does not adapt to the actual operating conditions. Due to this, the SoC working range is tight, since the controller is always aiming to the fixed SoC target. In some situations, as at 1000s, the actual SoC cannot reach the target value because the vehicle is still, and energy recuperation is not active.

In Table 7, the effects of the hybrid strategy activation on the fuel consumption are presented. The starting SoC is here set to 99%, assuming a completely charged energy accumulation system.

Table 7.WLTC fuel consumption improvement simulated results, for the Lamborghini 48V hybrid configuration with RBS on-board strategy.

	Phase 1	**Phase 2**	**Phase 3**	**Phase 4**	**Combined**
Strategy Deactivated %	100	54	44	42	53
On-Board Strategy %	-0,18	-0,22	-0,07	+0,00	-0,11

The results show that there is no big difference between the two simulations. The positive effect obtained through the EM activation is significant for comfort enhancement as it was shown in Figure 62 and Figure 64, but it is not enough to improve the vehicle's fuel economy. That was expected due to the fact that no function designed for fuel consumption reduction had been implemented. Moreover, a very scarce area of the LiC working range is used.

3.3.2. Dynamic Hybrid Control Strategy

As explained, the hybrid control strategy previously discussed works with a target SoC fixed by calibration. Consequently, the working range is limited, since the SoC is always targeting that value.

On this side, there is room for improvement, since an additional rule-based control function could be implemented, where the SoC target is determined dynamically through a function that considers the number of upshifts available and the actual vehicle speed.

The target of this activity is to improve the vehicle's fuel economy maintaining the same hardware and the same rule-based approach that has been introduced in the previous paragraphs. The idea could be to use more of the energy contained in the capacitor to support traction, so that it becomes also possible to recover more during braking phases.

However, as the main target of the strategy is comfort, a constraint is needed to always guarantee enough energy to cover the possible gear shifts that could take place depending on the gear inserted, in addition to the minimum level of energy necessary to not fail the component.

This could be achieved with a variable SoC target that, in addition to taking into account the possible gear shifts, tries to ensure energy for creeping and boost functions. This amount could be dependent on speed in order to set a target value that is low at high speed, as energy could be always recovered from regenerative braking, and a target value that is high at low and null speed, to guarantee the energy needed to activate the hybrid control functions. The target energy stored in the capacitor (i.e., the target SoC) could be established as follows, where:

- E_t is the total energy in the LiC,
- E_{min} is the minimum energy necessary for component protection, depending on the minimum voltage,
- E_{use} is the available energy for the hybrid strategy,
- E_{gear} is the energy necessary for upshifts (1st gear means the vehicle can upshift 6 times),
- E_{spd} is the remaining energy available for the additional hybrid control functions, as boost and creeping, and dependent on speed, without the E_{gear} and E_{min} component,
- E_{tgt} is the energy target of the LiC,
- $E_{kin,av}$ is the kinetic energy at the actual vehicle speed,
- $E_{kin,max}$ is the kinetic energy at the disconnection speed.

The energy necessary for upshifts varies depending on the chosen gear:

$$E_{gear} = E_{single\ upshift} \cdot n_{upshifts}$$

LXXXIV

The energy available for the additional hybrid control functions and dependent on speed may be determined as:

$$E_t = E_{min} + E_{use}$$

LXXXV

$$E_{use} = E_{gear} + E_{spd}$$

LXXXVI

So:

$$E_{spd} = E_t - E_{min} - E_{gear}$$

LXXXVII

Due to the limit on the maximum speed of the EM and the gear ratio between the EM and the wheels, the EM cannot work in the entire vehicle speed range and needs to be disengaged over a certain speed. In particular, the disconnection speed is fixed at 130 km/h. The percentage of kinetic energy available is:

$$\%_{kin} = \frac{\boldsymbol{E_{kin,av}}}{\boldsymbol{E_{kin,max}}}$$

LXXXVIII

This ratio shows the kinetic energy available at different speeds, until disconnection.

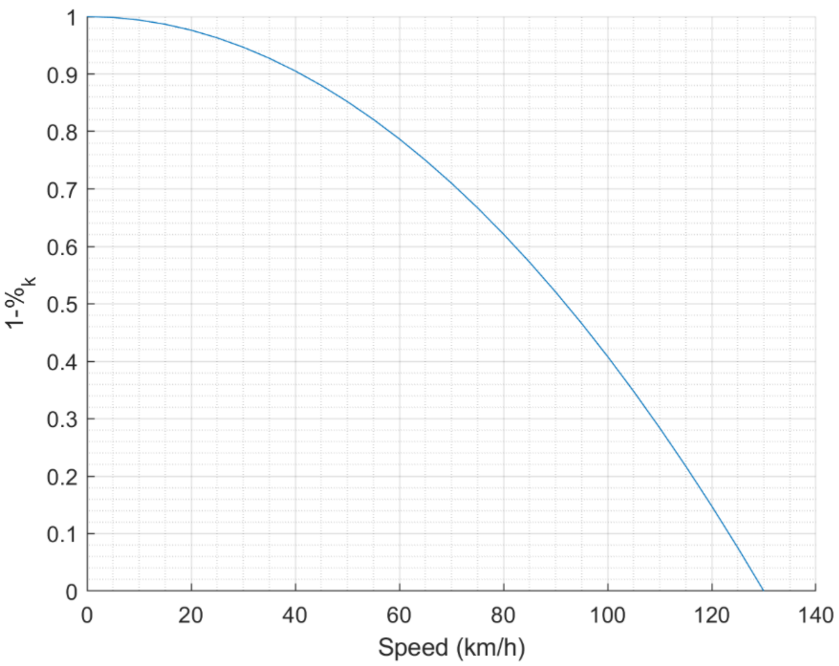

Figure 66. Percentage of energy in the LiC accumulation system at various speeds.

Since the kinetic energy can be used for recuperation, the aim is to have a fully charged LiC at null speed and a fully discharged LiC at disconnection speed.

$$E_{tgt} = E_{spd} \cdot (1 - \%_{kin}) + E_{gear} + E_{min}$$

LXXXIX

In conclusion, the scheme in Figure 67 sums up the distribution of the energy (as an example, relatively low speed is considered):

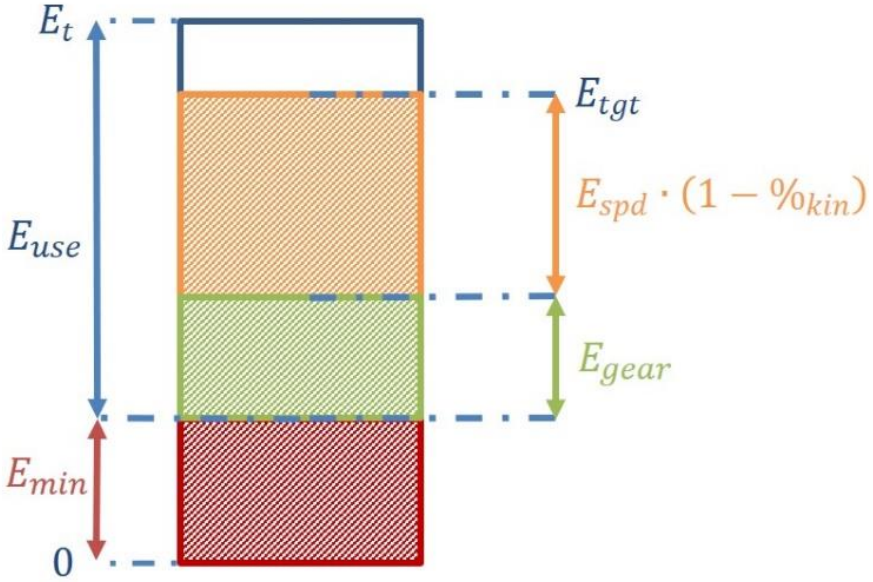

Figure 67. Energy distribution according to the new strategy block (at relatively low speed).

Further evaluations pointed out the limits for energy recuperation. The main limit is represented by the EM maximum power value in generator mode, that sets the minimum time for a completely charged LiC. In particular, in cut-off conditions (vehicle decelerating with the brake pedal released) the LiC could be fully charged, while in harsh braking conditions the EM would not guarantee enough power to recover all of the dissipated energy. If necessary, a minimum SoC value could be set according to calibration evaluations. It will fix a limit for component protection and for terminal voltage issues.

Alongside the introduction of the dynamic hybrid strategy, it could be possible to activate the EM in normal operating conditions, covering part of the ICE torque with EM torque.

A function is implemented, that provides electrical torque to power the vehicle. The function output is obtained comparing the actual SoC and the target SoC. As seen in Figure 68, the higher the actual SoC is compared with the target SoC value, the higher the torque that the EM can provide to the wheels.

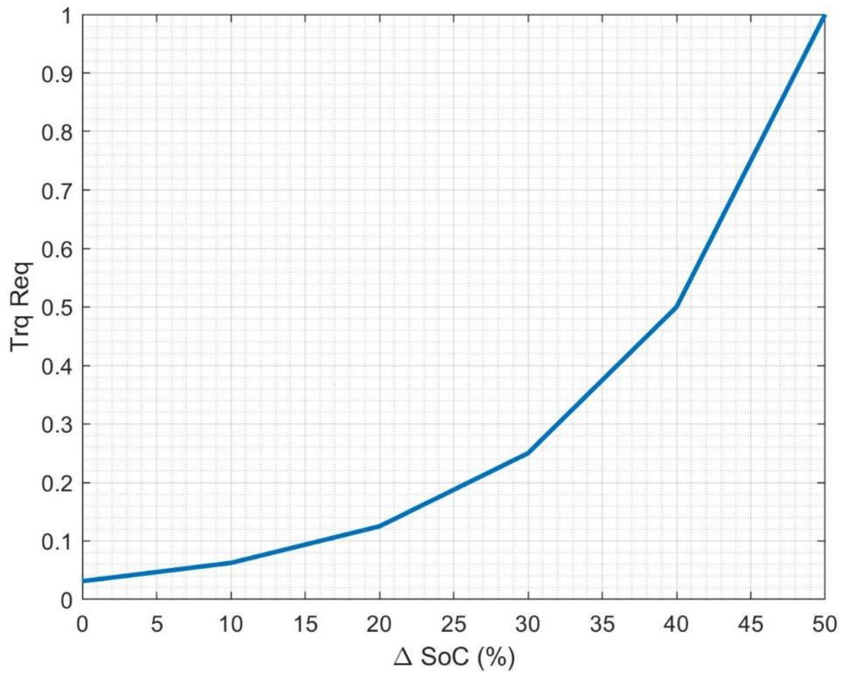

Figure 68. Normalized value of the torque request.

The modifications introduced in the dynamic hybrid control strategy take into account the possibility to implement load point shift strategies. The ICE torque is then corrected according to the electric torque contribution.

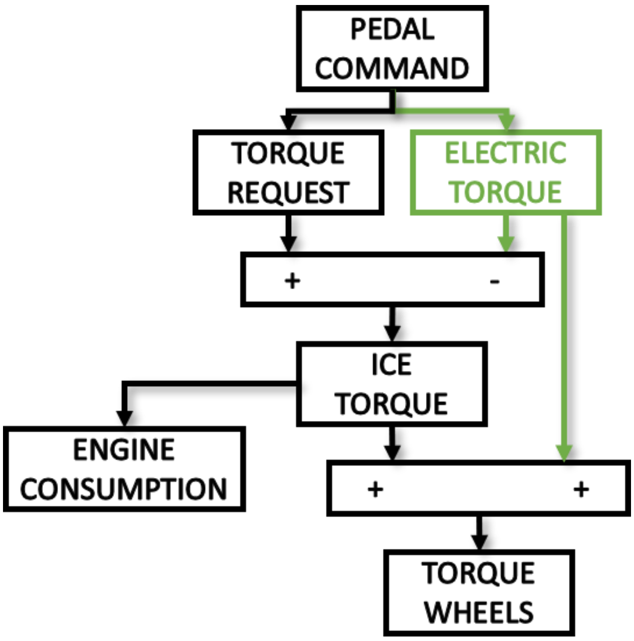

Figure 69. Torque and fuel consumption determination according to the modified strategy.

3.4. Second Architecture, RBS and ECMS

The second vehicle that has been modeled was introduced in 2.4, it is characterized by the presence of two EMs in P3-P4 or P2-P4 position and by an energy storage system initially composed solely of LiCs and subsequently by a HESS. This chapter focuses on hybrid control strategies that target fuel economy applied to that kind of vehicle.

MATLAB/Simulink allows the user to design various configurations and to activate only the desired one while keeping the others disabled. This is possible thanks to the Variant Subsystems [122], where the active choice is determined by the variant control, which can be a Boolean expression or a string. The decision to work with a Variant Subsystem (Figure 70) allows the user to choose the control strategy directly from the MATLAB environment, without necessarily entering Simulink. This means that the model is more easily accessible even to users who have not participated in the design of the model itself. Any unwanted changes in the Simulink environment could generate major problems, especially if the model is shared between users and departments. This is avoided when the model configuration selection is done via MATLAB.

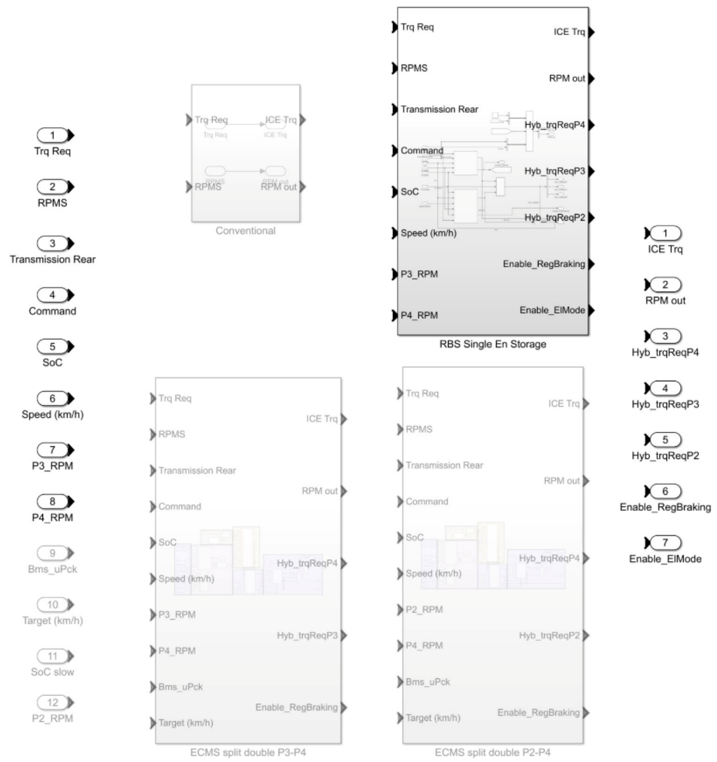

Figure 70. Simulink variant subsystem model for the hybrid control strategy choice.

In this regard, a GUI could be implemented to further facilitate operations for users who are not familiar with the software.

3.4.1. Rule Based Strategy

As shown in Figure 71, the main target of the RBS developed for the second architecture is to make the vehicle work in electric drive mode as soon as the electrical energy storage is full, i.e., the battery SoC reaches a value of 90%. Every time the electric drive mode is activated, the fuel consumption is reduced to the minimum, as the ICE can be shut down or it can work in idle conditions.

The strategy is activated only if the EMs are capable to apply all the power at the wheels that the ICE was delivering. If that condition is not met, the electric driving will not be possible.

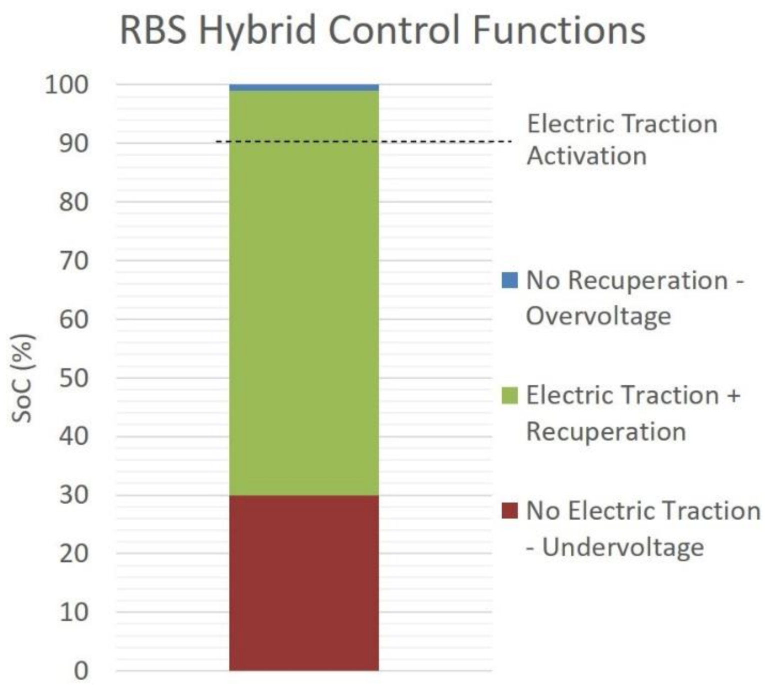

Figure 71. RBS control functions' activation range.

As it can be seen from Figure 71 the energy storage system can be discharged until a minimum SoC value chosen from calibration (i.e., SoC = 30%). When this value is reached, the electric driving mode is stopped, and only the regenerative braking function is kept active.

The SoC is not the only control variable of the strategy, the EMs speed and the torque request are also kept into account, as they will be compared with their corresponding limit values.

The feasibility of the pure electric mode activation has been analyzed, and the possibility to work with the ICE in shut down conditions has been discarded. If the ICE were to be turned off, we would have issues with the lubricant flow on the friction and on the heating of the powertrain components. Other issues would have been generated by the speed difference between the clutch and the gearbox components when the ICE reconnection takes place.

Then, the ICE will be kept in idle conditions, guaranteeing low fuel consumption values, and allowing the clutch and gearbox to work in conditions that do not heavily stress the mechanical components.

The strategy will be activated after the warm-up phase of the after-treatment system on the WLTC Class 3b to guarantee the usual heating strategy for the after-treatment components.

The warm-up phase of the WLTC Class 3b represents one of the most controversial intervals for the fuel consumption analysis. The introduction of the hybrid control strategy would necessarily generate changes in vehicle behavior during this starting phase. These changes are unpredictable, and it is very difficult to simulate them accurately. The decision to maintain the same behavior as the conventional vehicle guarantees the reduction of possible errors to the minimum since the results are analyzed as a comparison between cycle simulations.

3.4.2. Equivalent Consumption Minimization Strategy

The ECMS is designed (as shown in the diagram of Figure 72) to improve the power flow distribution to the wheels. During braking, the regenerative braking control function from the RBS will be maintained, and the strategy will also keep into account the delayed activation due to the catalyst heating.

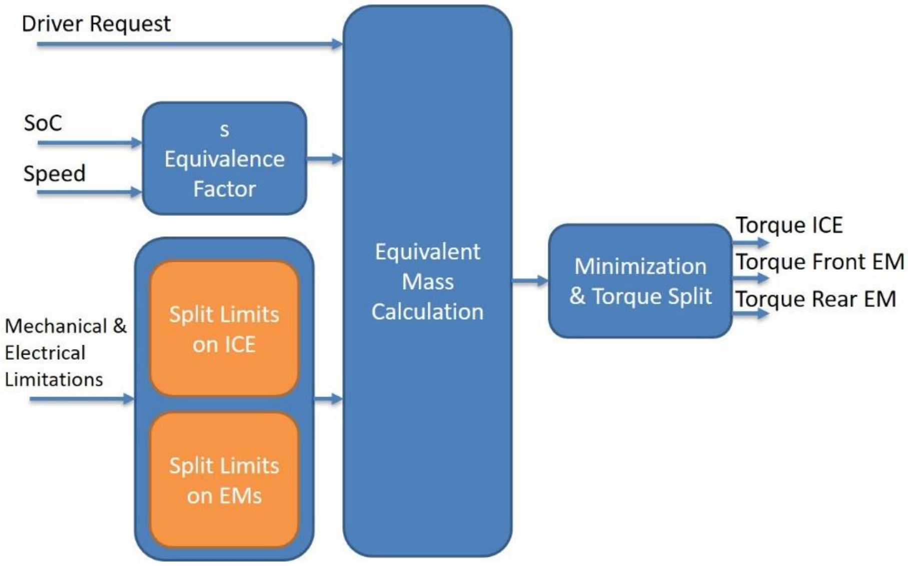

Figure 72. Equivalent Consumption Minimization Strategies (ECMS) Scheme.

Split Factor (u)

The control variable for this kind of strategy is u, the torque split factor between ICE and EMs. Once the torque working range is defined, both for the ICE and the EMs, the u factor that minimizes the equivalent fuel consumption is sought. The torque request must be fulfilled by combining the 2 power sources.

$$T_{REQ} = T_{ICE} + T_{HY}$$

XC

The torque split factor u is defined as follows:

$$T_{ICE} = (1 - u) \cdot T_{REQ}$$

XCI

$$T_{HY} = u \cdot T_{REQ}$$

XCII

The split factor u working window (Table 8), and consequently the ICE and EMs torque working window, are determined at each integration step through the EMs, ICE, and battery limits.

Table 8.Split factor u complete working range.

Split factor u	Driving Mode
u = 1	Electric Drive and Regenerative Braking
0 < u < 1	Hybrid Boost Operation
u = 0	ICE only
−n < u < 0	Battery Recharge (ICE load point shift)

Once the u working window is defined, it is discretized in 20 evenly spaced intervals to guarantee a fixed-size simulation array. The variable discretization that was chosen guarantees a real-time simulation.

Split Factor (hy)

Secondly, the torque fraction T_{HY} is split between the 2 EMs. The electrical limitations impose an operational range for the 2 EMs that must be considered. Hypothetically, we could decide to deliver all the electrical torque with the front EM instead of the rear one or vice versa. The hy factor (Table 9) will define the split.

$$T_{HY} = T_{FRONT} + T_{REAR}$$

XCIII

The torque split factor hy is defined as follows (apart from the transmission ratios):

$$T_{REAR} = (1 - hy) \cdot T_{HY}$$

XCIV

$$T_{FRONT} = hy \cdot T_{HY}$$

XCV

Table 9.Split factor hy complete working range.

Split factor hy	Electric Traction Mode
hy=1	Front Traction
0 < hy < 1	Torque Split
hy = 0	Rear Traction

Once the working window is defined, it is discretized in evenly spaced intervals, to guarantee a fixed-size simulation array. The variable discretization that was chosen guarantees a real-time simulation. The combination of the u and hy vectors will define a matrix of possible torque values, and subsequently of equivalent fuel consumption, from which the minimum value that satisfies the optimality criterion will be extracted.

Equivalent Fuel Consumption

The ECMS aims to identify the best power flow distribution between the energy converters at every integration step, such that the optimality criterion that has been chosen is achieved. At first, a global cost function is defined, that considers the usage of both the ICE and the EMs to power the vehicle. Their contribution is evaluated through the calculation of the equivalent consumption value, at every integration step, defined as follows:

$$\dot{m}_{eq} = \dot{m}_f + \dot{m}_{bat}$$

XCVI

where $\dot{m}_{eq}$ [g/s] is the equivalent fuel consumption flow, $\dot{m}_f$ [g/s] is the fuel consumption and $\dot{m}_{bat}$ [g/s] is the electrical energy equivalent consumption. $\dot{m}_f$ can be determined through interpolation of fuel consumption maps during the simulation of the longitudinal dynamics model, while the $\dot{m}_{bat}$ value will be calculated based on the electrical power request and to the cost function, which depends on the equivalent cost and on the system's working point.

The Lower Heating Value (LHV) [J/g] will divide the power request to the battery to convert, using the equivalent factor s, electrical energy into virtual fuel consumption.

$$\dot{m}_{bat} = s \cdot \frac{P_{bat}}{LHV}$$

XCVII

Consequently,

$$\dot{m}_{bat} = \frac{s}{LHV} \cdot \sum_i P_{EM,i} \cdot (\gamma_i \cdot \frac{1}{\eta_{EM,i}} + (1 - \gamma_i) \cdot \eta_{EM,i})$$

XCVIII

where η_{EM} is the efficiency of the EM, P_{EM} is the power request to the EM and γ is the factor that allows to properly evaluate if the EM is working as a generator (P_{EM} <0) or as an electric motor (P_{EM} >0), and it is defined as follows:

$$\gamma = \frac{1 + sign(P_{EM})}{2}$$

XCIX

This formulation can be easily implemented into the longitudinal dynamics model. The minimization of the equivalent fuel consumption $\dot{m}_{eq}$ brings along the definition of the power flow distribution between ICE and EM, as the T_{ICE} and T_{HY} pair is defined. The general formulation of the minimization problem refers to any kind of energy storage system and can be found in [11,117]. Defining ξ as the SoC, u the control variable, Q_{bat} the battery charge capacity, I_{bat} the battery current:

$$\dot{\xi}(t) = f(\xi, u, hy, t) = -\frac{I_{bat}(\xi, u, hy, t)}{Q_{bat}}$$

C

It is possible to define the Hamiltonian of the optimal control problem:

$$H(\xi, u, hy, \lambda, t) = -\lambda(t) \cdot f(\xi, u, hy, t) + \dot{m}_f(u, t)$$

CI

$$\dot{\lambda}(t) = -\lambda(t) \frac{\partial f(\xi, u, hy, t)}{\partial \xi}$$

CII

Thus, the Hamiltonian is the total equivalent fuel consumption. Introducing $s(t)$:

$$s(t) = -\lambda(t) \frac{LHV}{P_{bat}(t)}$$

CIII

At the end:

$$H(\xi, u, \lambda, hy, t) = \dot{m}_{eq}(\xi, u, hy, s, t) = s(t) \cdot \frac{P_{bat}(t)}{LHV} \cdot f(\xi, u, hy, t) \ldots + \dot{m}_f(u, t)$$

CIV

The optimal control satisfies:

$$u^*(t) = \underset{u}{\operatorname{argmin}}\, H(\xi, u, \lambda, t)$$

CV

The optimal control depends on $s(t)$, but its value is unknown a priori, thus the strategy is sub-optimal.

Battery Energy Cost Function (s)

The s factor indicates the cost of the electrical energy; it is dependent on the system's working conditions and in the present dissertation the following formulation has been adopted, to guarantee the respect of SoC limits and to track the SoC target [11,14]:

$$s = \left\{ 1 - k_p \cdot \left[\frac{SoC - \left(\frac{SoC_{max} + SoC_{min}}{2} \right)}{\left(\frac{SoC_{max} - SoC_{min}}{2} \right)} \right]^3 \right\} \cdot [k_a \cdot (SoC_{target} - SoC)]$$

CVI

The cost function is calculated at every integration step, and when its value is high, it makes it preferable to use the engine and recharge the battery, while if it is low, it makes the electric traction preferable.

The curly brackets contain a penalty term that modifies the s value when the SoC is near to the maximum or minimum acceptable values, making the electrical energy cost, respectively, lower, or higher. On the other hand, the second term is a proportional correction obtained considering the difference between the target value of the SoC, and the actual one.

The parameters k_p and k_a are calibrated with subsequent adjustments. Initial values based on literature [11] are chosen to perform a simulation, and these are subsequently modified to better fit the admissible SoC working range and to minimize the gap between actual and target SoC. Their value choice is decisive for the simulation results, as it directly impacts the cost function and consequently, the hybrid performance and the fuel consumption.

For this application, the electrical energy is low-cost since the LiC energy storage is a high-power system, and it can be charged and discharged rapidly. The values of the calibrated parameters are chosen accordingly.

The choice to work with a constant value is the simplest one, and it makes the strategy a Charge Sustaining (CS) one. Other possibilities that are commonly used for Li-ion Batteries-based vehicles are represented by the Charge-Depleting/Charge Sustaining (CD/CS), which firstly discharges the battery until a certain SoC value and then keeps the value around a target SoC, or the Charge-Blended (CB), which follows a SoC target that linearly decreases with the driven distance [11]. The calibrated parameters k_p and k_a could be kept the same when changing the vehicle mission and the control strategy. On the other hand, the calibration process could be run every time the control strategy is modified, to determine k_p and k_a that better fit the vehicle behavior and better adapt to the SoC variations. In any case, sensitive changes are expected only when the strategy undergoes significant modifications (for example moving from a constant SoC target as in a CS to a SoC target dependent on speed), otherwise only small variations are expected.

The present work is based on a LiC-based super sport car, and an alternative SoC target is formulated similarly as it has been previously done. According to LXXXIX, the SoC target is a speed-dependent quantity related to the detachment speed value of the EM (in this application it has been set equal to 190 km/h, the detachment speed of the front EM).

The SoC target was high at low speeds, as the kinetic energy was low, and this solution guaranteed a high energy quantity stored in the electrical system. On the other side, the SoC target was low at high speeds since energy was already existing in the form of kinetic energy that could be rapidly recovered through the EM. Moreover, if we were to have high electrical energy at high speed, the energy content would end up unused once the detachment speed was reached.

Since the detachment speed of the EM is now greater than the first vehicle configuration (where the P3 EM disconnected at 130 km/h), the dependency of the SoC target on speed is also modeled differently. If we were to keep a quadratic dependency as in Figure 66, the working range of the energy storage would be limited on a WLTC Class 3b, in fact at the maximum cycle speed we would have:

$$SoC_{target,min} = \left(1 - \left(\frac{132}{190}\right)^2\right) \cdot 100 = 52\%$$

CVII

This means that the SoC target would span between 52% and 100%, limiting the working range of our system. So, a linear dependency is adopted here to better fit the complete SoC range.

As already said, this alternative SoC target formulation, represented in Figure 73 for a WLTC Class 3b, is thought to fit better the behavior of LiCs that dispose of a high charge and discharge rate, and which can perform a high number of cycles [120,121].

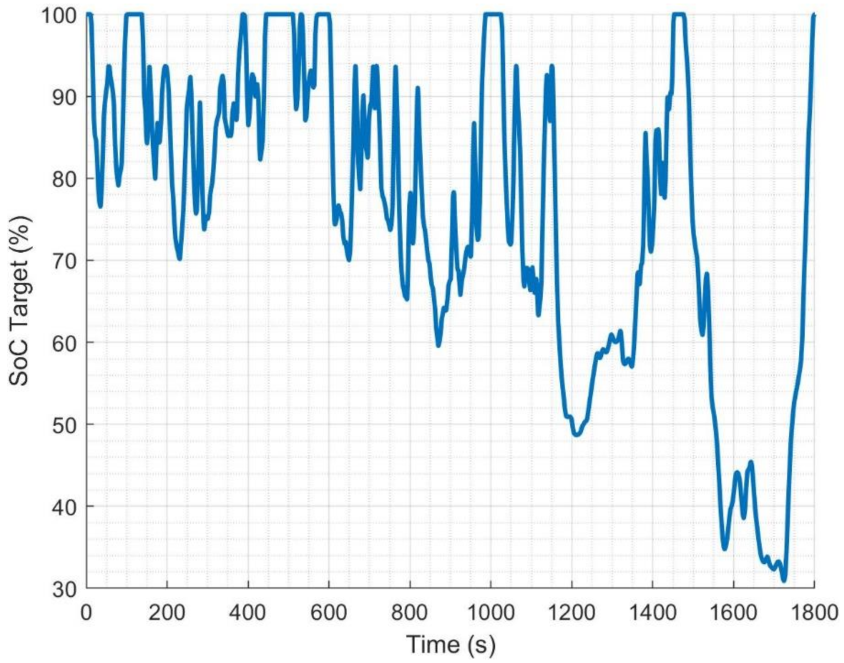

Figure 73. Speed-dependent state of charge (SoC) target profile for a WLTC Class 3b.

The purpose of this approach is to avoid unused energy and to maintain high energy content where it is mostly needed, ensuring the satisfaction of performance or drivability requests, important objectives for a super sports car. Different control functions can therefore be implemented to guarantee improvements in performance and drivability, especially at low speeds.

4. Results

This chapter illustrates the simulations that have been run on the various vehicle architectures, with a focus on fuel economy. The simulations aim to illustrate how the super sport car behaves as a result of a hybridization process, by describing its longitudinal dynamics on emission cycles. The model allows to study in detail each component and to act freely on the control of the system. The results in terms of fuel consumption and performance are used as a benchmark to assess the characteristics of the car in the initial concept phase.

The target of the work is to define which energy storage system's technology and which control strategy best suit the needs of the hybrid super sport car.

As explained in 2.2, the first vehicle configuration is based on a Lamborghini Aventador, while the second and third configurations are based on a Lamborghini Aventador SVJ. Both the conventional vehicle models will be simulated on a WLTC Class 3b and the results obtained for fuel consumption will be used as a reference, respectively for the first and the second vehicle configuration. Then, the results for the simulations with the active hybrid control strategies were reported as a fuel consumption comparison.

The WLTC Class 3b phases are defined as follows, as illustrated in [44] and shown in Figure 22:

- Phase 1: 0–589 s
- Phase 2: 590–1023 s
- Phase 3: 1024–1478 s
- Phase 4: 1479–1800 s

The tables reporting the results show in the first line the conventional vehicle simulation, while in the following lines, they show the simulated results for the various hybrid configurations.

The fuel consumption simulated results for the conventional vehicle were normalized (%) with respect to the maximum fuel consumption value obtained during the various cycle phases. As it has been shown in the previous chapters, Phase 1 was usually associated with the maximum value (i.e., 100%) since the engine works in cold-start conditions and at high fuel consumption operating points.

The simulated results for the hybrid vehicle configurations were reported as a fuel consumption comparison with the standard production vehicle, showing the percentage reduction.

4.1. First Configuration, single EM LiC-based

As explained in 3.3, the hybrid control strategy priority continues to be the passengers' comfort, moreover the energy content of the LiC is estimated to be 6% of the content of a Lithium-Ion Battery of the same volume (approximately 6L) typically used in automotive industry.

Due to these considerations, only small fuel consumption improvements are expected. Micro [123] and mild-hybrid technologies can reach approximately 16% fuel economy [124–127], Audi claims that the A8 mild hybrid technology is capable to recover up to 0,7 L/100km in real driving conditions (press released values), but none of these results refer to applications based on LiCs. However, they can represent a starting point for the comparison with existing hybrid technologies.

Figure 74 shows a simulation run on a WLTC Class 3b for the first vehicle configuration. The strategy introduced in 3.3.1 has been already tested also for fuel consumption as it can be seen in Table 7, it will be called 'On-Board Strategy'. On the other side, the strategy introduced in 3.3.2 is now tested on WLTC Class 3b simulations, and it will be called 'Dynamic Strategy'.

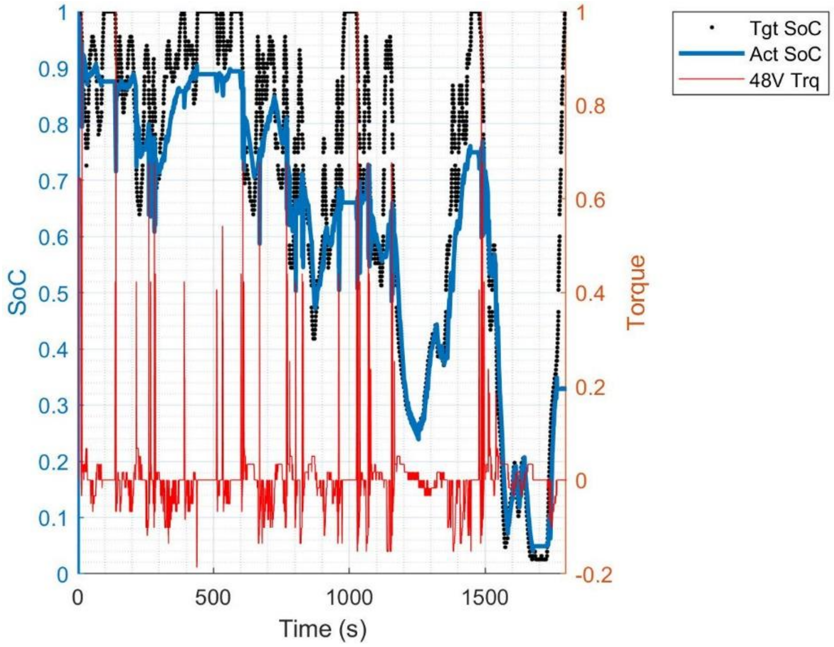

Figure 74. WLTC Class 3b simulation with a Dynamic Strategy.

At the start of Phase 1 the LiC is fully charged, SoC=99%. During this phase, the EM torque is overall positive, and less ICE torque is required to cover the torque request. During Phase 2 the SoC value is still high and the SoC target lowers due to higher speeds. The electrical energy available will help to cover the torque request and good improvements in the fuel economy are expected. At the end of this phase the SoC is quite low.

During Phase 3 the speed gets higher than before, the SoC target is lower and more electrical energy is available. However, due to the activity of Phase 2, a small amount of energy is available and recovering functions will be activated. Overall, the electrical effect on fuel consumption could be negative since more ICE torque is required to charge the LiCs.

Due to the energy recovered in Phase 3 and due to the highest speeds in the cycle, during Phase 4 a lot of EM energy is available and good fuel economy improvement is expected.

Table 10. WLTC Class 3b fuel consumption simulated results, for the Lamborghini 48V hybrid configuration with on-board strategy and dynamic strategy.

	Phase 1	Phase 2	Phase 3	Phase 4	Combined
Strategy Deactivated %	100	54	44	42	53
On-Board Strategy %	-0.18	-0.22	-0.07	+0.00	-0.11
Dynamic Strategy %	-0.79	-1.56	-0.34	-0.77	-0.83

Table 10 shows the results from Table 7 and, in addition, it shows the results referred to a Dynamic Strategy. The introduction of the Dynamic Strategy shows an improvement of about 1% through the cycle and the fuel consumption reduction reaches up to 0.3 L/100km.

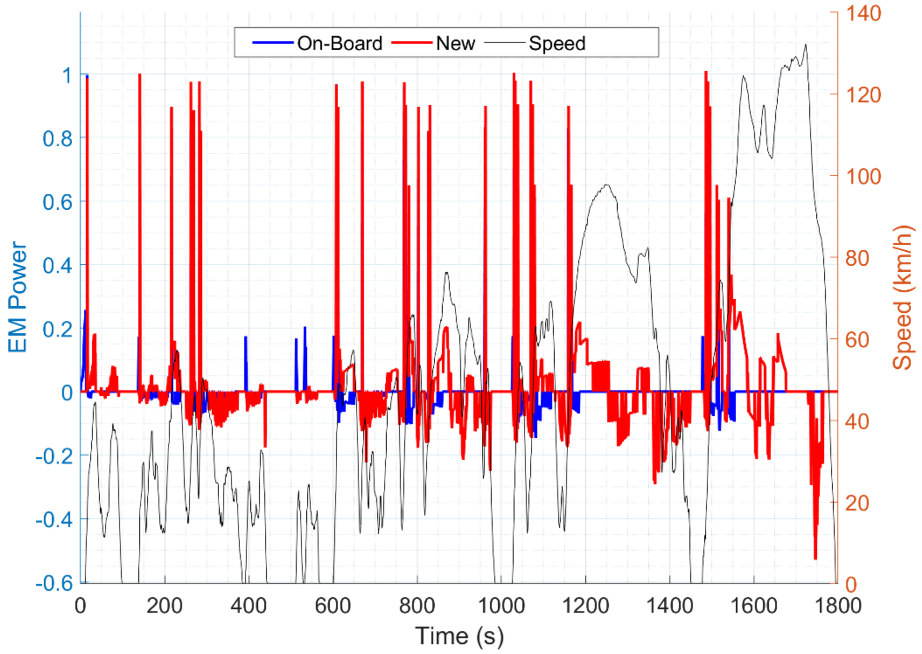

Figure 75. Comparison of power provided by the electric motor during WLTC Class 3b.

The comparison between the On-Board Strategy discussed in 3.3.1 and the Dynamic Strategy from 3.3.2 highlights a more frequent activation of the EM, without giving up the comfort target that is guaranteed by the torque gap covering.

However, the results that are reported in Table 10 do not consider the SoC variation that takes place between the initial SoC and the final SoC. In particular, from Figure 74 is evident that the final SoC is much lower than the initial one, meaning that the electrical energy that has been used during the cycle has not been recovered. This means that the results presented in Table 10 are not fully representative of the vehicle's fuel consumption.

So, a new simulation is run with the constraint to guarantee a final SoC equal to the initial one or slightly greater. The reason why a final SoC higher than the initial one is here accepted is that the energy stored in the LiCs system is low, therefore the impact of a variation of SoC (if small) is considered negligible.

The analysis is completed running a WLTC Class 3b immediately after the first one, with the hypothesis of a starting SoC equal to the final SoC (=32%). Differently from before, during the first phase the LiC accumulation system is recharged to reach SoC values compatible with the SoC target.

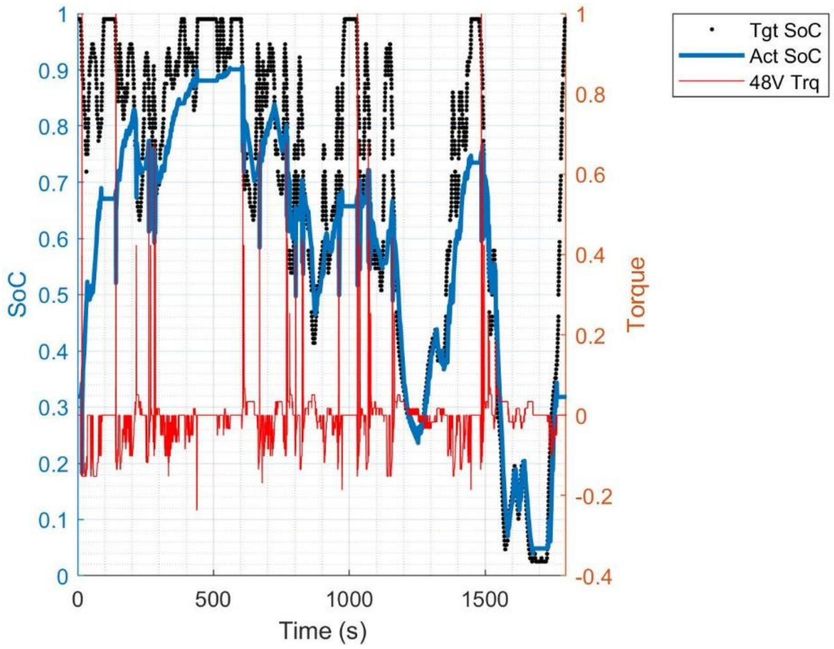

Figure 76. WLTC Class 3b simulation for a Dynamic Strategy with a starting SoC equal to the final SoC.

Table 11. WLTC Class 3b fuel consumption simulated results, for the Lamborghini 48V hybrid configuration with dynamic strategy and starting SoC equal to the final SoC.

	Phase 1	Phase 2	Phase 3	Phase 4	Combined
Strategy Deactivated %	100	54	44	42	53
Dynamic Strategy %	+0.38	-1.56	-0.34	-0.77	-0.56

As expected, the first phase produces a different result from Table 10, but the overall trend is consistent and produces an improvement on fuel consumption during the cycle.

As it has been said, the fuel consumption results for super sport cars are significantly high, since the engine displacement is big, and therefore the percentage improvements on fuel economy are quite low. Further evaluations are made through simulation, modifying the engine displacement and its performance, in order to evaluate the impact of the hybrid control strategy and the LiC hybrid architecture on a smaller engine. The displacement is supposed to be half (3.25 L) of the actual value. At the same time, the torque values and the engine frictions will be reduced to a half.

Table 12. WLTC Class 3b fuel consumption simulated results, for the half displacement hybrid configuration.

Half Displacement	Phase 1	Phase 2	Phase 3	Phase 4	Combined
Dynamic Strategy %	-1.48	-2.30	-0.38	-1.30	-1.37

The results show that the hybrid control strategy applied to the smaller engine configuration can get a steady improvement on the fuel consumption that goes up to 1.4% on the combined value for the WLTC 3b cycle.

The results are compared to the ones from hybrid vehicles commonly available on the market. According to these, the Lamborghini application falls within the sphere of micro-hybrid systems [123].

4.2. Second Configuration, 2 EMs LiC-based

The second vehicle configuration introduced in 2.4 is now tested on a WLTC Class 3b, and the hybrid control strategies that are used are the ones introduced in 3.4. Both the P3-P4 and the P2-P4 configurations are tested, first with respect to the RBS and then with respect to the ECMS.

4.2.1. Fuel Consumption Correction

As it was explained in the previous paragraph, the simulations will be considered acceptable if the final SoC of the LiCs' pack is equal or greater than the initial one. This is due to the fact that the energy stored in the LiCs' system is low, therefore the impact of a variation of SoC (if small) is considered negligible. However, it could happen that the variation of SoC between the final and initial one is not small and therefore not negligible. To this aim, a fuel consumption correction is carried out, based on the procedure implemented in [11] and explained below.

During the cycle, the energy requested at the wheels can be delivered by the ICE or the EMs since we are working with a hybrid vehicle, therefore two different situations can occur as the energy balance at the end of the cycle, expressed as ΔeC [kJ], could be positive or negative, i.e. the energy storage SoC at the end of the cycle is higher or lower than the initial value.

In the first scenario, it is assumed that the positive difference of the electric energy is covered by the ICE, consuming more fuel than required and recharging the energy storage systems through the EMs that are acting as generators. This means that on the right side of CVIII the EM efficiency is at the denominator because the energy content in the energy storage is lower than the starting energy content coming from the fuel. The virtual fuel consumption (to be subtracted to the actual one) is calculated using the average efficiencies of the machines, as shown in the following equation:

$$\Delta m_{fuel} \cdot LHV \cdot \bar{\eta}_{ICE} = \frac{\Delta eC}{\bar{\eta}_{EM}}$$

CVIII

Where LHV is the lower heating value of the fuel, and $\bar{\eta}_{ICE}$ and $\bar{\eta}_{EM}$ are the average efficiencies, respectively for the ICE and the EM.

In the second scenario, with a negative electrical energy balance, the difference is considered as a further request of torque addressed to the EMs instead of using the ICE. Therefore, it is possible to calculate the additional fuel consumption to be added to the actual one, to compensate the battery balance. The formulation is expressed as follows:

$$\Delta m_{fuel} \cdot LHV \cdot \bar{\eta}_{ICE} = \bar{\eta}_{EM} \cdot \Delta eC$$

CIX

Here, the EM efficiency on the right side of CIX multiplies the energy content of the energy storage since the EM is working as a motor, meaning that the energy content of the energy storage is higher than its equivalent in fuel energy. The fuel consumption correction is used to correct the combined final value of the various simulations. When the correction is applied, it will be properly reported.

4.2.2. RBS

At first, the RBS simulations were run, and the results were reported following the indications previously described. Table 13 and Figure 77 show the simulation results for the configuration P3 – P4, while Table 14 and Figure 78 are relative to the configuration P2 – P4.

Table 13.WLTC Class 3b simulated results, for a P3-P4 architecture with an RBS.

FC Reduction % 60s1p	Phase 1	Phase 2	Phase 3	Phase 4	Combined
Simulated %	100	54	43	41	52
RBS P3–P4	−0.8	−5.4	−1.9	+0.0	−1.8

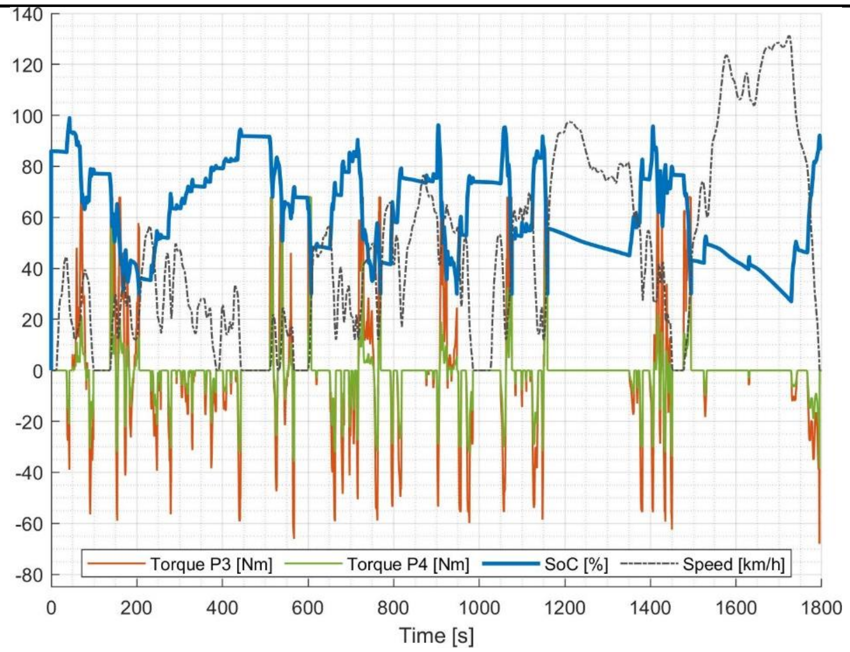

Figure 77. SoC and Torque profiles for P3–P4 RBS.

The powertrain system behaved as expected, allowing the activation of the electric mode when the SoC of the pack goes over the target value. During the energy storage recharge, the vehicle will be powered exclusively by the ICE.

Table 14.WLTC Class 3b simulated results, for a P2-P4 architecture with an RBS.

FC Reduction % 60s1p	Phase 1	Phase 2	Phase 3	Phase 4	Combined
Simulated %	100	54	43	41	52
RBS P2–P4	−1.2	−7.1	−2.7	+0.6	−2.3

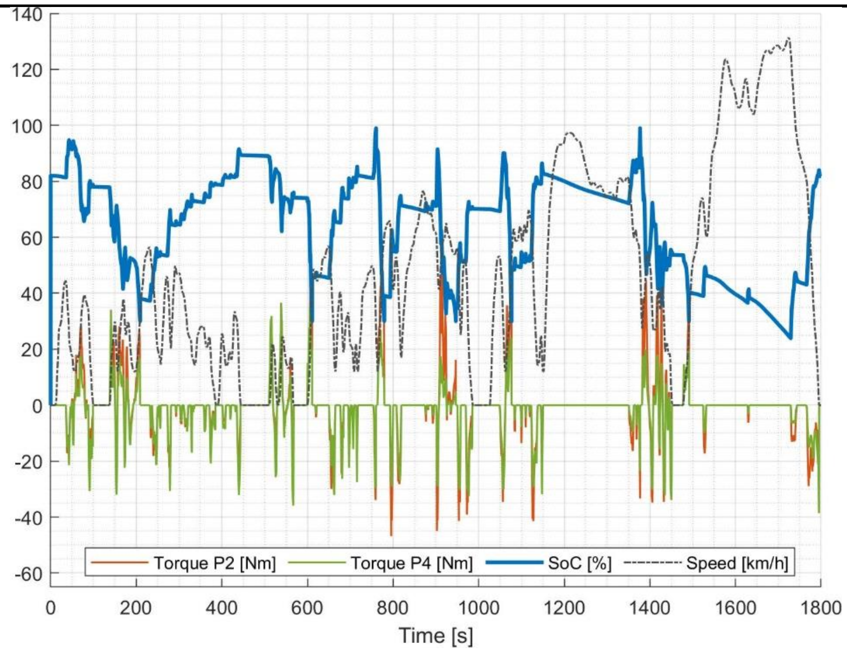

Figure 78. SoC and Torque profiles for P2–P4 RBS.

Both simulations show how the storage system recharged quickly, guaranteeing multiple discharges related to electric driving during the cycle.

Figure 79 reports the speed of both the P3 and P2 EMs during the WLTC Class 3b. Due to the different transmission ratios, the speed profiles were different.

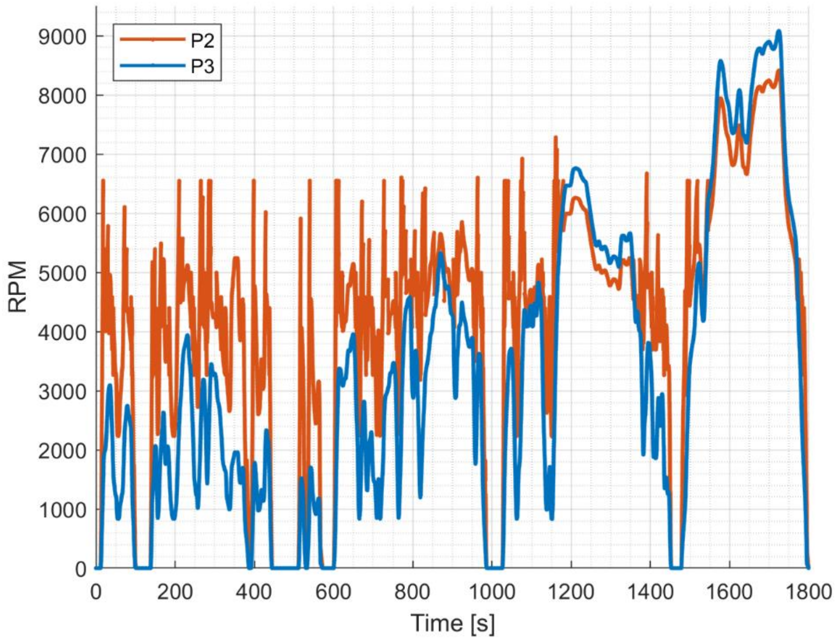

Figure 79. EM RPM comparison.

The results show an improvement in fuel economy, the RBS can reduce fuel consumption by up to 2.3%. In particular, the choice to work with a P2 instead of a P3 seems profitable.

As shown in Figure 79, the P2 and P3 EMs run at different speeds, since their gear ratio is different. In particular, the P2 EM can meet the torque demand at the wheels through a lower torque (and so a lower power consumption) with respect to the P3 EM, since its transmission ratio is higher overall. On the other hand, the P2 EM typically runs at speeds that are higher than the ones of the P3 EM, this has the opposite effect of generating a higher power consumption.

The effects are mixed, and they strictly depend on the EMs' maps that have been introduced in the model. However, for the RBS simulations, the P2 configuration is proficient. This is possible thanks to the fact that eventually the P2 EM requests less power, resulting in lower energy consumption and meaning that more time can be spent in electric drive mode. Consequently, different results for fuel consumption are generated in the two configurations, rewarding the case of P2–P4.

4.2.3. ECMS

The following simulations allow evaluating the impact of the ECMS, always according to the previously introduced indications. Table 15, Figure 80, and Figure 81 show the results for the configuration P3 – P4, while Table 16, Figure 82, and Figure 83 show the results for the configuration P2 – P4.

Table 15. WLTC Class 3b simulated results, for a P3-P4 architecture with an ECMS.

FC Reduction % 60s1p P3–P4	Phase 1	Phase 2	Phase 3	Phase 4	Combined	Corrected
Simulated %	100	54	43	41	52	\
ECMS CS 50%	−4.7	−6.5	−4.8	−0.8	−4.0	−5.2
ECMS Spd	−3.9	−8.2	−5.2	−2.7	−4.8	\

The ECMS results show a significant improvement in fuel economy, both for the CS and Spd Dependency hypothesis.

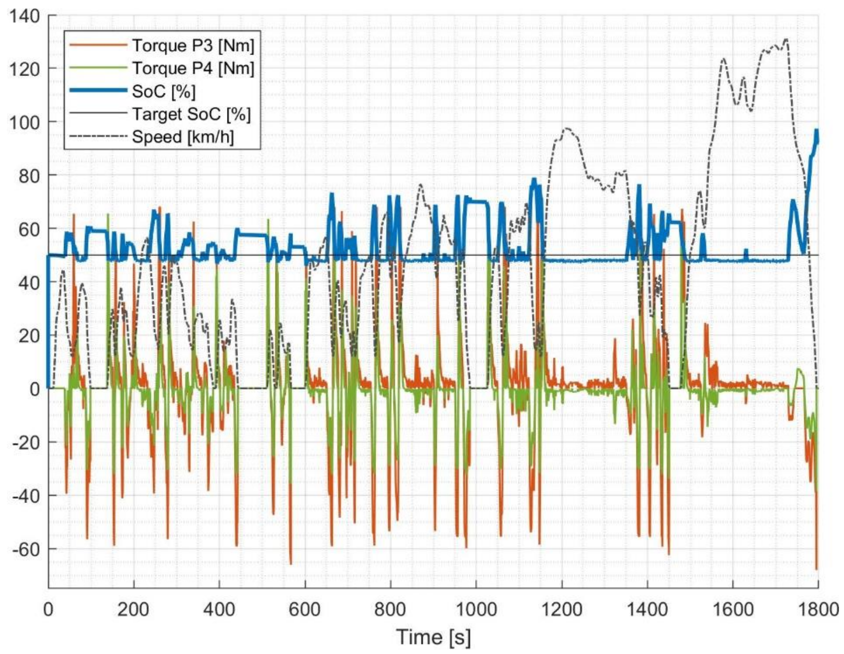

Figure 80. ECMS simulation for P3–P4 with an SoC target equal to 50%.

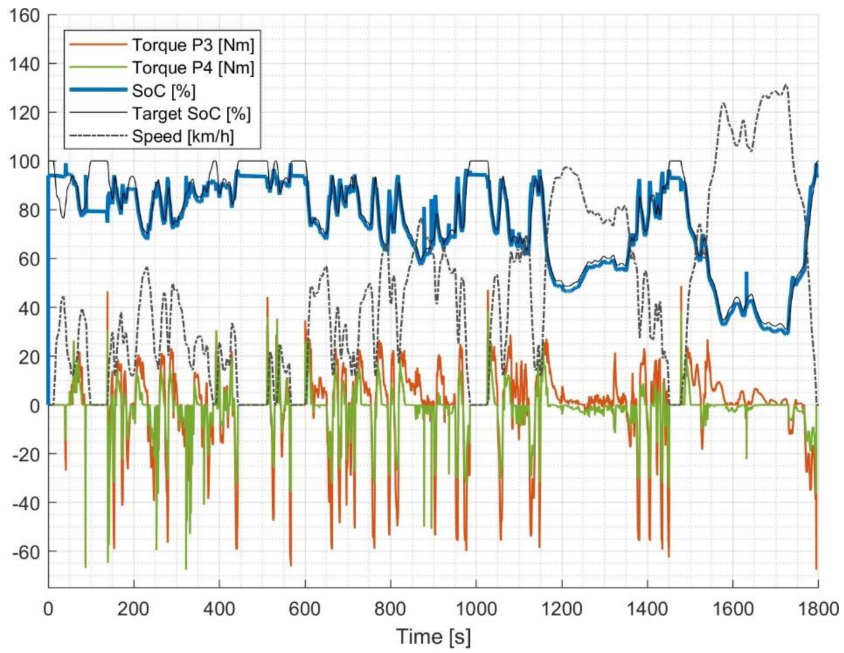

Figure 81. ECMS simulation for P3–P4 with an SoC target depending on speed.

The same simulations were run on the P2–P4 configuration as it has been done for the RBS.

Table 16. WLTC Class 3b simulated results, for a P2-P4 architecture with an ECMS.

FC Reduction % 60s1p P2–P4	Phase 1	Phase 2	Phase 3	Phase 4	Combined	Corrected
Simulated %	100	54	43	41	52	\
ECMS CS 50%	−4.7	−6.4	−4.9	−1.0	−4.1	−5.4
ECMS Spd	−2.3	−7.9	−5.1	−2.7	−4.3	\

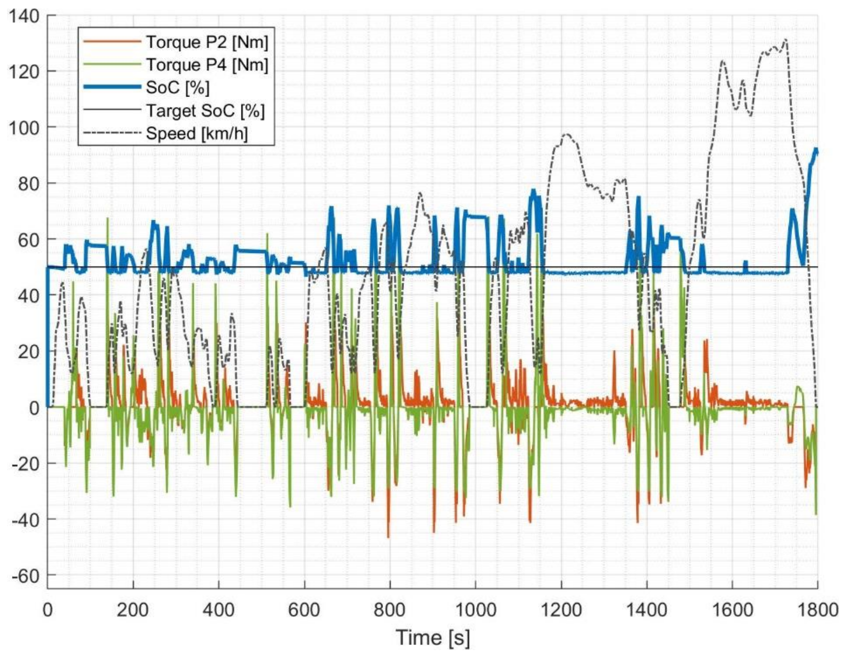

Figure 82. ECMS simulation for P2–P4 with an SoC target equal to 50%.

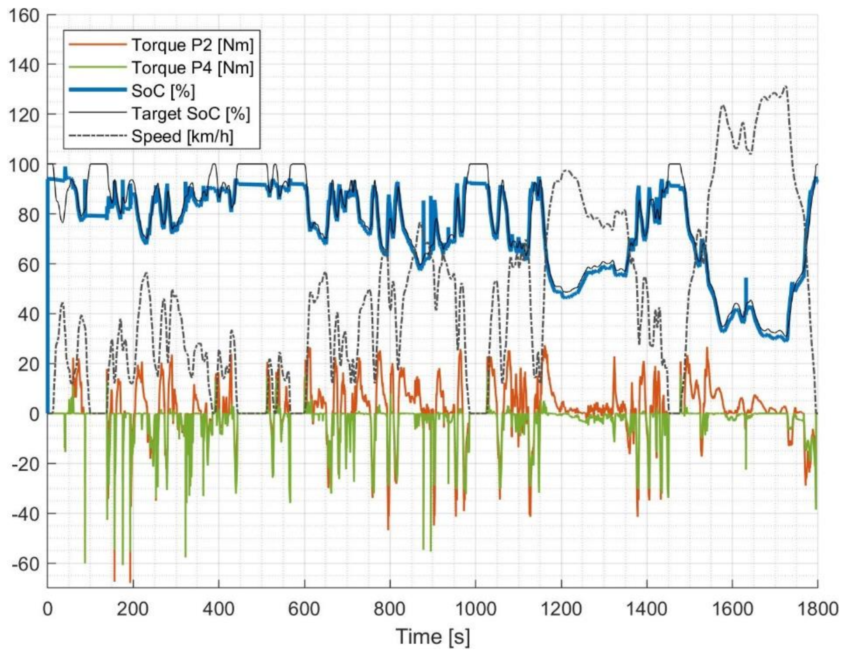

Figure 83. ECMS simulation for P2–P4 with an SoC target dependent on speed.

The CS calibration was tuned to guarantee an SoC value close to the target one at every instant. On the other side, the speed dependency configuration will guarantee a greater variability of the SoC, keeping space for any evaluations on performance or drivability. The ECMS simulations show that both P2-P4 and P3-P4 configurations can achieve fuel economy, in particular the P2-P4 is the most efficient in ECMS CS mode.

4.2.4. Half Displacement Results

Further evaluations were made through simulation, also in this case by modifying the engine displacement and its performance, to evaluate the impact of the hybrid control strategy and the LiC hybrid architecture on a smaller engine.

In particular, the RBS P2–P4, ECMS CS 50% P2-P4, and ECMS speed-dependent P3–P4 were simulated, as these represented the best solutions for the various control strategies. A conventional vehicle with half displacement was simulated to guarantee a reference for the fuel consumption comparison. The results are reported in Table 17.

Table 17. WLTC Class 3b simulated results for the best configurations.

FC Reduction % 60s1p	Phase 1	Phase 2	Phase 3	Phase 4	Combined	Corrected
Simulated %	100	55	45	47	55	\
RBS P2–P4	−8.3	−12.8	−7.0	+1.0	−6.1	\
ECMS CS 50% P2-P4	−9.7	−13.4	−10.6	-1.6	−8.2	−10.3
ECMS Spd P3–P4	−4.4	−14.8	−9.8	−3.4	−7.6	\

Figure 84, Figure 85, and Figure 86 show the impact of the various hybrid control strategies on a powertrain with a smaller engine. The behavior of the hybrid electric powertrian is similar to the one that was obtained in previous simulations, however the fuel consumption results show a bigger reduction, associated with better fuel economy.

This is due to the fact that usually the fuel consumption results for super sport cars are significantly high, since the engine displacement is big. However, to work with a smaller engine leads to greater percentage improvements that make the results comparable to the ones obtained for hybrid vehicles commonly available on the market.

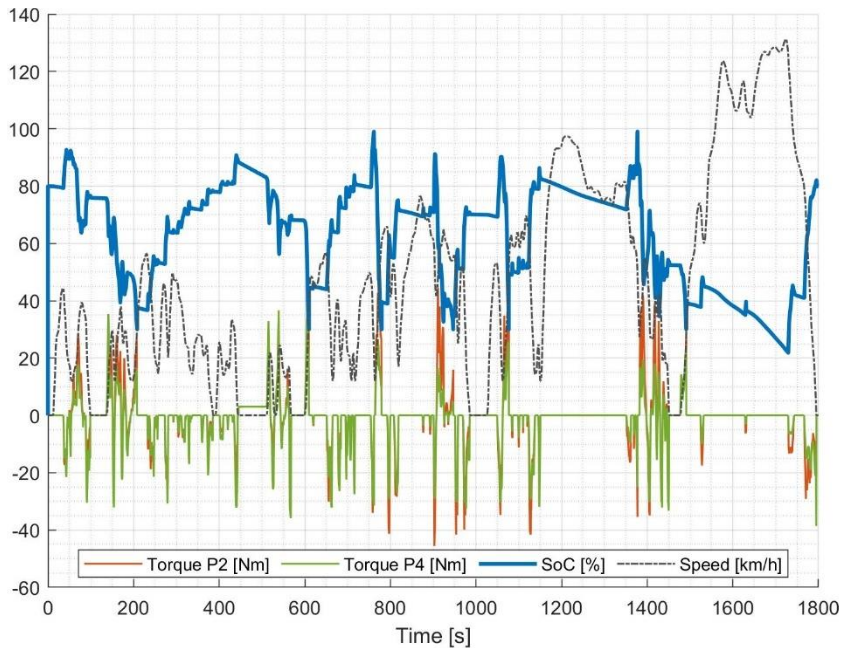

Figure 84. RBS simulation with half displacement for P2–P4.

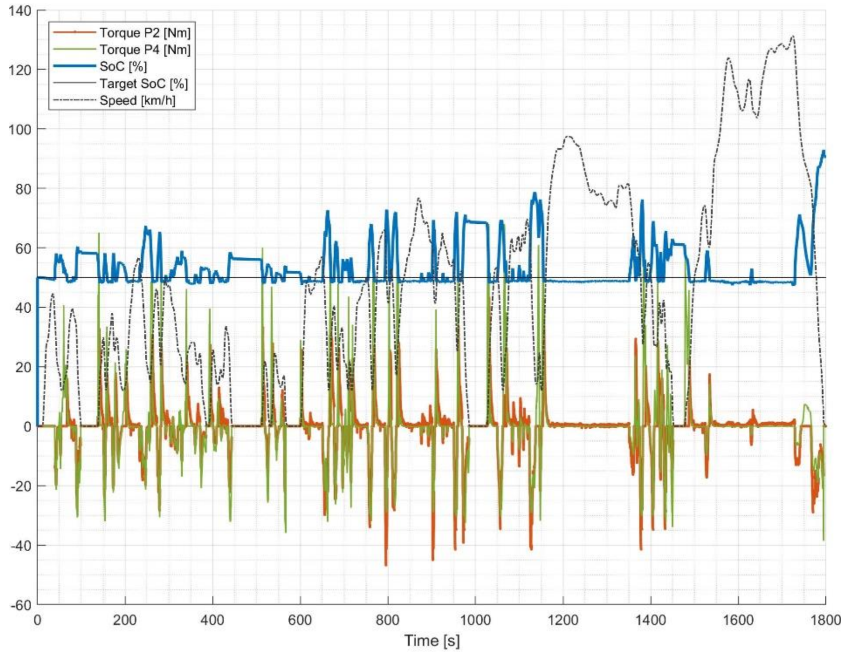

Figure 85. ECMS simulation with half displacement for P2–P4 with an SoC target equal to 50%.

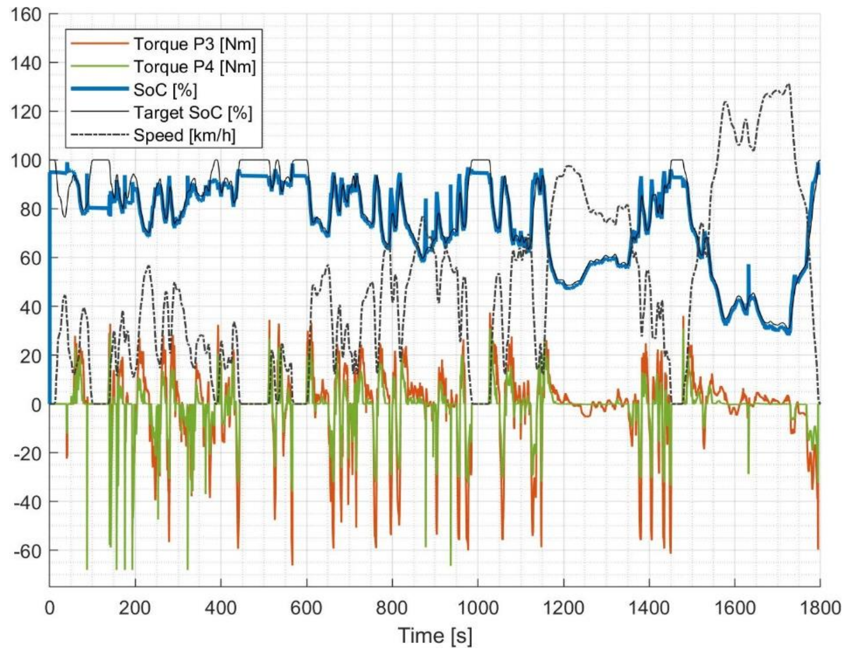

Figure 86. ECMS simulation with half displacement for P3–P4 with a target SoC dependent on speed.

The results of the simulations with half displacement are compared with the ones from hybrid vehicles commonly available on the market. According to these, the Lamborghini application would fall within the sphere of mild hybrid systems [14,16]. To sum up, the comparison between RBS and ECMS shows that it is possible to guarantee a greater fuel consumption reduction working on the hybrid control strategy.

The ECMS reduces fuel consumption by up to 5.4%. Both the P2–P4 and the P3–P4 configurations achieve better results, as the strategy will choose at every working point the best torque split solution between the front and rear EM.

Overall, the fuel consumption reduction is small, and that can be associated with the characteristics of the vehicle at our disposal (i.e., high displacement and high absolute values of fuel consumption). At the same time, the results show a positive trend on the fuel economy that is due to the hybrid control strategies chosen.

It must be noticed that the speed dependent SoC strategy guarantees good results. This kind of application shows that we can achieve fuel economy even if we do not maintain a fixed SoC target, but a speed-dependent one. This means that depending on the speed of the vehicle we could leave room for any functions more performance-related, which could be activated at the request of the driver.

This result represents an important element for the design of super sport cars, for which performance and drivability are notable elements. It should be noted, however, that these results are a consequence of the type of energy storage system chosen, which has as its main feature the high power and the consequent reduced charging and discharging times.

The hybrid control strategy comparison points out that the choice to invest in the ECMS has given benefits from the fuel economy point of view as it doubles the improvement on FC results.

4.2.5. Energy Storage Size Variation

At last, some simulations were run to evaluate the behavior of the energy storage with respect to its main limit represented by the low specific energy [5,60]. The simulations were run for the ECMS P3–P4 speed dependent scenario as it imposes rapid variations on the SoC, and it is considered the most interesting to be implemented on a super sport car, typically associated with high accelerations and decelerations. The capacity of the energy storage system is doubled and quadrupled and so 60s2p and 60s4p are simulated. A system of that kind will guarantee greater capacitance, lower internal resistance, and a greater mass. The results are reported in Table 18.

Table 18. WLTC Class 3b simulated results, for the various energy storage configurations.

FC Reduction % 60s1p P3–P4	Phase 1	Phase 2	Phase 3	Phase 4	Combined
Simulated %	100	55	45	47	55
60s1p	−3.9	−8.2	−5.2	−2.7	−4.8
60s2p	−5.0	−8.4	−5.5	−2.5	−5.1
60s4p	−5.0	−8.4	−5.7	−2.6	−5.2

Table 18 shows that a greater capacitance brings slightly better fuel economy results that tend to an asymptote. It is evident that although the results improve, the reward obtained is not sufficient to justify an investment in a system that becomes more complex, heavier, and larger. Above all, because the system is inserted in a supercar, which typically seeks maximum performance and has dimensional limits related to design and aerodynamics.

Such an outcome points out that for an application of this kind the low specific energy limit of the energy storage system does not compromise the results, indeed this hybrid powertrain can achieve fuel economy thanks to its high power, which results in a high charge and discharge rate.

4.3. Third Configuration, 2 EMs HESS-based

The simulations for the third configuration are run under the conditions previously explained, and the possibility to work with a system based on a HESS is explored. The vehicle configuration that is here adopted is equal to the second vehicle configuration introduced in 2.4, however, only the P2-P4 is here considered.

As it has been done previously, the fuel consumption (L/100km) is established as the assessment parameter for comparison. The simulated conventional vehicle model reproducing a Lamborghini Aventador SVJ is considered as a reference. Moreover, the simulations that were done in 4.2 for the second vehicle configuration, with a P2-P4 and an energy storage system uniquely based on LiCs, are reported under the name 'LiC 60s1p'.

In 4.2.1 a fuel consumption correction has been introduced. The application of this fuel consumption correction is essential for the following simulations as we are no more working with an energy storage uniquely based on LiCs.

The presence of a HESS is associated with higher energy content and so even a small variation in the SoC of the HESS could produce an impact on the fuel consumption results. As the fuel consumption correction in 4.2.1 took into account an energy storage system uniquely based on LiCs, there were no problems in determining the energy difference between the final state and the initial one, since the pack worked alone. However, with the introduction of HESS, two different energy storage systems are present, and so both the energy balance of the LiCs and the one of the batteries must be taken into account.

Once the total energy balance is calculated thanks to the equations shown in XX and XXVIII, the fuel consumption correction can be determined as in 4.2.1.

4.3.1. Passive HESS

At first, the vehicle model is simulated with a passive HESS as energy storage system. Both the RBS and the ECMS impact is analyzed.

RBS

The third vehicle configuration is simulated on a WLTC Class 3b, and the results can be seen in Figure 87 and Table 19. As previously introduced, Table 19 shows the results for the reference configurations given by the Lamborghini Aventador SVJ conventional vehicle and by the second vehicle configuration in P2-P4 with an energy storage uniquely based on LiCs. Moreover, the fuel consumption results for the passive HESS are shown.

Figure 87 shows the simulation of the passive HESS on an RBS. The LiCs' SoC is chosen as the state variable, therefore the RBS is activated or deactivated when the LiCs' SoC reaches the respective target values. This way, every time the electrical driving is activated, the traction power will be guaranteed by the LiCs.

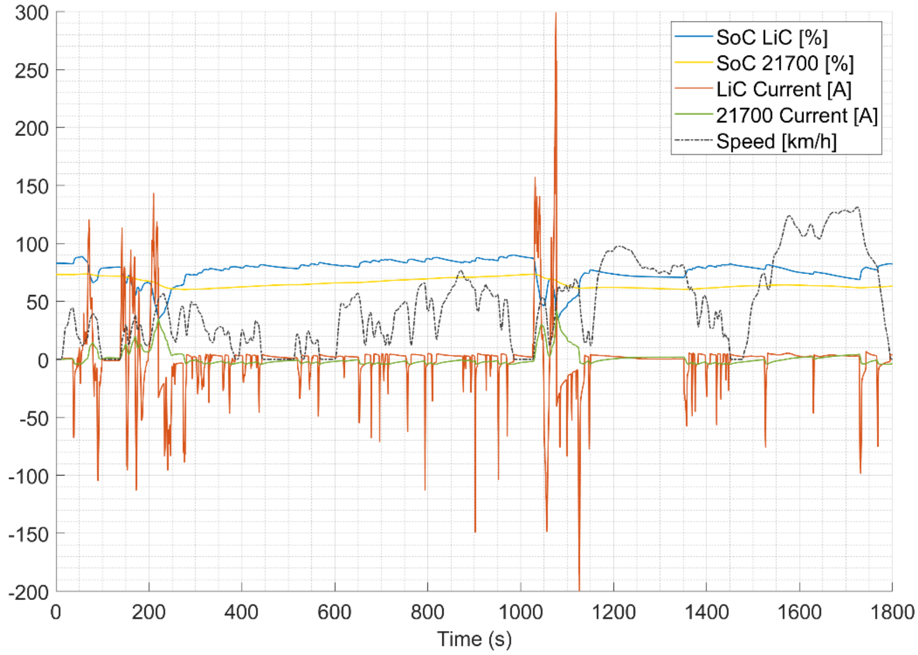

Figure 87. Passive HESS WLTC Class 3b on an RBS.

Table 19. WLTC Class 3b simulated results, for a P2-P4 hybrid configuration with a passive HESS and an RBS.

P2-P4 RBS	Phase 1	Phase 2	Phase 3	Phase 4	Combined	Corrected
Simulated %	100	54	43	41	52	\
LiC 60s1p	-1.2	-7.1	-2.7	+0.6	-2.3	\
Passive HESS	-2.1	+1.5	-3.5	+1.2	-0.7	-0.2

The RBS ensures a reduction of fuel consumption, respecting the HESS current limits. As it can be seen, the fuel consumption is reduced in those phases where the hybrid powertrain is activated, otherwise it increases due to the greater weight.

As the final SoC differs from the initial one, the fuel consumption correction is applied. The simulation of an RBS for a passive HESS shows a reduction of approximately -0.2% after the fuel consumption correction. If compared with the value obtained for a LiC-based hybrid powertrain (LiC 60s1p), the passive HESS gets a worse result, making the addition of batteries apparently useless in this case.

The major problem of the passive HESS is represented by the fact that it cannot recover all the energy available through regenerative braking due to current limitations introduced for safety reasons through the control strategy presented in Control. On the other side, a LiC-based configuration does not experience the same current limitations derived from the presence of additional batteries, making it capable of recovering more energy.

ECMS

An ECMS simulation is run to complete the analysis on the passive HESS. The ECMS splits the torque to guarantee the minimization of the equivalent fuel consumption, keeping into account the system's limitations. The results are reported in Figure 88 and Table 20:

In particular, the strategy that is here simulated is the ECMS CS 50%. The ECMS with an SoC depending on speed is not simulated for the passive HESS, in fact a passive HESS would not be ideal for a strategy of this kind as the direct connection typical of a passive HESS between the battery and the LiCs would make the SoC variation slow and uncapable of following properly the fast variations of the target SoC due to the current limits of the battery. This highlights that the power limit has a major importance for the energy storage systems, especially for super sport cars.

The simulation done in 4.2.3 is considered for the 'LiC 60s1p' reference.

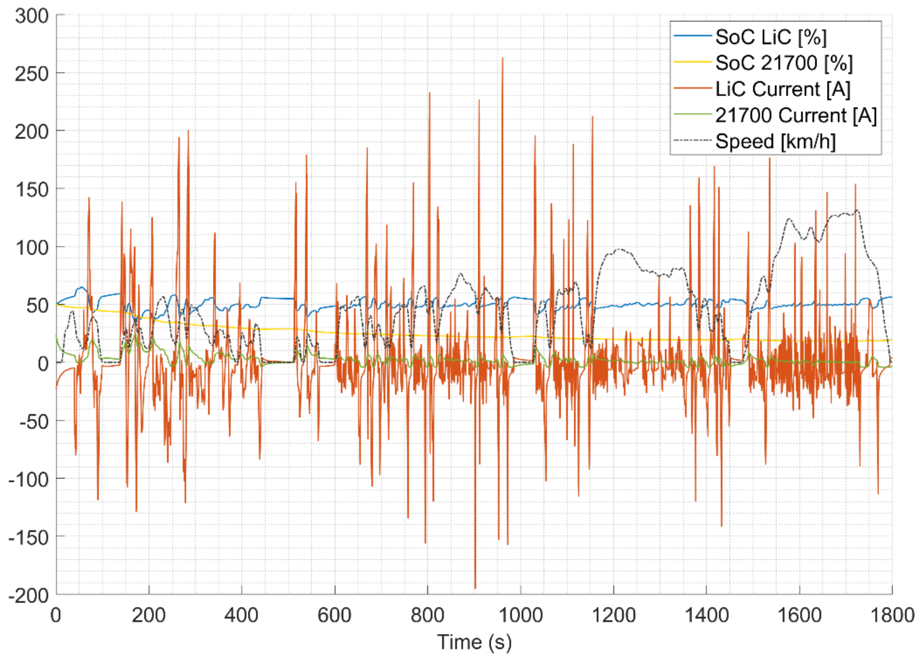

Figure 88. Passive HESS WLTC Class 3b on an ECMS.

Table 20. WLTC Class 3b simulated results, for a P2-P4 hybrid configuration with a passive HESS and an ECMS CS.

P2-P4 ECMS CS	Phase 1	Phase 2	Phase 3	Phase 4	Combined	Corrected
Simulated %	100	54	43	41	52	\
LiC 60s1p	-4.7	-6.4	-4.9	-1.0	-4.1	-5.4
Passive HESS	-7.9	-3.0	-1.7	+0.1	-3.0	-1.7

Figure 88 shows the simulation for the passive HESS on an ECMS CS 50%. During the simulation the LiCs' SoC is considered the reference, and it will follow the SoC target of 50%. On the other hand, the battery's SoC is not controlled, and it is progressively discharged, even if the battery maintains the same terminal voltage of the LiCs being in a parallel connection.

The graph shows a current that varies very frequently, especially for LiCs. This is also due to the strategy calibration that has been chosen, which could be adjusted to ensure smoother activation profiles.

Table 20 shows the fuel consumption results for the ECMS CS 50%. The ECMS guarantees a fuel consumption reduction, but, as in the RBS, the configuration cannot recover all the energy available through regenerative braking due to the control strategy that needs to be adopted for safety reasons, explained in Control. So, even in this case the results are not as good as the ones obtained through the LiC-only simulation. Moreover, since the system cannot be actively controlled, the capacitor energy cannot be fully used [5,78] as it is bound to the battery voltage.

In conclusion, for the passive HESS, fuel consumption reduction is achieved, but the current limits of the 21700 batteries are too challenging and the passive HESS cannot achieve better recuperation than the LiCs alone. This makes a passive system with a bigger capacity worse than a LiC-only system with respect to fuel consumption reduction.

4.3.2. Semi-Active HESS

The simulations for a semi-active HESS have been run to evaluate the performance of this solution. The configuration that is here tested is the one based on Figure 58 and based on the theory presented in DC-DC Converter.

RBS

As in 3.4.1, the RBS makes the vehicle work in electric drive mode once the SoC is over a certain target value. The current system is characterized by two energy storage systems, and the LiCs' SoC represents the strategy reference. This allows to activate the hybrid components only when the electric traction power is available. On the other side, as it was described in 2.5.4 and in [75,89] the battery deals with the average power and it is charged or discharged until it reaches its limits as it can be seen in Figure 89 and Table 21.

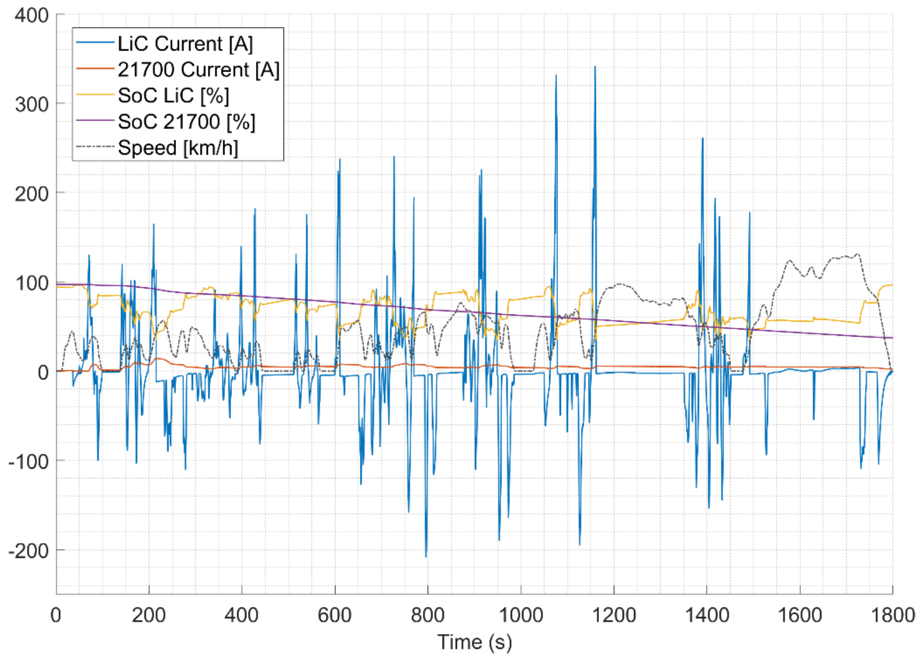

Figure 89. RBS simulation for a semi-active configuration.

Table 21. WLTC Class 3b simulated results, for a P2-P4 hybrid configuration with a passive and a semi-active HESS, and an RBS.

P2-P4 RBS	Phase 1	Phase 2	Phase 3	Phase 4	Combined	Corrected
Simulated %	100	54	43	41	52	\
LiC 60s1p	-1.2	-7.1	-2.7	+0.6	-2.3	\
Passive HESS	-2.1	+1.5	-3.5	+1.2	-0.7	-0.2
Semi-Active HESS	-1.9	-7.1	-5.1	+1.0	-3.0	+0.7

Figure 89 shows the activation of the RBS on the semi-active configuration. The LiCs' SoC is the reference, and the phases in which it is rapidly discharged correspond to the electrical driving activation. With respect to the passive HESS, the electrical driving is here activated more frequently. This is due to the fact that the semi-active HESS separates the current limits of the two different energy storages, allowing the HESS to react better at dynamic situations. This means also that better recuperation can be achieved without the same strict limits on currents that are present for passive HESS.

However, the semi-active configuration is not proficient for fuel economy, as shown in Table 21. This is true once the fuel consumption correction is applied, as the battery is discharged in an uncontrolled manner and ends the cycle at a SoC much lower than the initial one. It can be noticed that even if the RBS guarantees a fuel consumption reduction for the LiC-based hybrid powertrain and for the passive HESS, it is not capable to guarantee the same results for a semi-active HESS.

So, the additional energy present in the form of additional batteries does not guarantee improvements on this side. Different solutions could be analyzed for a HESS with a larger battery pack, that could compensate for the additional weight by extending the driving periods in electrical drive. Further analysis could be carried out by actuating a control on the battery SoC, in addition to the control already done on the LiCs' SoC.

ECMS

The ECMS is focused on optimizing the equivalent fuel consumption at every instant. The LiCs' SoC is taken as a reference for the strategy, and it follows the SoC target throughout the whole cycle. On the other side, the battery is charged or discharged with respect to the average power. The results for a ECMS in CS mode are shown in Figure 90 and Table 22.

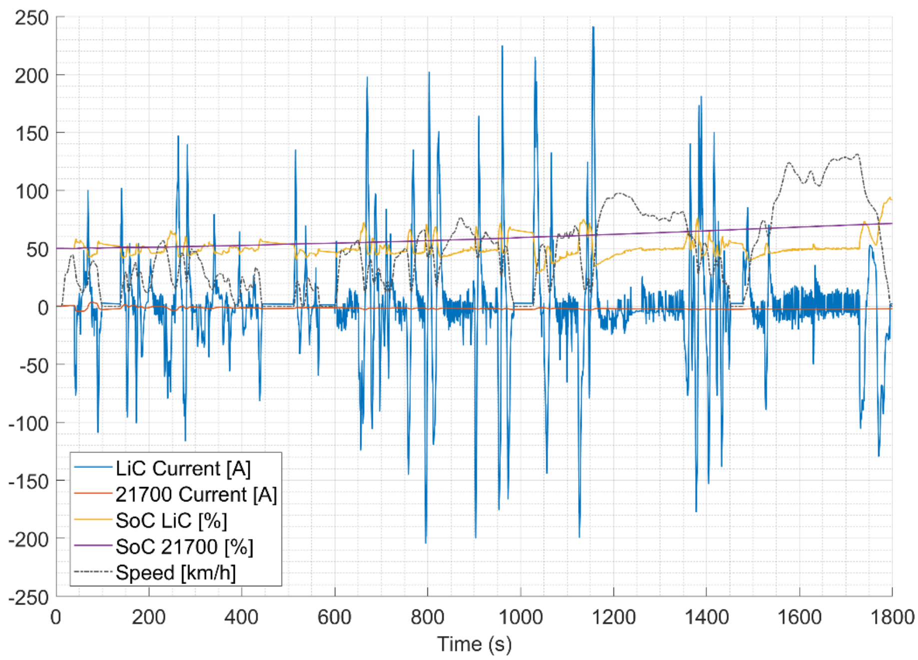

Figure 90. ECMS CS simulation for a semi-active configuration.

Table 22. WLTC Class 3b simulated results, for a P2-P4 hybrid configuration with a passive and a semi-active HESS, and an ECMS CS.

P2-P4 ECMS CS	Phase 1	Phase 2	Phase 3	Phase 4	Combined	Corrected
Simulated %	100	54	43	41	52	\
LiC 60s1p	-4.7	-6.4	-4.9	-1.0	-4.1	-5.4
Passive HESS	-3.6	-1.8	-1.2	+0.3	-1.5	-1.7
Semi-Active HESS	-4.2	-5.3	-3.9	+0.3	-3.1	-6.8

Figure 90 shows that the battery's SoC increases during the cycle, and this leads to a final SoC higher than the initial one. So, the fuel reduction correction is applied. The application of an ECMS CS on a semi-active system is proficient for fuel economy. Differently from the RBS, the ECMS is designed to target the minimization of the equivalent fuel consumption at every instant, and this can be seen in the results that have been obtained.

Table 22 shows that a semi-active HESS configuration can reduce fuel consumption up to 6.8%, making this solution better than the LiC 60s1p and the passive HESS. The advantage of the semi-active configuration is the major flexibility in the system's control that makes it possible to work better in dynamic situations. However, the drawback is represented by the high complexity and the addition of a component that involves greater weights and dimensions.

Later, an ECMS Spd is tested. The LiCs' SoC follows the target SoC varying with speed, and the battery works with the average power. The results are shown in Figure 91 and Table 23.

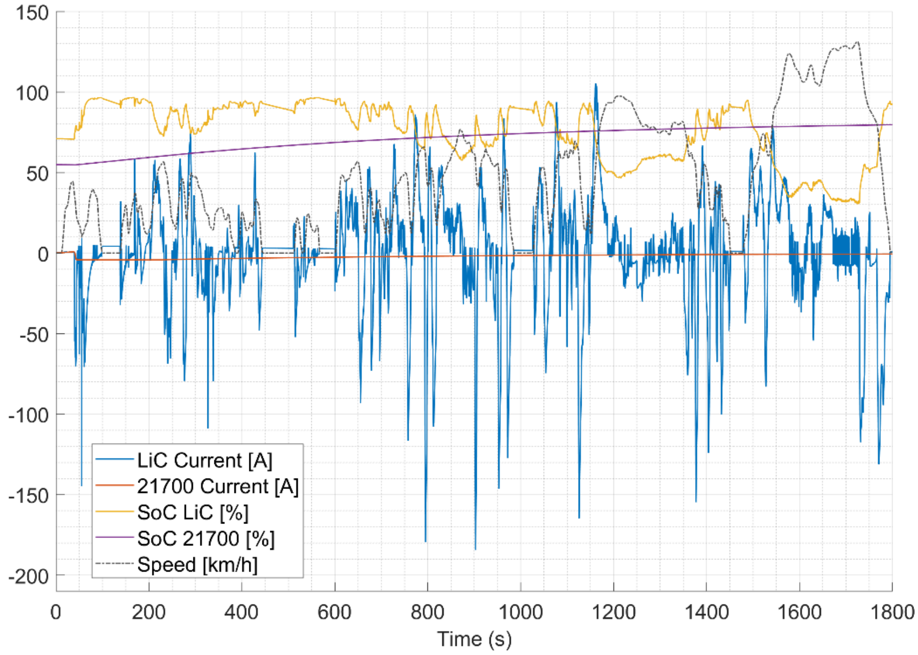

Figure 91. ECMS Spd simulation for a semi-active configuration.

Table 23. WLTC Class 3b simulated results, for a P2-P4 hybrid configuration with a semi-active HESS, and an ECMS Spd.

P2-P4 ECMS Spd	Phase 1	Phase 2	Phase 3	Phase 4	Combined	Corrected
Simulated %	100	54	43	41	52	\
LiC 60s1p	-2.3	-7.9	-5.1	-2.7	-4.3	\
Semi-Active HESS	+2.0	-5.8	-3.6	-1.5	-2.0	-5.5

Figure 91 shows the activation of an ECMS with a SoC target dependent on speed, for a semi active HESS. The capacity of the semi active configuration to unbind the two energy storages and the current that is flowing through them, is relevant for this application. In fact, it is thanks to this that the LiCs can follow a rapidly varying SoC target while the battery can deal with the average power, recharging through the entire cycle and acting as an energy reserve whether it would be needed. As shown in Table 23, this configuration guarantees a fuel consumption reduction.

This application is of particular interest for super sport cars, as the energy reserve that is guaranteed by the varying SoC target could be used for the activation of additional hybrid control functions. This guarantees great flexibility. and ensures the possibility to follow rapid variations of the target SoC.

4.3.3. Fixed Ratio HESS

At last, the fixed ratio configuration is analyzed, both on RBS and ECMS simulations. The fixed ratio HESS is based on Figure 58 and based on the theory presented in Fixed Ratio DC-DC.

RBS

As for the semi-active configuration, the system is characterized by two energy storage systems, and the LiCs' SoC represents the strategy reference. This allows to activate the electric drive mode only when the traction power, mainly given by the LiCs, is available. On the other side, the battery is controlled by the fixed ratio DC-DC and it is charged or discharged until it reaches its limits as it can be seen in Figure 92 and Table 24.

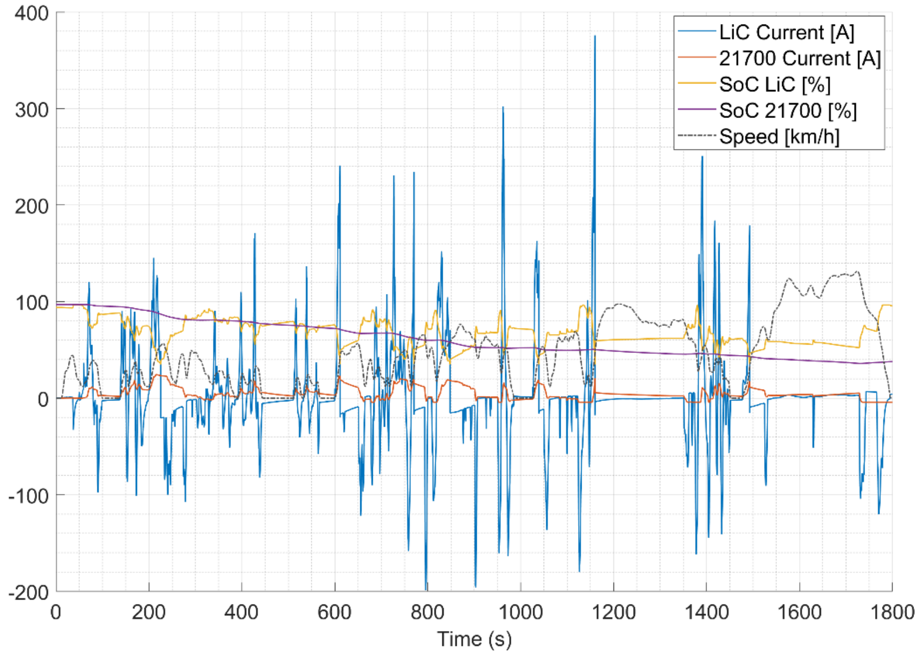

Figure 92. RBS simulation for a fixed ratio configuration.

Table 24. WLTC Class 3b simulated results, for a P2-P4 hybrid configuration with a passive, a semi-active, a fixed-ratio HESS, and an RBS.

P2-P4 RBS	Phase 1	Phase 2	Phase 3	Phase 4	Combined	Corrected
Simulated %	100	54	43	41	52	\
LiC 60s1p	-1.2	-7.1	-2.7	+0.6	-2.3	-2.3
Passive HESS	-2.1	+1.5	-3.5	+1.2	-0.7	-0.2
Semi-Active HESS	-1.9	-7.1	-5.1	+1.0	-3.0	+0.7
Fixed Ratio HESS	-3.1	-8.1	-3.9	+0.9	-3.2	+0.3

The fixed ratio HESS shows a frequent activation of the electrical drive, and it behaves as the semi-active configuration previously simulated. Further analysis should be carried out by actuating a control on the battery SoC, in addition to the control already actuated on the LiCs' SoC. Table 24 shows that the fixed ratio HESS is not capable to achieve a reduction of fuel consumption once the fuel consumption correction is applied to the result.

ECMS

The results for a ECMS in CS mode are shown in Figure 93 and Table 25.

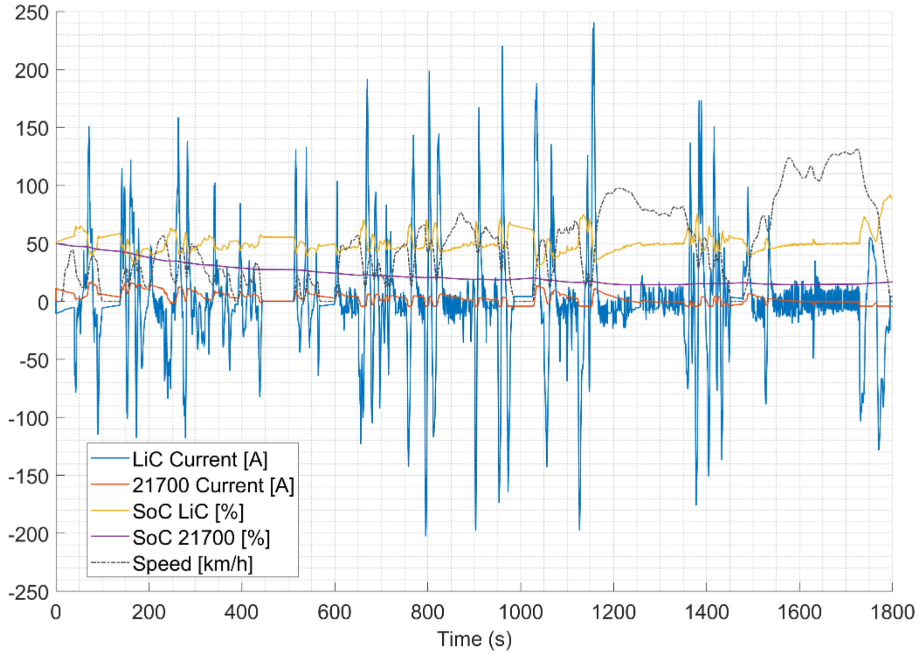

Figure 93. ECMS CS simulation for a fixed ratio configuration.

Table 25. WLTC Class 3b simulated results, for a P2-P4 hybrid configuration with a passive, a semi-active, a fixed-ratio HESS, and an ECMS CS.

P2-P4 ECMS CS	Phase 1	Phase 2	Phase 3	Phase 4	Combined	Corrected
Simulated %	100	54	43	41	52	\
LiC 60s1p	-4.7	-6.4	-4.9	-1.0	-4.1	-5.4
Passive HESS	-3.6	-1.8	-1.2	+0.3	-1.5	-1.7
Semi-Active HESS	-4.2	-5.3	-3.9	+0.3	-3.1	-6.8
Fixed Ratio HESS	-8.3	-7.4	-5.5	-0.1	-5.1	-4.0

The results in Table 25 show that the fixed ratio HESS configuration guarantees fuel consumption reduction when simulated on an ECMS CS 50%. This makes the fixed ratio HESS a viable solution for fuel economy. However, the control simplicity of the fixed-ratio DC-DC is here paid with worse results with respect to the semi-active configuration.

At last, an ECMS Spd is tested. The LiCs' SoC follows the target SoC that varies with speed. The results are shown in Figure 94 and Table 26.

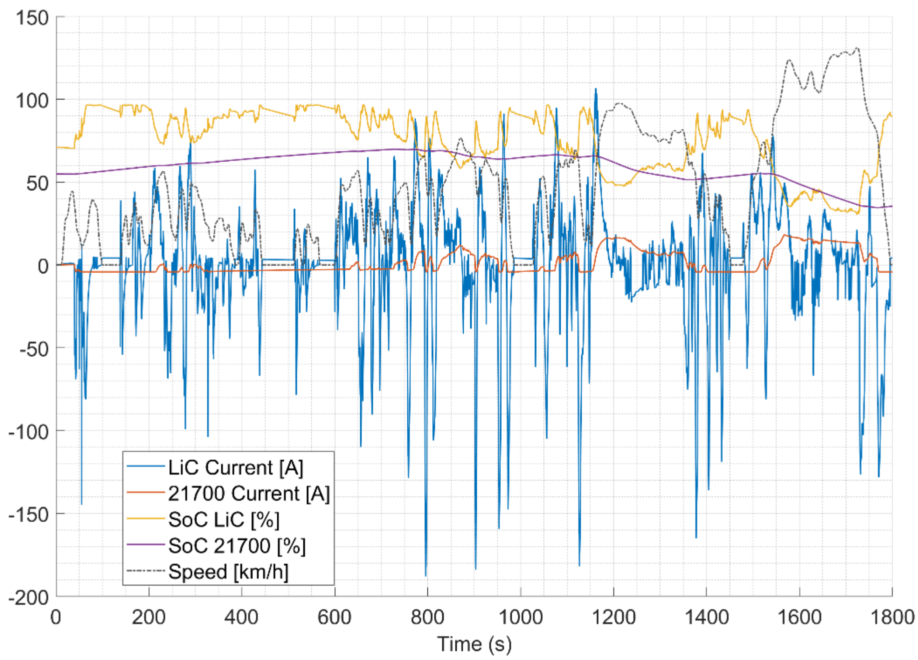

Figure 94. ECMS Spd simulation for a fixed ratio configuration.

Table 26. WLTC Class 3b simulated results, for a P2-P4 hybrid configuration with a semi-active, a fixed-ratio HESS, and an ECMS Spd.

P2-P4 ECMS Spd	Phase 1	Phase 2	Phase 3	Phase 4	Combined	Corrected
Simulated %	100	54	43	41	52	\
LiC 60s1p	-2.3	-7.9	-5.1	-2.7	-4.3	\
Semi-Active HESS	+2.0	-5.8	-3.6	-1.5	-2.0	-5.5
Fixed Ratio HESS	+1.7	-8.3	-6.3	-3.1	-3.8	-3.0

Table 25 and Table 26 show that the fixed ratio DC-DC is capable to achieve fuel economy when the hybrid control strategy targets the minimization of equivalent fuel consumption as the ECMS does. However, the results that are obtained do not improve what was previously simulated on the semi active HESS.

The current profiles that are obtained in Figure 94 resemble the ones obtained for the semi active simulations in Figure 91, especially for the LiCs' current that in both cases is capable to react at the SoC target variations. On the other hand, the battery's current has a different profile as in the semi-active configuration is meant to deal with the average load power, while here aims to maintain the same voltage between battery and load as explained in Fixed Ratio DC-DC.

To sum up, these simulations make it clear that a passive HESS, despite guaranteeing simplicity and being cheap, is not good for performance and control. On the other side, the semi-active configuration is more complex but has the great advantage of being controllable and this results in a more consistent fuel consumption reduction and reliability.

The fixed ratio DC-DC achieves fuel economy; however, it is not as proficient as the semi-active HESS. At the same time, it represents a simpler system that would allow to save complexity. Improvements could be obtained updating the control strategies and making them best suited to work with a HESS by controlling both the LiCs' SoC and the batteries' SoC, this would make an additional fuel consumption reduction possible. Another improvement could be given by the introduction of batteries with greater limits on current, that would be capable of guaranteeing better energy recuperation.

Another consideration is related to the comparison between the HESS and an energy storage uniquely based on LiCs. The choice to work with a HESS allows to improve the system's flexibility, as greater energy content could be guaranteed, while maintaining the power of the LiCs. However, the results for the RBS show that in some situations, the energy storage system uniquely based on LiCs could achieve better fuel economy results. On one side, this clarifies the importance of high-power density systems for super sports car, that can guarantee fuel economy even if characterized by low energy density. On the other side, it makes clear that the hybrid system carries more weight and that it needs a more accurate management of the additional energy that it makes available (for example with strategies targeting the minimization of fuel consumption), which otherwise will not lead to the expected benefits.

4.3.4. Performance

The last part of the activity has been destined to the study of dynamic conditions (typically seen for sport driving or use on the track). The energy storage system is here dimensioned to recover all the energy available for high-speed braking. The study aims to understand what kind of solutions would be needed to satisfy this target and whether these solutions are viable. The semi-active fixed ratio HESS is now analyzed for performance. Simulations for a 0-200 km/h acceleration and a 200-0 km/h braking are run.

At first, a braking from 200 km/h to 0 km/h is analyzed as this represent an extremely challenging condition, especially for the battery due to its stringent current limit. During braking, energy is usually dissipated through mechanical brakes, but here it can be recovered through regenerative braking. The target is to design a HESS capable of storing all the energy generated from braking. The hybrid powertrain as it has been described until now is not capable of recovering the whole amount of energy, so a new HESS is designed.

Since the batteries are strongly limited in current, they are not capable of recovering great energy quantities during hard braking and their impact in a high-power situation, like the 200-0 km/h braking, is low. So, the battery maintains the 54s1p configuration. On the other side, the LiCs are sized to recover all the available energy and a configuration of 60s5p is chosen, maintaining the same voltage range of the previous hybrid configuration. Furthermore, EMs about 5 times more powerful than the previous configuration are chosen to satisfy the peak power. The new hybrid powertrain, which we refer to as Hybrid 60s5p, is simulated as shown in Figure 95.

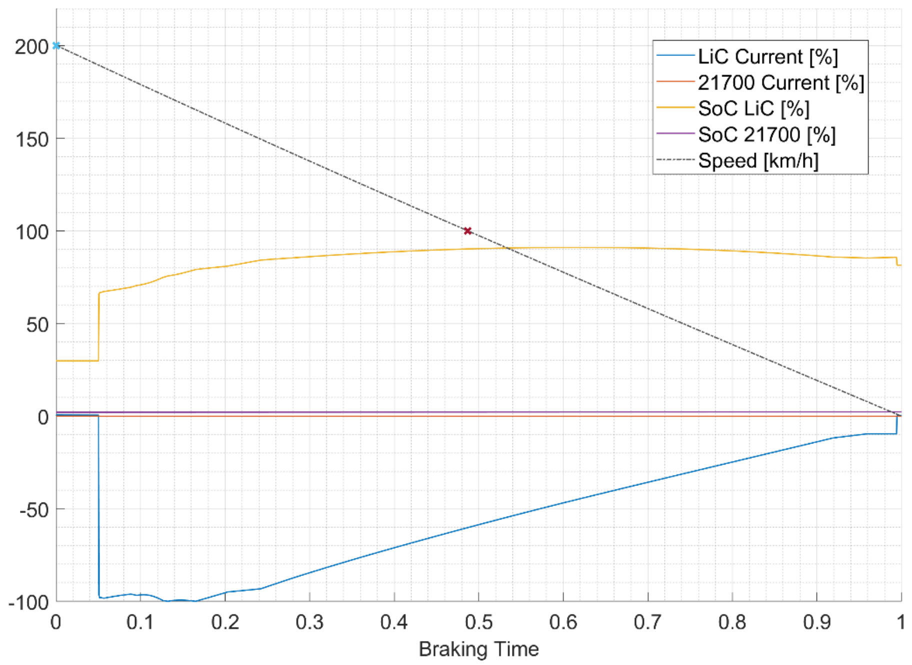

Figure 95. Hybrid 60s5p simulation for the 200-0 km/h braking.

The simulation demonstrated that during recuperation the braking energy is coming from the EMs and not the mechanical brakes, allowing to recover all the available energy. In this simulation the battery and the LiCs are starting at the same voltage (respectively corresponding to a LiCs SoC=30% and a battery SoC=2%), and, as soon as the vehicle speed gets under 190 km/h, the regenerative braking strategy is activated as the front EM is attached.

A negative current start flowing in the HESS, and the battery immediately reaches its lower limit while the LiCs can manage all the remaining current (here the values are normalized with respect to the maximum LiCs' current). The LiCs' SoC in Figure 95 is calculated as in XIX, meaning that it depends on the terminal voltage of the LiCs' pack, that is formulated as in XV. This means that its variation depends both on the internal voltage that increases during a braking simulation, and on the voltage drop generated by the negative current.

This is evident at the beginning of the simulation (approximately instant 0.05), when a rapid spike takes place because of the sudden demand of current. Moreover, this explains the curvilinear pattern of the SoC during the braking phase.

As the braking phase ends, the current goes back to zero and the system is left with a voltage imbalance between LiCs and batteries. The two components start exchanging low values of current to bridge this gap and the LiCs start delivering positive current to the battery until voltage equilibrium is reached. This is shown in Figure 96, where the LiCs current becomes positive and the SoC of the batteries slowly increases to reach the same LiCs voltage as explained in Fixed Ratio DC-DC.

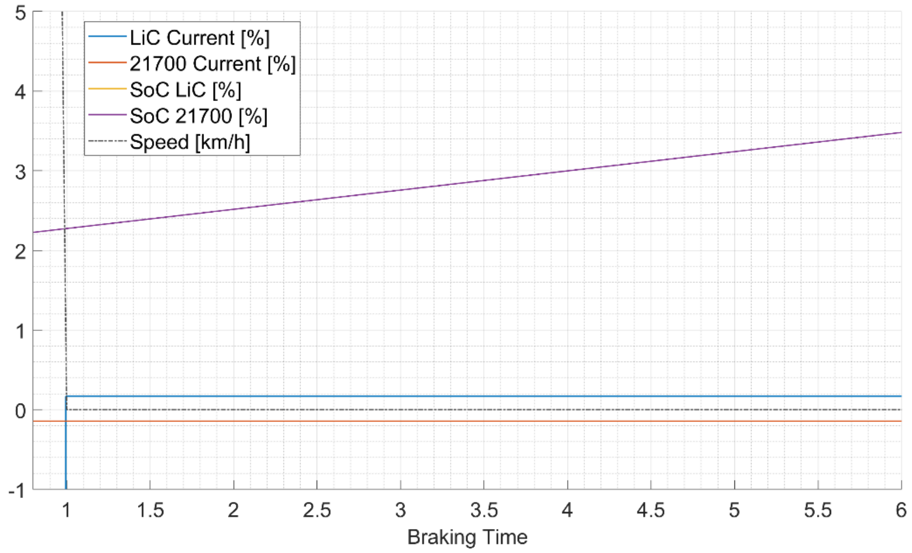

Figure 96. Detail of the system's currents.

Figure 97 shows the energy dissipated through mechanical braking. The Hybrid 60s5p makes use of the mechanical brake mainly in the initial phase as the regenerative braking is activated under 190 km/h. The remaining braking energy is almost completely given by regenerative braking, meaning that the HESS is properly sized.

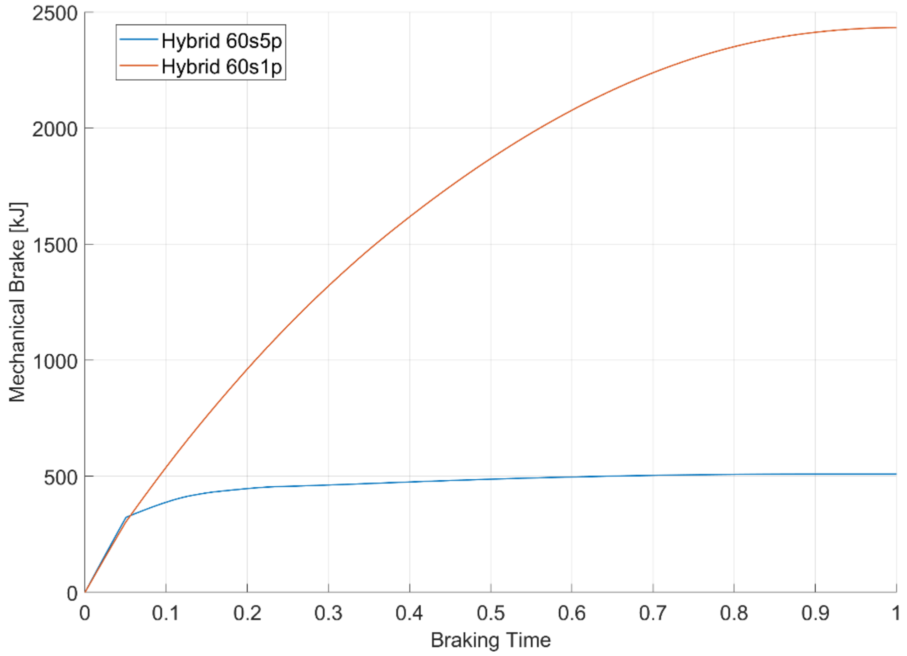

Figure 97. Mechanical contribution for the 200-0 km/h braking.

The Hybrid 60s5p is tested also for a 0-200 km/h acceleration. At first, the conventional vehicle is simulated for a 0-200 km/h acceleration and the times of 0-100 km/h, and 0-200 km/h are recorded and normalized with respect to the greatest of the two.

Later, simulations for the Hybrid 60s1p and for the Hybrid 60s5p are run and the results are compared to the conventional ones, showing the percentage improvement or reduction, as shown in Table 27, Figure 98, and Figure 99

Table 27. 0- 200 km/h simulated performance results.

Time	0-100 km/h	0-200 km/h
Conventional (%)	36	100
Hybrid 60s1p (%)	+15	+6
Hybrid 60s5p (%)	-14	-25

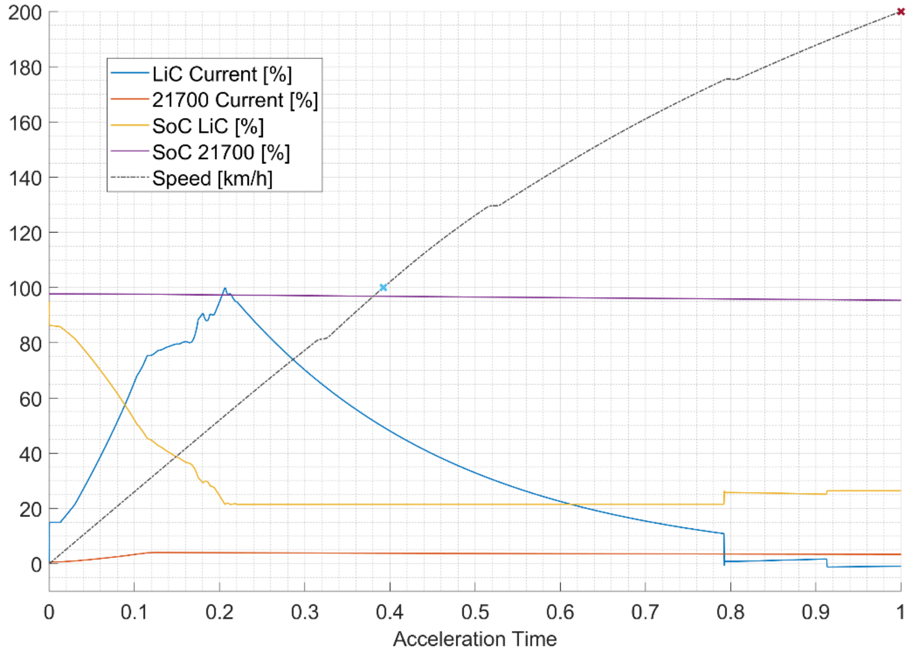

Figure 98. Hybrid 60s1p simulation for the 0-200 km/h acceleration.

The Hybrid 60s1p is less performant than the conventional vehicle. This is because in hybrid configuration the P4 EM is the only power source at the front axle, and it is not capable to output the same power that was split to the front from the ICE in conventional configuration all-wheel drive.

Moreover, as soon as the LiCs reach the minimum SoC, the hybrid contribution ends leaving the ICE alone. In fact, the battery is not capable to satisfy the power request by itself. As the hybrid contribution ends, the battery continues to deliver positive current to the LiCs, as the HESS tries to bridge the difference in voltage between the LiCs and the battery.

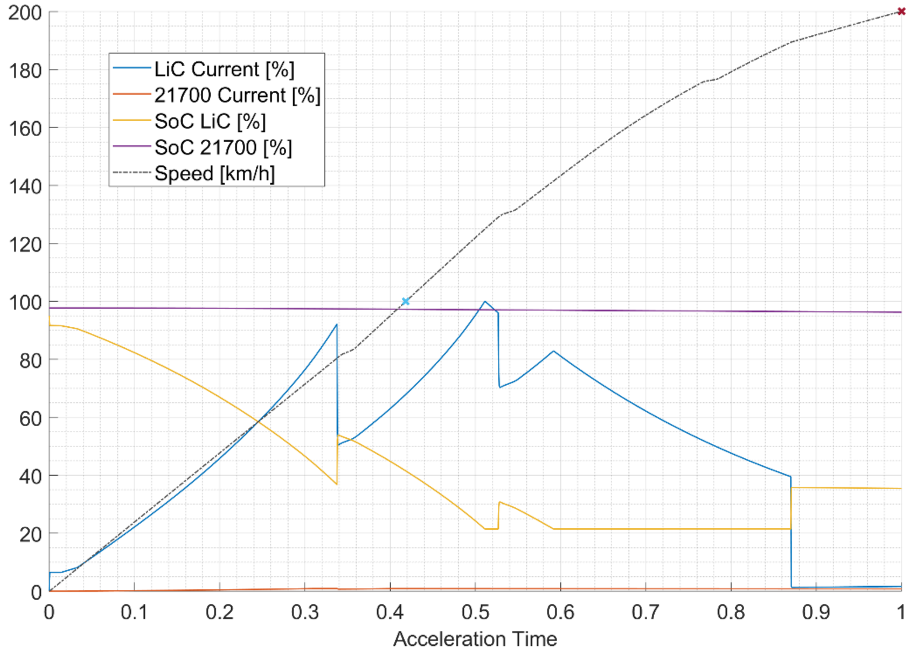

Figure 99. Hybrid 60s5p simulation for the 0-200 km/h acceleration.

In Figure 99, at approximately instant 0.87, the vehicle speed of 190km/h is reached, and the front EM is detached modifying the current requests. In the Hybrid 60s5p configuration the front EM delivers more power than before and the LiCs deliver higher currents. Moreover, the presence of parallels lowers the internal resistance and the voltage drop, and this allows to run in hybrid mode for longer time.

The results highlight that a HESS can guarantee improvements on the 0-200 km/h acceleration and energy recuperation on the 200-0 km/h braking. While the battery can be seen as the responsible for the energy target, the LiCs are capable to achieve the power target. Performance tests highlight the possibility of using a HESS to achieve both power and energy targets, focusing on proper LiCs and battery sizing.

5. Models' Management

This chapter refers to the ways models were managed during the research project. Proper models' management is often overlooked, and small time is destined to this activity that, on the other side, requires accurate management and solid procedures.

5.1. Data sharing and archive

During the research project, solid procedures have been established to properly track the models' development and to maintain good and consistent management of models and files, keeping a data archive of the file versions and establishing a way for model sharing.

It is extremely important to keep an archive of the file versions, especially when lots of people work on the same model, to avoid problems when modifications are made and to track every change that is done. Eventually, various versions of the model need to be merged without losing the work of other people. Another request is the need of fast and stable ways to share models. With respect to these topics, TortoiseGit and GitHub have been adopted.

5.1.1. GitHub

GitHub [128] is a provider of internet hosting especially designed for software development and version control using Git. Git is a software capable of tracking changes in any set of files and it is particularly indicated for programmers collaboratively developing source code. GitHub offers the functionalities of Git and provides among the others bug tracking, feature requests, task management, and continuous integration for every project.

GitHub allows the user to start a pull request, detaching momentarily the code from the core and giving the chance to experiment, debug, and build new features. This way, changes can be proposed, and any modification can be made. Once the modified code is reviewed it can be merged with the original. GitHub has been adopted to work in collaboration with other people on the same hybrid control strategies.

5.1.2. TortoiseGit

TortoiseGit [129] is a Windows Shell Interface to Git, and supports by regular task, such as committing, showing logs, creating branches and tags, creating patches and so on.

All commands are available through Windows Explorer, making it easy for all users. The main highlight is that it allows to manage software versions easily and keep a data archive, giving the chance to recover the past versions of the models.

5.2. Model Sharing

Other considerations have been made speaking strictly of the model management on MATLAB/Simulink.

5.2.1. Variant Subsystems

During the research project various vehicle configurations have been analyzed, starting from a conventional vehicle, and progressively adding components to reproduce the hybrid behavior. As different vehicles were built, different models were used. On the other side, the same vehicle could host various hybrid configuration with the introduction of multiple EMs in P2-P4 and P3-P4 configurations. Alongside this, various strategies could be implemented as RBS and ECMS.

MATLAB/Simulink allows the user to design various configurations and to activate only the desired one, while keeping the others disabled. This is possible thanks to the Variant Subsystems as shown in Figure 70.

Variant Subsystems [122] allow to manage all the configurations hosted by a single model through the MATLAB environment, without necessarily entering Simulink. This way, the model can be tuned without modifying blocks in Simulink, but just by giving input through the MATLAB command window, making it easy also for users who have not participated in the model design or who have no experience in that kind of software. This solution can be adopted for safety reasons, as any unwanted changes in the Simulink environment could generate major problems, especially if the model is shared between users and departments. This is avoided when the model control is done via MATLAB.

5.2.2. Graphic User Interface

The adoption of Variant Subsystems goes along with the introduction of a GUI, in fact the presence of a GUI could lead to major advantages:

- Keeps the work organized and traceable,
- Makes the model accessible to all kind of users, as direct access to Simulink is not needed,

On the other side:

- Requires working effort, at least in the first realization phase,
- Requires models adequate to the GUI implementation.

So, the GUI brings with itself complexity as its development and the management of the interaction between GUI, MATLAB and Simulink need to be continuously updated.

Simulink versions of the vehicle model need to be specifically designed for GUI integration, in particular a database with the final version of the vehicle model should be created and no modifications should be made on that version. Alongside the Simulink model, the MATLAB code needed for data input is included in the database.

A GUI has been realized for the longitudinal dynamics' simulations of a hybrid vehicle model, it allows to configure a vehicle and simulate its behavior on a chosen real driving speed cycle or an emission cycle.

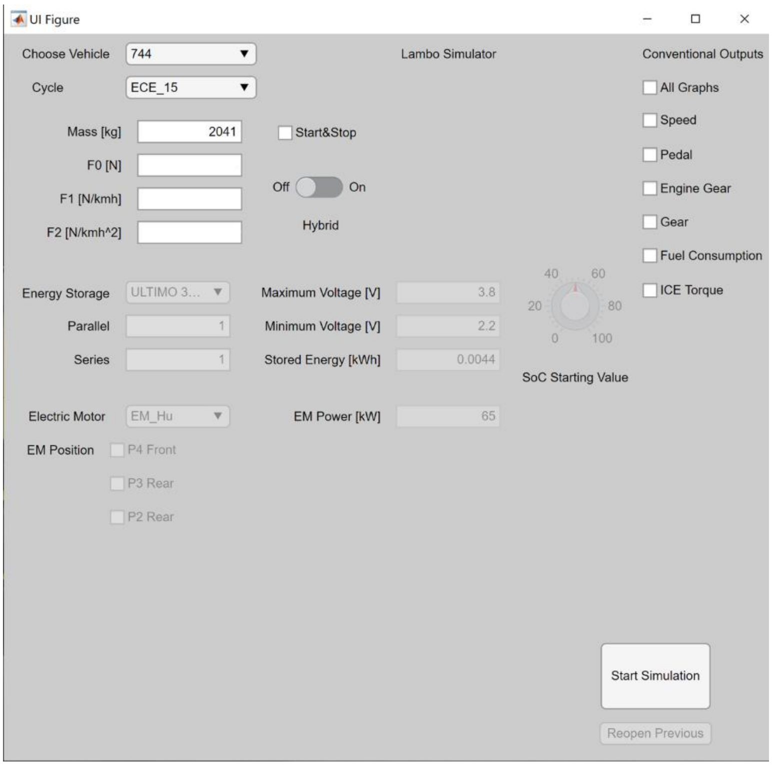

Figure 100. GUI starting window.

The GUI has been developed to simulate both the behavior of a conventional and hybrid vehicle, and it allows to choose between various powertrain configurations as P2-P4 and P3-P4. The vehicle mass and vehicle resistances are editable; moreover, the energy storage system and its configuration and the hybrid control strategies can be chosen.

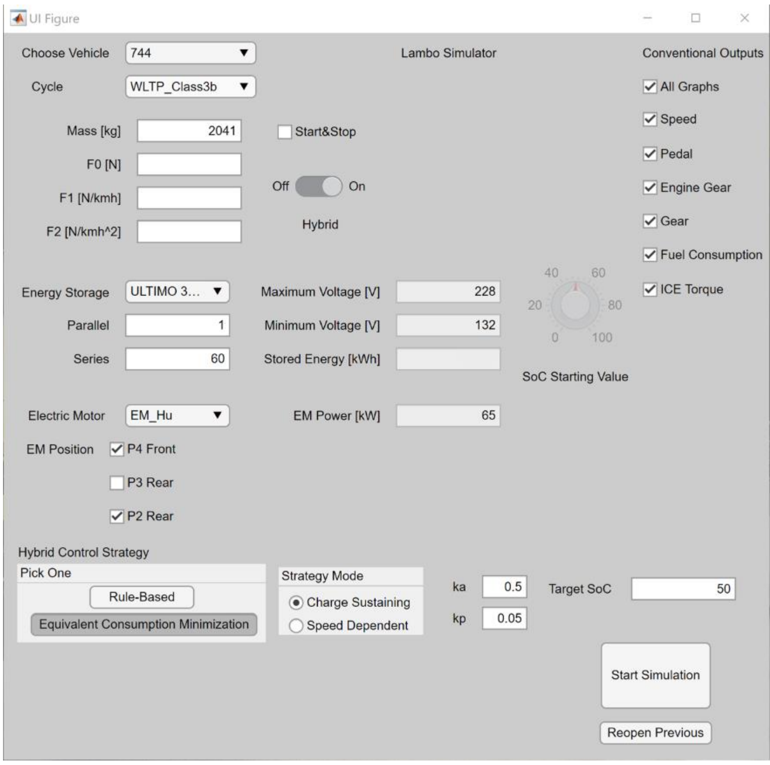

Figure 101. GUI window for a hybrid vehicle configuration.

As output, various graphs showing the vehicle and the powertrain behavior can be plotted. Then, the choice to save data for further analysis is allowed, a .mat file will be generated. All these selections can be made without entering the simulation environment.

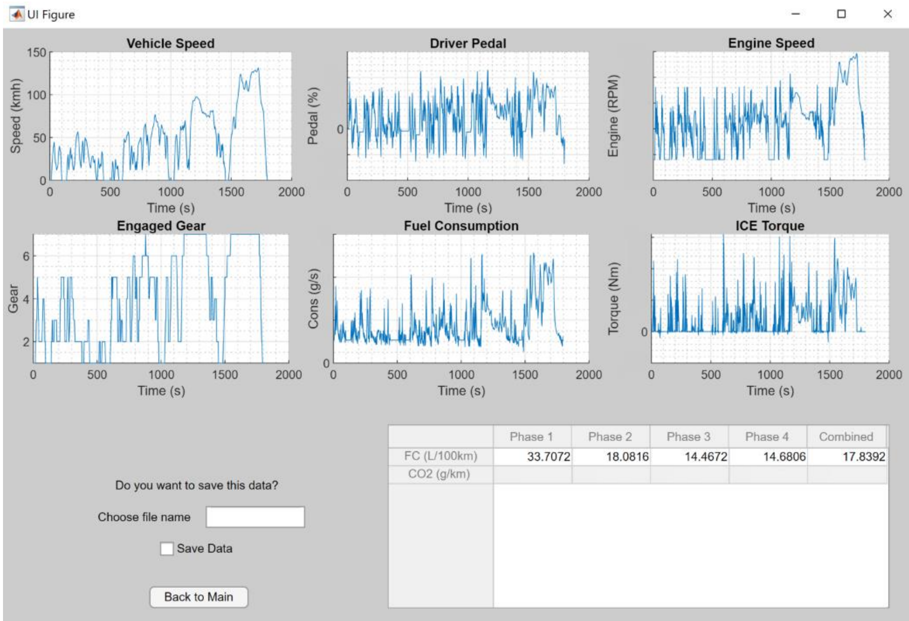

Figure 102. Simulation results, the GUI allows to save the simulation's results.

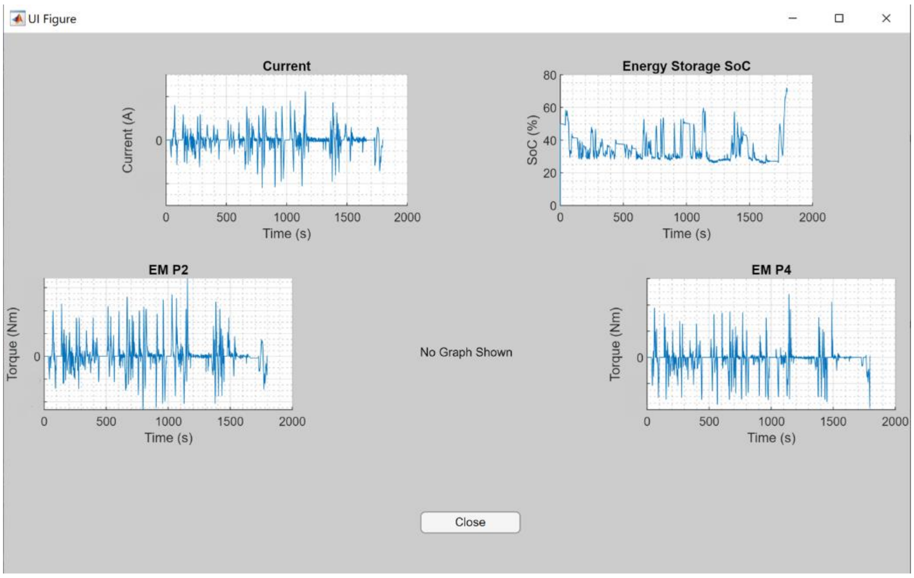

Figure 103. Simulation's results referred to the hybrid powertrain.

The GUI has been developed in AppDesigner [130], that is an interactive development environment for designing an app layout and programming its behavior. It provides a fully integrated version of the MATLAB Editor and a set of interactive UI components. It also offers a grid layout manager to organize the user interface, and automatic reflow options to make the app detect and respond to changes in screen size. It makes also possible to distribute apps by packaging them into installer files directly from the App Designer toolstrip, or by creating a standalone desktop or web app. AppDesigner allows to work on apps both in Design View and Code View, to guarantee maximum editability.

6. Conclusions

This dissertation thesis analyzes hybrid electric vehicles and focuses on super sport car applications. It starts with the modeling of a simple hybrid powertrain and goes on by enriching the architecture, generating a more complex powertrain based on innovative energy storage technologies and introducing hybrid control strategies capable of satisfying various requests.

The first vehicle configuration, based on the hybridization of a conventional Lamborghini Aventador model, is composed of an energy storage uniquely based on LiCs, a single EM in P3 position and a rule-based control strategy that aims at comfort as the first objective.

The simulations run on this configuration show that a high-power density storage system as LiCs is ideal for covering torque requests of short duration. Moreover, modifications are made to the control strategy, that allow to conclude that a system of this type can be rethought to obtain fuel economy. In particular, a dynamic strategy that links the SoC target to the vehicle speed has been designed. It has been verified that this strategy could achieve the comfort target, while leaving room for additional functions more related to performance or fuel economy. The fuel consumption improvement that is achieved for this hybrid configuration goes up to 0.56%.

The second configuration, that is based on the hybridization of a Lamborghini Aventador SVJ, sees the introduction of two EMs, that can be disposed in P3-P4 or P2-P4 configuration. The energy storage system is always uniquely based on LiCs, while the hybrid control strategies' study is deepened. At first, an RBS that allows the vehicle to run in electric mode is introduced. Then, an ECMS targeting the minimization of the equivalent fuel consumption is evaluated.

The simulations show that a hybrid vehicle of this kind is capable of achieving fuel economy, theoretically falling within the sphere of mild hybrid systems [14,16]. In particular, the choice to invest in an ECMS seems proficient as it doubles the improvements on fuel economy if compared with the previously adopted solutions. The ECMS, in fact, reduces fuel consumption by up to 5.4%, while the RBS can achieve a reduction of 2.3%.

The third vehicle configuration is always based on the hybridization of a Lamborghini Aventador SVJ with two EMs but works uniquely with a P2-P4 configuration. The control strategies that are destined to this configuration are the same RBS and ECMS that were introduced for the second one. However, the energy storage system is modified, and a HESS is studied. The target of this application is to guarantee both power and energy, by combining two different energy storage systems as LiCs and batteries.

The HESS is studied as a simple passive HESS, where the LiCs and batteries are directly connected in parallel, or as a semi-active HESS, where a DC-DC converter is the interface for the two energy storage systems. Also, a fixed ratio DC-DC is introduced and analyzed. Every one of these configurations has its own advantages and disadvantages, in fact the passive HESS is a simple system that ensures low weight and small size; however, it cannot be actively controlled, and it limits the energy that would be available from LiCs. The results on fuel economy show a reduction of 0.2% for the RBS and 1.7% for the ECMS.

The semi-active HESS introduces a DC-DC converter, increasing the weight, size, and complexity. On the other hand, it allows to properly control the currents flowing in both batteries and LiCs. While the application of an RBS does not achieve fuel economy, the use of a ECMS and so the minimization of the equivalent fuel consumption instant by instant, makes the semi-active HESS proficient as it achieves a reduction of 6.8% in CS mode, and 5.5% in speed dependent mode.

The adoption of a fixed ratio DC-DC converter is seen as an alternative to maintain the complexity low, while still controlling the current limits of the HESS. However, this simplicity is paid with worse results on fuel economy, if compared with the other semi-active configuration. In fact, the ECMS guarantees a reduction of 4.0% in CS mode, and 3.0% in speed dependent mode, while the RBS is not capable to achieve fuel economy in this configuration.

Overall, the simulations show that the HESS is capable to guarantee fuel economy, reducing the fuel consumption of the vehicle with respect to a conventional one. However, the HESS introduction is not necessarily proficient with respect to the second vehicle configuration that was previously adopted, uniquely based on LiCs. This is partially due to the fact that the strategies that have been adopted are not specifically designed for a HESS. However, the main limit of the configuration is represented by the battery current limit, that impacts on the whole system. With respect to this, the introduction of high-power batteries should be prioritized.

The final analysis is run by simulating the performance of the super sport HEV fitted with a semi-active HESS. The HESS is specifically sized to recover all the energy available during a 200-0 km/h braking and to guarantee a reduction in the time performance for a 0-100 km/h and 0-200 km/h acceleration. These simulations show that the HESS can be an interesting solution to cover both the energy and power requirements that are typically associated to a super sport HEV.

To sum up, it is evident that the LiC technology is limited for energy performance at the moment, but with a proper development of the control strategy and keeping into account the growth of the technology [59,120,121,131], the system capabilities could lead to major applications in the hybrid environment.

The high-power characteristic of the LiCs makes them interesting for applications like super sport cars, which greatly evaluate features such as performance and drivability along with fuel economy. The development of the capacitors' technology to achieve better energy density performance is one of the future steps for this research activity. Other interesting steps are the deepening of the HESS technology and an experimental study of its feasibility, while from the control point of view the work on the RBS and ECMS could go on to better fit the energy storage system's characteristics. The introduction of optimal control strategies is seen as another aspect to be explored; however, it is not priority given that these strategies are suitable only for off-line implementation.

7. Bibliography

1. Climate Change Evidence: How Do We Know?, https://climate.nasa.gov/evidence, Jun. 2021.

2. Economides, G., Papandreou, A., Sartzetakis, E., and Xepapadeas, A., "The Economics of Climate Change," ISBN 978-960-7032-86-7, 2018.

3. US EPA, O., "Overview of Greenhouse Gases," Overviews and Factsheets, https://www.epa.gov/ghgemissions/overview-greenhouse-gases, 2015.

4. Ferrari, G., "Motori a Combustione Interna," 2nd ed., Esculapio, ISBN 88-7488-971-2, 2016.

5. Ehsani, M., ed., "Modern electric, hybrid electric, and fuel cell vehicles: fundamentals, theory, and design," CRC Press, Boca Raton, ISBN 978-0-8493-3154-1, 2005.

6. Watzenig, D. and Brandstätter, B., eds., "Comprehensive Energy Management – Eco Routing & Velocity Profiles," Springer International Publishing, Cham, ISBN 978-3-319-53164-9, 2017, doi:10.1007/978-3-319-53165-6.

7. Olin, P., Aggoune, K., Tang, L., Confer, K., Kirwan, J., Rajakumar Deshpande, S., Gupta, S., Tulpule, P., Canova, M., and Rizzoni, G., "Reducing Fuel Consumption by Using Information from Connected and Automated Vehicle Modules to Optimize Propulsion System Control," *SAE Technical Paper*, 2019-01–1213, 2019, doi:10.4271/2019-01-1213.

8. Zhao, Y., Song, H., Liu, Y., and Yu, Z., "Energy Management of Dual Energy Source of Hydrogen Fuel Cell Hybrid Electric Vehicles," *SAE Technical Paper*, 2020-01–0595, 2020, doi:10.4271/2020-01-0595.

9. Jeffers, M.A., Miller, E., Kelly, K., Kresse, J., Li, K., Dalton, J., Kader, M., and Frazier, C., "Development and Demonstration of a Class 6 Range-Extended Electric Vehicle for Commercial Pickup and Delivery Operation," *SAE Technical Paper*, 2020-01–0848, 2020, doi:10.4271/2020-01-0848.

10. Jager, B. de, Keulen, T. van, and Kessels, J., "Optimal Control of Hybrid Vehicles," Springer London, London, ISBN 978-1-4471-5075-6, 2013, doi:10.1007/978-1-4471-5076-3.

11. Caramia, G., "Modelling and Optimization of Energy Management Strategies for Hybrid Vehicles," Dissertation Thesis, Università di Bologna, 2020.

12. Emadi, A., ed., "Handbook of automotive power electronics and motor drives," Taylor & Francis, Boca Raton, ISBN 978-0-8247-2361-3, 2005.

13. Guzzella, L. and Sciarretta, A., "Vehicle Propulsion Systems," Springer Berlin Heidelberg, Berlin, Heidelberg, ISBN 978-3-642-35912-5, 2013, doi:10.1007/978-3-642-35913-2.

14. Cerofolini, A., "Optimal Supervisory Control of Hybrid Vehicles," Dissertation Thesis, Università di Bologna, 2014, doi:10.6092/unibo/amsdottorato/6357.

15. Liu, W., "Hybrid electric vehicle system modeling and control," 2nd edition, Wiley, Chichester, West Sussex, UK ; Hoboken, NJ, USA, ISBN 978-1-119-27894-8, 2017.

16. Onori, S., Serrao, L., and Rizzoni, G., "Hybrid Electric Vehicles," Springer London, London, ISBN 978-1-4471-6779-2, 2016, doi:10.1007/978-1-4471-6781-5.

17. UltimoLithiumIonCapacitorsMay2017.pdf, Oct. 2021.

18. Guzzella, L. and Amstutz, A., “CAE tools for quasi-static modeling and optimization of hybrid powertrains,” *IEEE Transactions on Vehicular Technology* 48(6):1762–1769, 1999, doi:10.1109/25.806768.

19. Guzzella, L. and Amstutz, A., The QSS Toolbox Manual, 2005.

20. Rizzoni, G., Guzzella, L., and Baumann, B.M., “Unified modeling of hybrid electric vehicle drivetrains,” *IEEE/ASME Transactions on Mechatronics* 4(3):246–257, 1999, doi:10.1109/3516.789683.

21. Lin, C.-C., Filipi, Z., Wang, Y., Louca, L., Peng, H., Assanis, D.N., and Stein, J., “Integrated, Feed-Forward Hybrid Electric Vehicle Simulation in SIMULINK and its Use for Power Management Studies,” 2001-01–1334, 2001, doi:10.4271/2001-01-1334.

22. US EPA, O., “Advanced Light-Duty Powertrain and Hybrid Analysis (ALPHA) Tool,” Data and Tools, https://www.epa.gov/regulations-emissions-vehicles-and-engines/advanced-light-duty-powertrain-and-hybrid-analysis-alpha, 2016.

23. ADVISOR Documentation, http://adv-vehicle-sim.sourceforge.net/, Sep. 2021.

24. CIUFFO, B., “CO2MPAS,” Text, https://e3p.jrc.ec.europa.eu/articles/co2mpas, 2016.

25. Lee, B., Lee, S., Cherry, J., Neam, A., Sanchez, J., and Nam, E., “Development of Advanced Light-Duty Powertrain and Hybrid Analysis Tool,” 2013-01–0808, 2013, doi:10.4271/2013-01-0808.

26. Kargul, J., Moskalik, A., Barba, D., Newman, K., and Dekraker, P., “Estimating GHG Reduction from Combinations of Current Best-Available and Future Powertrain and Vehicle Technologies for a Midsized Car Using EPA’s ALPHA Model,” 2016-01–0910, 2016, doi:10.4271/2016-01-0910.

27. Markel, T., Brooker, A., Hendricks, T., Johnson, V., Kelly, K., Kramer, B., O’Keefe, M., Sprik, S., and Wipke, K., “ADVISOR: a systems analysis tool for advanced vehicle modeling,” *Journal of Power Sources* 110(2):255–266, 2002, doi:10.1016/S0378-7753(02)00189-1.

28. Wipke, K.B. and Cuddy, M.R., “Using an advanced vehicle simulator (ADVISOR) to guide hybrid vehicle propulsion system development,” National Renewable Energy Lab. (NREL), Golden, CO (United States), 1996.

29. Walsdorff, A. and Université de Liège > Master ing. civ. méc., À.F., “Longitudinal vehicle’s dynamics, energy consumption and performance modeling of sport cars,” 2016.

30. Lamborghini Murciélago - Scheda Tecnica, Prestazioni, Foto, https://www.lamborghini.com/it-en/capolavori/murcielago, Sep. 2021.

31. Autonomie - Home, https://www.autonomie.net/, Oct. 2021.

32. AVL CRUISE™, https://www.avl.com/cruise/, Oct. 2021.

33. GT-DRIVE+ Next Generation Vehicle Modeling Framework | GT-SUITE, Oct. 2021.

34. IGNITE, https://software.ricardo.com/products/ignite, Oct. 2021.

35. Jazar, R.N., “Vehicle dynamics: theory and applications,” Corrected at 3. printing, Springer, New York, NY, ISBN 978-0-387-74243-4, 2009.

36. Wong, J.Y., “Theory of ground vehicles,” 3rd ed, John Wiley, New York, ISBN 978-0-471-35461-1, 2001.

37. Allen, R.W., Rosenthal, T.J., and Hogue, J.R., “Modeling and Simulation of Driver/Vehicle Interaction,” *SAE Transactions* 105:81–89, 1996.

38. Kessels, J.T.B.A., Koot, M.W.T., Ellenbroek, R.M.L., Pesgens, M.F.M., Veldpaus, F.E., Bosch, van den, P.P.J., Eifert, M., and Kok, D.B., “Vehicle modeling for energy management strategies: conference; 7th AVEC Symposium 2004; 2004-08-23; 2004-08-27,” *Proceedings of the 7th International Symposium on Advanced Vehicle Control 2004, AVEC '04 : August 23-27, 2004, Arnhem, The Netherlands* 465–470, 2004.

39. Preda, I., Covaciu, D., and Ciolan, G., “Coast Down Test – Theoretical and Experimental Approach,” 2010, doi:10.13140/RG.2.1.4048.5925.

40. Sivanesan, M. and Jayabalaji, G., “Modelling, Analysis and Simulation of Clutch Engagement Judder and Stick-Slip,” *SAE Int. J. Passeng. Cars - Mech. Syst.* 10(1):54–64, 2016, doi:10.4271/2016-01-2355.

41. Viscosity of Engine Oil – viscosity table and viscosity chart :: Anton Paar Wiki, https://wiki.anton-paar.com/en/engine-oil/, Sep. 2021.

42. Pacejka, H.B., “Tire and Vehicle Dynamics,” 2° edizione, Society of Automotive Engineers, Warrendale, Pa, ISBN 978-0-7680-1702-1, 2005.

43. Miller, J.M., “Propulsion Systems for Hybrid Vehicles,” IET, ISBN 978-0-86341-336-0, 2004.

44. Addendum 15: Global technical regulation No. 15, Worldwide harmonized Light vehicles Test Procedure, Established in the Global Registry on 12 March 2014, United Nations.

45. Thiel, W., Gröf, S., Hohenberg, G., and Lenzen, B., “Investigations on Robot Drivers for Vehicle Exhaust Emission Measurements in Comparison to the Driving Strategies of Human Drivers,” 982642, 1998, doi:10.4271/982642.

46. Okui, N., “Effects of the Differences in Driving Behavior on Fuel Economy and Emission Characteristics during Vehicle Simulator Execution,” 2018-01–1768, 2018, doi:10.4271/2018-01-1768.

47. Guse, D., Roehrich, H., Lenz, M., and Pischinger, S., “Influence of Vehicle Operators and Fuel Grades on Particulate Emissions of an SI Engine in Dynamic Cycles,” 2018-01–0350, 2018, doi:10.4271/2018-01-0350.

48. Lamborghini announces its roadmap for electrification: “Direzione Cor Tauri,” https://www.volkswagenag.com/en/news/2021/05/lamborghini-announces-its-roadmap-for-electrification.html#, Sep. 2021.

49. New Maserati Electrification way | Maserati, https://www.maserati.com/sg/en/news/mmxx/maserati-electrification, Sep. 2021.

50. Annual Report, https://www.astonmartinlagonda.com/investors/annual-report, Sep. 2021.

51. Lamborghini Huracán Rwd - Technical Specifications, Pictures, Videos, https://www.lamborghini.com/en-en/brand/masterpieces/huracan-rwd, Sep. 2021.

52. Baraszu, R.C. and Cikanek, S.R., “Torque fill-in for an automated shift manual transmission in a parallel hybrid electric vehicle,” *Proceedings of the 2002 American Control Conference (IEEE Cat. No.CH37301)*, IEEE, Anchorage, AK, USA, ISBN 978-0-7803-7298-6: 1431–1436 vol.2, 2002, doi:10.1109/ACC.2002.1023222.

53. Shelton, M.J., Teslak, C.J., and Dai, Z., “Torque hole filling in a hybrid vehicle during automatic transmission shifting,” US8808141B2, 2014.

54. Aravindan, V., Gnanaraj, J., Lee, Y.-S., and Madhavi, S., “Insertion-Type Electrodes for Nonaqueous Li-Ion Capacitors,” *Chem. Rev.* 114(23):11619–11635, 2014, doi:10.1021/cr5000915.

55. Sheberla, D., Bachman, J.C., Elias, J.S., Sun, C.-J., Shao-Horn, Y., and Dincă, M., “Conductive MOF electrodes for stable supercapacitors with high areal capacitance,” *Nature Mater* 16(2):220–224, 2017, doi:10.1038/nmat4766.

56. Bi, S., Banda, H., Chen, M., Niu, L., Chen, M., Wu, T., Wang, J., Wang, R., Feng, J., Chen, T., Dincă, M., Kornyshev, A.A., and Feng, G., “Molecular understanding of charge storage and charging dynamics in supercapacitors with MOF electrodes and ionic liquid electrolytes,” *Nat. Mater.* 19(5):552–558, 2020, doi:10.1038/s41563-019-0598-7.

57. Ronsmans, J. and Lalande, B., “Combining energy with power: Lithium-ion capacitors,” *2015 International Conference on Electrical Systems for Aircraft, Railway, Ship Propulsion and Road Vehicles (ESARS)*, 1–4, 2015, doi:10.1109/ESARS.2015.7101494.

58. BU-107: Comparison Table of Secondary Batteries, https://batteryuniversity.com/article/bu-107-comparison-table-of-secondary-batteries, 2010.

59. Valmra, E., “A New Approach for Ultracapacitor-Battery Hybrid Energy Storage Solutions,” *International Workshop on Supercapacitor and Energy Storage*, Skeleton Technologies GmbH, Bologna, 2019.

60. Burke, A. and Miller, M., “The power capability of ultracapacitors and lithium batteries for electric and hybrid vehicle applications,” *Journal of Power Sources* 196(1):514–522, 2011, doi:10.1016/j.jpowsour.2010.06.092.

61. Xun, Q., Liu, Y., and Holmberg, E., “A Comparative Study of Fuel Cell Electric Vehicles Hybridization with Battery or Supercapacitor,” *2018 International Symposium on Power Electronics, Electrical Drives, Automation and Motion (SPEEDAM)*, IEEE, Amalfi, ISBN 978-1-5386-4941-1: 389–394, 2018, doi:10.1109/SPEEDAM.2018.8445386.

62. Thounthong, P., Chunkag, V., Sethakul, P., Davat, B., and Hinaje, M., “Comparative Study of Fuel-Cell Vehicle Hybridization with Battery or Supercapacitor Storage Device,” *IEEE Trans. Veh. Technol.* 58(8):3892–3904, 2009, doi:10.1109/TVT.2009.2028571.

63. Gao, Y., Moghbelli, H., Ehsani, M., Frazier, G., Kajs, J., and Bayne, S., “Investigation of High-Energy and High-Power Hybrid Energy Storage Systems for Military Vehicle Application,” SAE Technical Paper: 2003-01–2287, 2003, doi:10.4271/2003-01-2287.

64. Nagai, H., Morita, M., and Satoh, K., “Development of the Li-ion Battery Cell for Hybrid Vehicle,” *SAE Technical Paper*, 2016-01–1207, 2016, doi:10.4271/2016-01-1207.

65. Rahmani, F., Niknejad, P., Agarwal, T., and Barzegaran, M., “Gallium Nitride Inverter Design with Compatible Snubber Circuits for Implementing Wireless Charging of Electric Vehicle Batteries,” *Machines* 8(3):56, 2020, doi:10.3390/machines8030056.

66. Zubieta, L. and Bonert, R., “Characterization of double-layer capacitors for power electronics applications,” *IEEE Transactions on Industry Applications* 36(1):199–205, 2000, doi:10.1109/28.821816.

67. Shah, V.A., Karndhar, S.G., Maheshwari, R., Kundu, P., and Desai, H., “An energy management system for a battery ultracapacitor Hybrid Electric Vehicle,” *2009 International Conference on Industrial and Information Systems (ICIIS)*, IEEE, Peradeniya, Sri Lanka, ISBN 978-1-4244-4836-4: 408–413, 2009, doi:10.1109/ICIINFS.2009.5429825.

68. Kumar, S. and Ikkurti, H.P., “Design and control of novel power electronics interface for battery-ultracapacitor hybrid energy storage system,” *International Conference on Sustainable Energy and Intelligent Systems (SEISCON 2011)*, IET, Chennai, India, ISBN 978-93-80430-00-3: 236–241, 2011, doi:10.1049/cp.2011.0367.

69. Walvekar, A.S., Bhateshvar, Y.K., and Vora, K., “Active Hybrid Energy Storage System for Electric Two Wheeler,” *SAE Technical Paper 2020-28-0516*, 2020, doi:10.4271/2020-28-0516.

70. Aharon, I. and Kuperman, A., “Topological Overview of Powertrains for Battery-Powered Vehicles With Range Extenders,” *IEEE Trans. Power Electron.* 26(3):868–876, 2011, doi:10.1109/TPEL.2011.2107037.

71. Kuperman, A. and Aharon, I., “Battery–ultracapacitor hybrids for pulsed current loads: A review,” *Renewable and Sustainable Energy Reviews* 15(2):981–992, 2011, doi:10.1016/j.rser.2010.11.010.

72. Lerman, C., Horosov, A., and Kuperman, A., “Capacitor semi-active battery-ultracapacitor hybrid energy source,” *2012 IEEE 27th Convention of Electrical and Electronics Engineers in Israel*, IEEE, Eilat, Israel, ISBN 978-1-4673-4681-8: 1–4, 2012, doi:10.1109/EEEI.2012.6377027.

73. Aharon, I. and Kuperman, A., “Design of semi-active battery-ultracapacitor hybrids,” *2010 IEEE 26-th Convention of Electrical and Electronics Engineers in Israel*, IEEE, Eilat, Israel, ISBN 978-1-4244-8681-6: 000593–000597, 2010, doi:10.1109/EEEI.2010.5662148.

74. Seim, L.H., “Modeling, control and experimental testing of a supercapacitor/battery hybrid system : passive and semi-active topologies,” Norwegian University of Life Sciences, Department of Mathematical Sciences and Technology, 2012.

75. Gao, L., Dougal, R.A., and Liu, S., “Power Enhancement of an Actively Controlled Battery/Ultracapacitor Hybrid,” *IEEE Trans. Power Electron.* 20(1):236–243, 2005, doi:10.1109/TPEL.2004.839784.

76. Neenu, M. and Muthukumaran, S., “A battery with ultra capacitor hybrid energy storage system in electric vehicles,” *IEEE-International Conference On Advances In Engineering, Science And Management (ICAESM - 2012)*, 731–735, 2012.

77. Chuan, Y., Mi, C., and Zhang, M., “Comparative Study of a Passive Hybrid Energy Storage System Using Lithium Ion Battery and Ultracapacitor,” *WEVJ* 5(1):83–90, 2012, doi:10.3390/wevj5010083.

78. Dougal, R.A., Liu, S., and White, R.E., “Power and life extension of battery-ultracapacitor hybrids,” *IEEE Trans. Comp. Packag. Technol.* 25(1):120–131, 2002, doi:10.1109/6144.991184.

79. Villa, A. and Piegari, L., “Impiego di supercondensatori in parallelo a batterie per estendere l’autonomia di veicoli elettrici a basse temperature,” Politecnico di Milano, Scuola di Ingegneria Industriale e dell’Informazione, Corso di Laurea in Ingegneria Elettrica, 2016.

80. Where fixed-ratio converters fit in high-power delivery systems - Power Electronic Tips, https://www.powerelectronictips.com/where-fixed-ratio-converters-fit-in-high-power-delivery-systems-faq/, May 2021.

81. Mukherjee, S., Kumar, A., and Chakraborty, S., “Comparison of DAB and *LLC* DC–DC Converters in High-Step-Down Fixed-Conversion-Ratio (DCX) Applications,” *IEEE Trans. Power Electron.* 36(4):4383–4398, 2021, doi:10.1109/TPEL.2020.3019796.

82. Salato, M., “A novel approach to industrial rectifier systems: dense, efficient and modular architecture enabled by fixed-ratio bus converters,” *Power Solution Brief, Vicor*, 2014.

83. Salmasi, F.R., “Control Strategies for Hybrid Electric Vehicles: Evolution, Classification, Comparison, and Future Trends,” *IEEE Transactions on Vehicular Technology* 56(5):2393–2404, 2007, doi:10.1109/TVT.2007.899933.

84. Böhme, T.J. and Frank, B., “Hybrid Systems, Optimal Control and Hybrid Vehicles: Theory, Methods and Applications,” Springer International Publishing, Cham, ISBN 978-3-319-51315-7, 2017, doi:10.1007/978-3-319-51317-1.

85. Chao Sun, Xiaosong Hu, Moura, S.J., and Fengchun Sun, “Velocity Predictors for Predictive Energy Management in Hybrid Electric Vehicles,” *IEEE Trans. Contr. Syst. Technol.* 23(3):1197–1204, 2015, doi:10.1109/TCST.2014.2359176.

86. Trovão, J.P., Pereirinha, P.G., Jorge, H.M., and Antunes, C.H., “A multi-level energy management system for multi-source electric vehicles – An integrated rule-based meta-heuristic approach,” *Applied Energy* 105:304–318, 2013, doi:10.1016/j.apenergy.2012.12.081.

87. Zhang, Q. and Li, G., “Experimental Study on a Semi-Active Battery-Supercapacitor Hybrid Energy Storage System for Electric Vehicle Application,” *IEEE Transactions on Power Electronics* 35(1):1014–1021, 2020, doi:10.1109/TPEL.2019.2912425.

88. Schouten, N.J., Salman, M.A., and Kheir, N.A., “Energy Management Strategies for Parallel Hybrid Vehicles Using Fuzzy Logic,” *IFAC Proceedings Volumes* 33(26):83–88, 2000, doi:10.1016/S1474-6670(17)39125-5.

89. Gao, L., Dougal, R.A., and Liu, S., “Active power sharing in hybrid battery/capacitor power sources,” *Eighteenth Annual IEEE Applied Power Electronics Conference and Exposition, 2003. APEC '03.*, IEEE, Miami Beach, FL, USA, ISBN 978-0-7803-7768-4: 497–503, 2003, doi:10.1109/APEC.2003.1179259.

90. Song, Z., Hofmann, H., Li, J., Han, X., and Ouyang, M., “Optimization for a hybrid energy storage system in electric vehicles using dynamic programing approach,” *Applied Energy* 139:151–162, 2015, doi:10.1016/j.apenergy.2014.11.020.

91. Ramoul, J., Chemali, E., Dorn-Gomba, L., and Emadi, A., “A Neural Network Energy Management Controller Applied to a Hybrid Energy Storage System using Multi-Source Inverter,” *2018 IEEE Energy Conversion Congress and Exposition (ECCE)*, 2741–2747, 2018, doi:10.1109/ECCE.2018.8558326.

92. Shen, J. and Khaligh, A., “A Supervisory Energy Management Control Strategy in a Battery/Ultracapacitor Hybrid Energy Storage System,” *IEEE Transactions on Transportation Electrification* 1(3):223–231, 2015, doi:10.1109/TTE.2015.2464690.

93. Xiong, R., Cao, J., and Yu, Q., “Reinforcement learning-based real-time power management for hybrid energy storage system in the plug-in hybrid electric vehicle,” *Applied Energy* 211:538–548, 2018, doi:10.1016/j.apenergy.2017.11.072.

94. Chen, Z., Hu, H., Wu, Y., Xiao, R., Shen, J., and Liu, Y., "Energy Management for a Power-Split Plug-In Hybrid Electric Vehicle Based on Reinforcement Learning," *Applied Sciences* 8(12):2494, 2018, doi:10.3390/app8122494.

95. Chen, H., Xiong, R., Lin, C., and Shen, W., "Model predictive control based real-time energy management for hybrid energy storage system," *CSEE Journal of Power and Energy Systems* 7(4):862–874, 2021, doi:10.17775/CSEEJPES.2020.02180.

96. Lamborghini Aventador SVJ, https://www.lamborghini.com/en-en/models/aventador/aventador-svj, Sep. 2020.

97. INR-21700-P42A – Molicel, http://www.molicel.com/product/inr-21700-p42a/, Apr. 2021.

98. Ahmed, R., Gazzarri, J., Onori, S., Habibi, S., Jackey, R., Rzemien, K., Tjong, J., and LeSage, J., "Model-Based Parameter Identification of Healthy and Aged Li-ion Batteries for Electric Vehicle Applications," *SAE Int. J. Alt. Power.* 4(2):233–247, 2015, doi:10.4271/2015-01-0252.

99. Yao, L.W., Aziz, J.A., Kong, P.Y., and Idris, N.R.N., "Modeling of lithium-ion battery using MATLAB/simulink," *IECON 2013 - 39th Annual Conference of the IEEE Industrial Electronics Society*, IEEE, Vienna, Austria, ISBN 978-1-4799-0224-8: 1729–1734, 2013, doi:10.1109/IECON.2013.6699393.

100. Ma, T., Yang, H., and Lu, L., "Development of hybrid battery–supercapacitor energy storage for remote area renewable energy systems," *Applied Energy* 153:56–62, 2015, doi:10.1016/j.apenergy.2014.12.008.

101. Lukic, S.M., Wirasingha, S.G., Rodriguez, F., Cao, J., and Emadi, A., "Power Management of an Ultracapacitor/Battery Hybrid Energy Storage System in an HEV," *2006 IEEE Vehicle Power and Propulsion Conference*, IEEE, Windsor, UK, ISBN 978-1-4244-0158-1: 1–6, 2006, doi:10.1109/VPPC.2006.364357.

102. Cao, J. and Emadi, A., "A new battery/ultra-capacitor hybrid energy storage system for electric, hybrid and plug-in hybrid electric vehicles," *2009 IEEE Vehicle Power and Propulsion Conference*, 941–946, 2009, doi:10.1109/VPPC.2009.5289744.

103. Banvait, H., Anwar, S., and Chen, Y., "A rule-based energy management strategy for Plug-in Hybrid Electric Vehicle (PHEV)," *2009 American Control Conference*, 3938–3943, 2009, doi:10.1109/ACC.2009.5160242.

104. Lin, C.-C., Peng, H., Grizzle, J.W., and Kang, J.-M., "Power management strategy for a parallel hybrid electric truck," *IEEE Transactions on Control Systems Technology* 11(6):839–849, 2003, doi:10.1109/TCST.2003.815606.

105. Lin, C.-C., Kang, J.-M., Grizzle, J.W., and Peng, H., "Energy management strategy for a parallel hybrid electric truck," *Proceedings of the 2001 American Control Conference. (Cat. No.01CH37148)*, 2878–2883 vol.4, 2001, doi:10.1109/ACC.2001.946337.

106. Cavina, N., Caramia, G., Patassa, S., and Caggiano, M., "Predictive Energy Management Strategies for Hybrid Electric Vehicles: Fuel Economy Improvement and Battery Capacity Sensitivity Analysis," 2018-01–0998, 2018, doi:10.4271/2018-01-0998.

107. Serrao, L., Onori, S., and Rizzoni, G., "A Comparative Analysis of Energy Management Strategies for Hybrid Electric Vehicles," *Journal of Dynamic Systems, Measurement, and Control* 133(3):031012, 2011, doi:10.1115/1.4003267.

108. Musardo, C., Rizzoni, G., and Staccia, B., “A-ECMS: An Adaptive Algorithm for Hybrid Electric Vehicle Energy Management,” *Proceedings of the 44th IEEE Conference on Decision and Control*, IEEE, ISBN 0-7803-9567-0: 8, 2005, doi:10.1109/CDC.2005.1582424.

109. Kural, E. and Güvenç, B.A., “Predictive-Equivalent Consumption Minimization Strategy for Energy Management of A Parallel Hybrid Vehicle for Optimal Recuperation,” Journal of Polytechnic, 2015:113–124, 2015.

110. Kouvaritakis, B. and Cannon, M., “Model Predictive Control: Classical, Robust and Stochastic,” Springer International Publishing, ISBN 978-3-319-24851-6, 2016, doi:10.1007/978-3-319-24853-0.

111. Zhang, J., He, H., and Wang, X., “Model Predictive Control Based Energy Management Strategy for a Plug-In Hybrid Electric Vehicle,” Atlantis Press, ISBN 978-94-6252-098-1: 875–879, 2015, doi:10.2991/icmeis-15.2015.165.

112. Ambhül, D., Guzzella, L., and Savaresi, S., “Energy Management Strategies for Hybrid Electric Vehicles,” Doctoral Thesis, ETH Eidgenössische Technische Hochschule Zürich, ETH/ Measurement and Control Laboratory, 2009.

113. Larsson, V., “Route optimized energy management of plug-in hybrid electric vehicles,” Chalmers Univ. of Technology, Göteborg, ISBN 978-91-7597-002-8, 2014.

114. Zhang, J., Richter, J.-M., and Kaczmarek, C., “Catalysts for Post Euro 6 Plug-In Hybrid Electric Vehicles,” 2020-01–0354, 2020, doi:10.4271/2020-01-0354.

115. Hofstetter, J., Boucharel, P., Atzler, F., and Wachtmeister, G., “Fuel Consumption and Emission Reduction for Hybrid Electric Vehicles with Electrically Heated Catalyst,” *SAE Int. J. Adv. & Curr. Prac. in Mobility* 3(1):702–714, 2020, doi:10.4271/2020-37-0017.

116. Okui, N., “Estimation of Fuel Economy and Emissions for Heavy-Duty Diesel Plug-In Hybrid Vehicle with Electrical Heating Catalyst System,” SAE International, Warrendale, PA, 2017, doi:10.4271/2017-01-2207.

117. Serrao, L., Onori, S., and Rizzoni, G., “ECMS as a realization of Pontryagin’s minimum principle for HEV control,” *2009 American Control Conference*, 3964–3969, 2009, doi:10.1109/ACC.2009.5160628.

118. Nguyen, C.T., Zhang, N., Walker, P.D., and Ruan, J., “Power-split strategy of a novel dual-input series-parallel hybrid electric vehicle,” *2019 IEEE International Conference on Industrial Technology (ICIT)*, 1610–1615, 2019, doi:10.1109/ICIT.2019.8755079.

119. Haußmann, M., Barroso, D., Vidal, C., Bruck, L., and Emadi, A., “A Novel Multi-Mode Adaptive Energy Consumption Minimization Strategy for P1-P2 Hybrid Electric Vehicle Architectures,” *2019 IEEE Transportation Electrification Conference and Expo (ITEC)*, 1–6, 2019, doi:10.1109/ITEC.2019.8790525.

120. Faraji, S. and Ani, F.N., “The development supercapacitor from activated carbon by electroless plating—A review,” *Renewable and Sustainable Energy Reviews* 42:823–834, 2015, doi:10.1016/j.rser.2014.10.068.

121. Raza, W., Ali, F., Raza, N., Luo, Y., Kim, K.-H., Yang, J., Kumar, S., Mehmood, A., and Kwon, E.E., “Recent advancements in supercapacitor technology,” *Nano Energy* 52:441–473, 2018, doi:10.1016/j.nanoen.2018.08.013.

122. Variant Subsystems - MATLAB & Simulink, https://www.mathworks.com/help/simulink/slref/variant-subsystems.html;jsessionid=f084b11c17d6bec1a2eeb0e61320, Sep. 2020.

123. Rick, A. and Sisk, B., "A Simulation Based Analysis of 12V and 48V Microhybrid Systems Across Vehicle Segments and Drive Cycles," 2015-01–1151, 2015, doi:10.4271/2015-01-1151.

124. Liu, Z., Ivanco, A., and Filipi, Z.S., "Impacts of Real-World Driving and Driver Aggressiveness on Fuel Consumption of 48V Mild Hybrid Vehicle," *SAE Int. J. Alt. Power.* 5(2):249–258, 2016, doi:10.4271/2016-01-1166.

125. Joshi, A., "Review of Vehicle Engine Efficiency and Emissions," 2019-01–0314, 2019, doi:10.4271/2019-01-0314.

126. Liu, Z., Shi, T., Chen, K., Hao, H., and Zhao, F., "Cost and Effectiveness Study of Hybrid Electric Vehicle Technologies Based on China Data," 7(1):16, 2017.

127. Kim, T.S., Manzie, C., and Watson, H., "Fuel Economy Benefits of Look-ahead Capability in a Mild Hybrid Configuration," *IFAC Proceedings Volumes* 41(2):5646–5651, 2008, doi:10.3182/20080706-5-KR-1001.00952.

128. GitHub: Where the world builds software, https://github.com/, Sep. 2021.

129. TortoiseGit – Windows Shell Interface to Git, https://tortoisegit.org/, Sep. 2021.

130. MATLAB App Designer, https://ch.mathworks.com/products/matlab/app-designer.html, Sep. 2021.

131. Muzaffar, A., Ahamed, M.B., Deshmukh, K., and Thirumalai, J., "A review on recent advances in hybrid supercapacitors: Design, fabrication and applications," *Renewable and Sustainable Energy Reviews* 101:123–145, 2019, doi:10.1016/j.rser.2018.10.026.